Distribution Agreement

In presenting this thesis or dissertation as a partial fulfillment of the requirements for an advanced degree from Emory University, I hereby grant to Emory University and its agents the non-exclusive license to archive, make accessible, and display my thesis or dissertation in whole or in part in all forms of media, now or hereafter known, including display on the world wide web. I understand that I may select some access restrictions as part of the online submission of this thesis or dissertation. I retain all ownership rights to the copyright of the thesis or dissertation. I also retain the right to use in future works (such as articles or books) all or part of this thesis or dissertation.

Signature:

_____ _____

Matthew A. Bryson Date

AN INVESTIGATION OF SPINAL ECTOPIC EPILEPTIFORM ACTIVITY

By

Matthew A. Bryson

Doctor of Philosophy

Neuroscience

_____

Shawn Hochman, Ph.D.

Advisor

_____

Peter Wenner, Ph.D.

Advisor

_____

Sandra M. Garraway, Ph.D.

Committee Member

_____

Nicholas Au Yong, MD, Ph.D.

Committee Member

Accepted:

_____

Kimberly Jacob Arriola, Ph.D., MPH.

Dean of the James T. Laney School of Graduate Studies

_____

Date

AN INVESTIGATION OF SPINAL ECTOPIC EPILEPTIFORM ACTIVITY

By

Matthew A. Bryson

B.S., Washington and Lee University, 2018

Advisor: Shawn Hochman, PhD

Advisor: Peter Wenner, PhD

An abstract of

A dissertation submitted to the Faculty of the James T. Laney School of Graduate Studies of Emory University in partial fulfillment of the requirements for the degree of Doctor of Philosophy in Neuroscience

2023

Abstract

AN INVESTIGATION OF SPINAL ECTOPIC EPILEPTIFORM ACTIVITY

By

Matthew Allen Bryson

Spinal cord injury (SCI) leads to sensory dysfunction including neuropathic pain, which is resistant to treatment with classical analgesics. Previous work has established spinal somatosensory network hyperexcitability as a critical driver of neuropathic pain after SCI. This network hyperexcitability shares common cellular mechanisms with epileptic conditions, including perturbations in ion channels, loss of GABAergic inhibition, and dysregulation of intracellular chloride concentration. Given the mechanistic similarities between the conditions, I sought to determine whether dorsal horn somatosensory circuitry exhibits epilepsy-like (epileptiform) network characteristics after SCI. Here, using a mouse lower thoracic contusion injury model and an isolated spinal cord preparation that enables recordings from sensory axons in multiple segmental dorsal roots (DRs), I demonstrated expression of GABA interneuron-driven ectopic bursting in primary afferents after SCI. This bursting synchronized across dorsal roots, ostensibly driven by dysfunction in primary afferent depolarization (PAD) through conversion from subthreshold inhibition to suprathreshold spiking. Synchronous bursting occurred spontaneously and could be evoked by afferent stimulation, including optogenetic stimulation of non-pain encoding afferents (Aδ-LTMRs and C-LTMRs). Indeed, SCI-induced bursting expressed distinguishing traits of an epileptiform circuit including stereotyped bursting activity that exhibited hypersynchrony, post-burst refractory period, recruitment by afferent stimulation, and functional reorganization of circuitry. Thus, SCI unmasks dorsal horn circuits that drive ectopic epileptiform bursting. All emergent features of bursting after SCI could be reproduced in naïve animals with the convulsant K_V blocker 4-aminopyridine (4-AP), the K_V blocker tetraethylammonium (TEA), and the KCC2 blocker VU0240551, suggesting that epileptiform burst circuitry expresses degeneracy such that ectopic bursting can arise from multiple alterations. Bursting is ostensibly generated by PAD-evoking GABAergic interneurons and propagates through Aδ and C fibers, including LTMRs, by which it is likely to directly activate pain circuitry. Overall, epileptiform bursting enables profound corruption of sensory signaling, as ectopic bursts propagate bidirectionally to aberrantly activate spinal circuitry and acutely perturb mechanosensitivity. This work contributes to the understanding of post-SCI somatosensory dysfunction by identifying a manifestation of dorsal horn hyperexcitability that is epileptiform, exhibits features indicative of degeneracy, and provides a substrate for crossing of sensory modalities, which could explain features of neuropathic pain after SCI.

AN INVESTIGATION OF SPINAL ECTOPIC EPILEPTIFORM ACTIVITY

By

Matthew A. Bryson

B.S., Washington and Lee University, 2018

Advisor: Shawn Hochman, PhD

Advisor: Peter Wenner, PhD

A dissertation submitted to the Faculty of the James T. Laney School of Graduate Studies of Emory University in partial fulfillment of the requirements for the degree of Doctor of Philosophy in Neuroscience

2023

Contents

List of tables

Table of figures

Chapter 1: Introduction

Neuropathic pain after spinal cord injury (**SCI**) is a significant clinical concern and is notoriously resistant to existing treatment options, largely due to our poor understanding of its etiology . The goal of this dissertation is to explore a novel phenotype of SCI-induced circuit hyperexcitability with similarities to epilepsy. Below, I will first describe the general mechanisms of somatosensory perception, including the peripheral and spinal organization of the somatosensory system. Then, I will discuss current hypotheses explaining how neuropathic pain can arise from somatosensory system dysfunction after SCI, as well as known similarities between neuropathic pain and epilepsy. Finally, I will briefly address the brain's role in pain, as it will not be discussed at length in this work. I will end the chapter by highlighting remaining gaps in knowledge and outlining experiments designed to address these limitations.

1.1 The importance of somatosensation

Somatosensation is a critical facet of our everyday sensory experience. It is easy to take for granted the complicated encoding strategies that create our perception of touch: numerous populations of highly specialized low threshold receptors allow us to feel temperature, vibration, fine touch, pressure, and more; noxious receptors allow us to detect and respond to potentially dangerous chemical, thermal, and mechanical stimuli; sensory adaptation allows us to wear clothing without constantly feeling it against our skin [1]. Spinal cord dorsal horn circuitry processes all this incoming information before it is transmitted to the brain. Dysfunctions in somatosensory circuitry induce conditions ranging from sensory deficits like complete insensitivity to pain [2] to seemingly miraculous neuropathic pain conditions like phantom limb syndrome.

1.2 Primary afferent populations and somatosensory coding

Somatosensation is incredibly complex, partially due to the rich variety of cutaneous sensory primary afferents, which are the first-order neurons of sensation. Primary afferents are pseudounipolar axons whose cell bodies lie in dorsal root ganglia (DRG) and whose axons collectively form dorsal roots (DR) that project to the spinal cord dorsal horn (DH). Afferent DRG and spinal projections are somatotopically organized in a dermatomal fashion, with segments divided into cervical, thoracic, lumbar, and sacral spinal segments, distributed rostrocaudally **(Figure 1-1B)**.

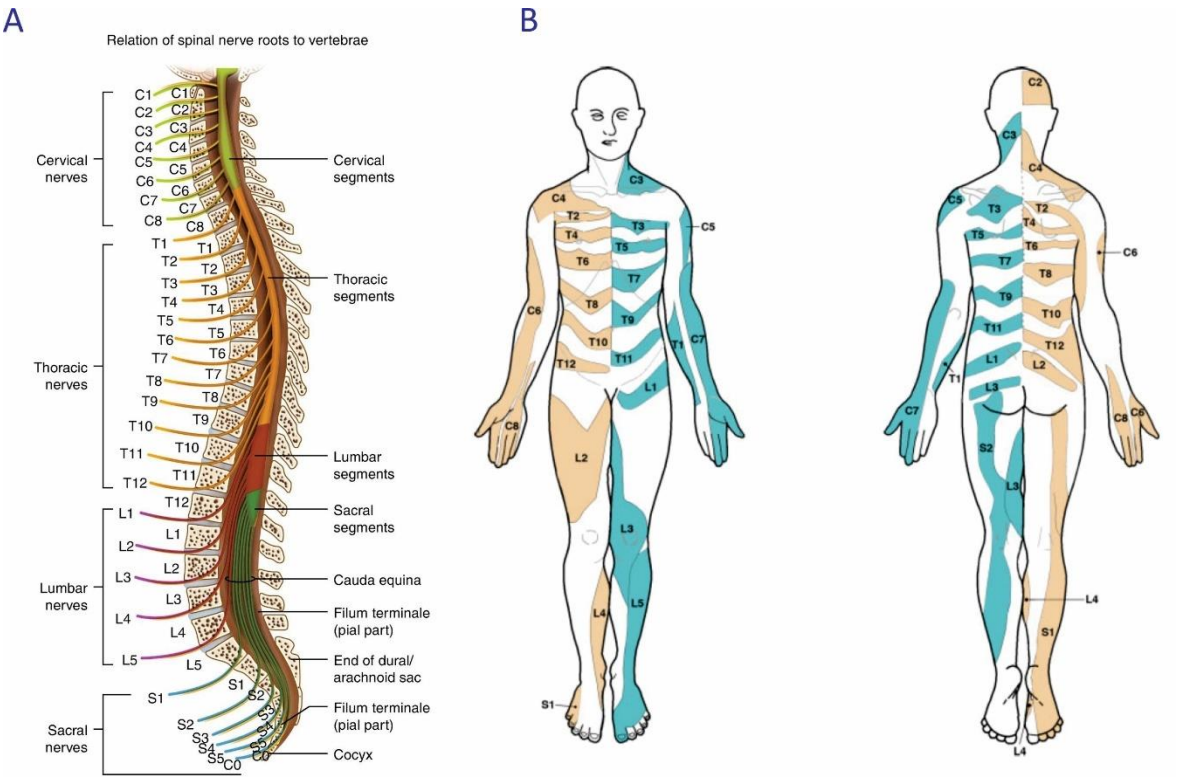

Figure 1-1: Dermatomal organization of spinal cord and tactile sensation

***(A)** Map of spinal and spinal nerve levels. (Figure from [3]) **(B)** Evidence-based map of dermatomal organization of tactile perception in human. Regions are based on activation of*

dorsal nerve root with tactile stimulation. Blank regions indicate areas of significant variability and overlap. (Figure from [4]).

Traditionally, primary afferents have been categorized by modality (the type of stimulus the receptor responds to) and conduction speed (owing to axon diameter and degree of myelination). Low threshold mechanoreceptors (LTMRs) are those that respond to innocuous touch and fall into three conduction velocity categories: C-LTMR (small unmyelinated fibers, slow conduction, <2.5 m/s at room temperature), Aδ-LTMR (mid-sized unmyelinated fibers, intermediate conduction, 4-30 m/s at room temperature), and Aβ-LTMRs (large, myelinated fibers, fast conducting, 30-100 m/s at room temperature) [5]. These primary afferent subtypes are pseudounipolar neurons that innervate hair follicles in the cutaneous periphery and terminate in a region of the superficial dorsal horn termed the LTMR recipient zone (LTMR-RZ) [6]. Nociceptors are Aδ and C fibers that transmit noxious information (mechanical, thermal, or chemical) from the periphery [7]. Although these numerous populations are conserved in structure and function between mice, cats, primates, and humans [8, 9], the wide variety of primary afferent subtypes is just beginning to be appreciated. For example, Aδ-, Aβ-, and C-LTMR (called C-tactile afferents in humans) populations can be further broken down into functional subpopulations based on genetic markers (Zheng et al., 2019). These genetic markers have allowed selective targeting of receptor subtypes for imaging and optogenetic approaches. Of particular interest in this study are C- and Aδ-LTMR afferents, which co-innervate hair follicles in hairy skin and form a functional unit of light touch reception [9, 10] **(Figure 1-2A)**. C-LTMRs have been implicated as mediators of pleasant touch, highlighting their role as receptors for the affective aspect of stimuli, while Aδ-LTMRs are thought to encode the representational aspect of light touch [11-13].

1.3 Organization of primary afferent projection to the dorsal horn

Primary afferent axons, bundled by dermatome in DRs, enter the spinal cord and form a wide variety of synaptic connections. Upon entry, Aβ fibers branch extensively, forming a broad network of connections rostrocaudally from their spinal entry point [14] before contacting interneurons in lamina III-IV[15]. After Aδ and C fibers enter the cord, short range projections of high threshold C and longer range projections of high threshold Aδ fibers travel through Lissauer's Tract (LT), which has been implicated in gating of receptive field size and transduction of nociceptive information through the spinothalamic tract [16]. These axons then enter the spinal gray matter and synapse onto interneurons in lamina I and II. Non-painful (innocuous) C- and Aδ-LTMRs exhibit topographical and non-overlapping receptive field organization in lamina II-III of the superficial dorsal horn, retaining their dermatomal tiling as they innervate the LTMR-RZ (**Figure 1-2B**). The superficial dorsal horn, particularly lamina II, is a critical site of sensory modulation and computation before projection neurons carry somatosensory information to supraspinal loci. The LTMR-RZ alone is made up of a variety of 14 excitatory and inhibitory interneurons, all of which receive mixed local interneuron, afferent, and cortical input [17] (**Figure 1-2C)**. Indeed, the dorsal horn is a complex web of interconnected somatosensory processing before information is projected to supraspinal regions.

Nociceptive projection neurons in lamina I receive direct excitatory input from Aδ and C nociceptors, as well as excitatory and inhibitory input from local and diffuse interneurons [18, 19]. Wide-dynamic range (WDR) neurons also reside in the dorsal horn and respond to both innocuous and noxious stimuli, coding the modality of their input with firing rate, with high frequency firing indicating a more noxious stimulus [20]. Nociceptive and WDR projection neurons comprise the spinal origin of the anterolateral system, or spinothalamic tract **(Figure 1-**

2B), which is responsible for transducing pressure, crude touch, temperature, and painful stimuli to the brain [21]. Through various dorsal horn circuits, Aδ- and C-LTMR inputs are critical for modulating the tone of interneurons that contact this highly sensitive system. For example, parvalbumin^{+} interneurons, a single inhibitory interneuron subtype that provides indirect input to spinothalamic projection neurons, are critical for gating allodynia [18]. This same work showed that silencing of inhibitory parvalbumin^{+} interneurons using viral vectors unmasked dorsal horn circuitry such that mice expressed constitutive hypersensitivity to mechanical stimuli. This circuit interaction is a concrete example of Gate-control theory, first proposed in 1965 by Melzack and Wall [22], a seminal hypothesis explaining how innocuous sensation can override, or "gate", painful sensation through dorsal horn circuits. While the canonical "gate" as initially proposed is mediated by Aβ innocuous input, we now know that the dorsal horn expresses multiple gating mechanisms [23-26].

Non-painful, or innocuous, stimuli, specifically fine touch, proprioception, and vibration, are processed through the dorsal column-medial lemniscus (DCML) system. Here, a minority of primary afferents form a direct pathway to the dorsal column nuclei (DCN) for further supraspinal processing [17]. Most primary afferent spinal projections, however, after branching within their tiled borders as described above, synapse onto second-order neurons in the LTMR-RZ, where they provide excitatory input for a complex circuit modulating both presynaptic afferent tone and postsynaptic projection circuitry, including modulation of ascending pain pathways through feedforward inhibition [25, 27]. The most prominent output pathway of innocuous circuitry is through DCML system **(Figure 1-2B)**, the projection neurons of which receive some direct monosynaptic Aβ input, some direct polysynaptic Aδ input, and mixed LTMR-RZ interneuron input [17].

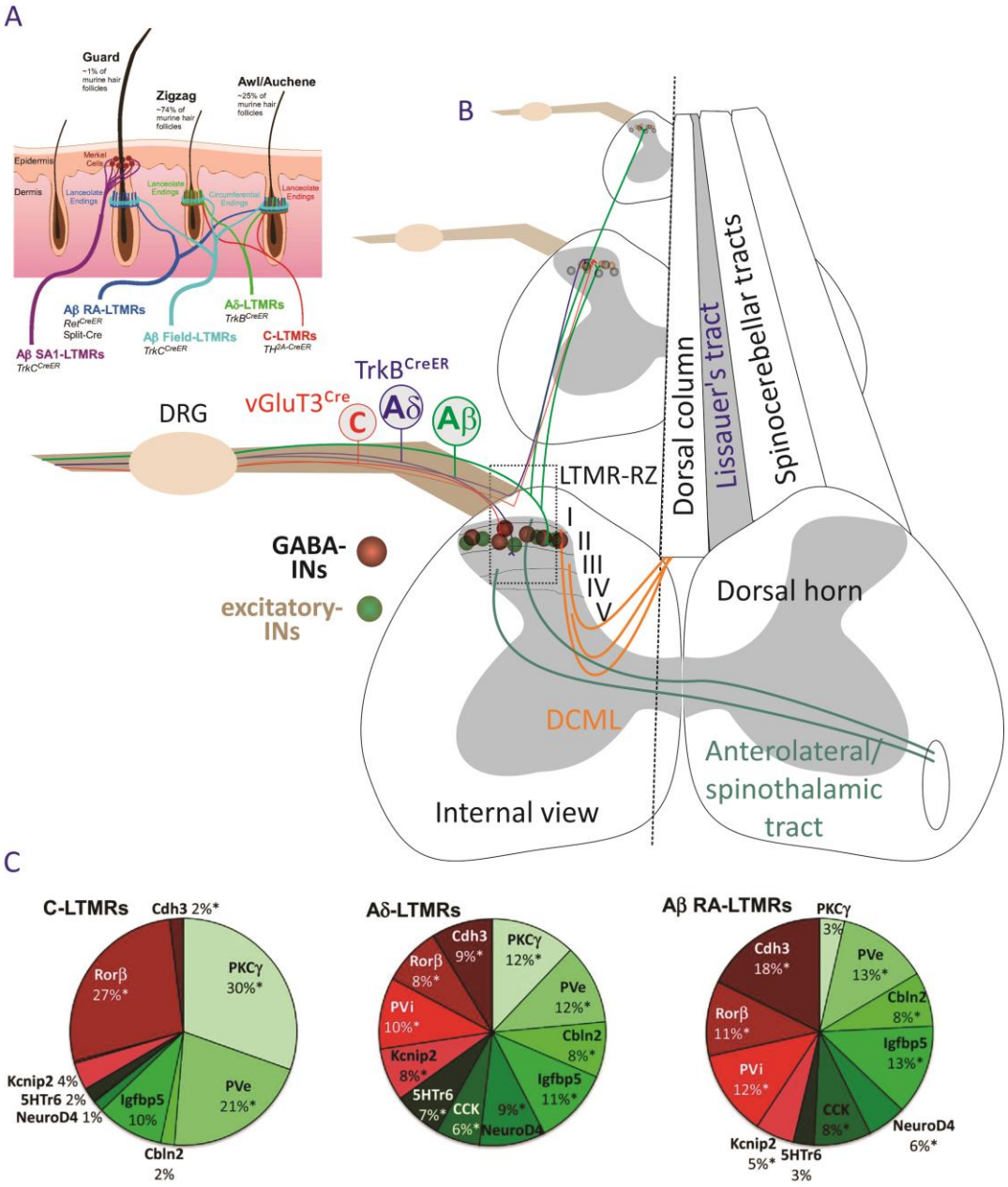

Figure 1-2: Basic organization of peripheral and spinal hairy skin somatosensation

(A) *Hairy skin is innervated by a wide variety of low threshold mechanoreceptors, many of which form lanceolate endings around hair follicles, including C- and Aδ- LTMRs (figure adapted from [14]).* ***(B)*** *Diagram of three rostrocaudal segments illustrating spinal projection of LTMRs as described in text above.* ***(C)*** *Excitatory (green) and inhibitory (red) interneuron*

subtypes contacted by LTMRs. Each LTMR type contacts a diverse and unique subset of interneurons (figure adapted from [17]).

1.4 Presynaptic inhibition and modulation in sensory coding

Not only are interneuron-projection neuron relationships complex, but primary afferents and dorsal horn interneurons also interact reciprocally [28, 29]. As discussed above, primary afferents synapse onto a variety of spinal interneurons. A subset of these interneurons form reciprocal synapses onto primary afferents [30], where they mediate a form of presynaptic inhibition called primary afferent depolarization (PAD) **(Figure 1-3)** [31-35]. As primary afferents highly express the Na-K-Cl cotransporter NKCC1, but express the chloride-extruding counterpart KCC2 at low levels, their intracellular chloride concentrations are higher than most neurons, leading GABA to produce depolarizing current rather than its canonical hyperpolarizing current [36]. Counterintuitively, this depolarization is inhibitory rather than excitatory, due to inactivation of sodium channels [37], inactivation of calcium channels [38], inhibition of afferent glutamate release [39], and action potential shunting due to increased cellular conductance [40]. More recent work into the synaptic mechanisms of PAD has called into question whether the canonical GABAergic interneuron-mediated depolarization is the only kind of PAD [41, 42]. Now, it is known that both $GABA_A$ and NMDA receptors underly PAD of different afferent types [42]. In general, PAD plays a critical role in modulating somatosensory circuits by controlling the gain of signals propagating from the periphery to the spinal cord and acting as a gating mechanism for painful stimuli by inhibiting nociceptive afferents [36, 43, 44].

As PAD is depolarizing, temporal or spatial summation of PAD can result in suprathreshold depolarization and the initiation of an ectopic action potentials at the axo-axonic interneuron-primary afferent synapse [45, 46]. These ectopic action potentials are referred to as dorsal root

reflexes (DRRs) and are hypothesized to travel orthodromically [47, 48], activating spinal circuitry, and antidromically, where they have been shown to produce neurogenic inflammation and hypersensitivity [49, 50]. Although these DRR action potentials are obviously not inhibitory, they do represent a perturbation in peripheral somatosensory function, as action potentials traveling antidromically collide with incoming action potentials from cutaneous receptors, resulting in loss of cutaneous receptor information [51]. Antidromic afferent action potentials also release inflammatory factors in the periphery, maintaining pathogenic states like neurogenic inflammation [49, 52]. Furthermore, it has been hypothesized that antidromic discharges could alter peripheral receptors' spike generation, further inhibiting orthodromic transmission during bouts of DRRs [48]. PAD is a powerful form of presynaptic inhibition that is critical to modulating peripheral somatosensory tone [53] and DRRs can act with a similar magnitude of modulatory control when they occur.

The dorsal horn also receives significant descending modulation. Perhaps the best-known descending pain pathway projections are those from the periaqueductal gray (**PAG**), which are responsible for the peripheral pain modulation achieved by opioids and the peripheral effects of endogenous enkephalin [54, 55]. The PAG's descending projections to dorsal horn are largely indirect – involving reciprocal connections with the rostral ventromedial medulla (**RVM**) serotonergic and locus coeruleus (**LC**) adrenergic neurons – which have long been major targets of supraspinal opioid-based analgesia [56, 57]. The entirety of the spinal somatosensory system – interneurons, projection neurons, and primary afferents – receive both serotonergic and noradrenergic input from RVM and LC, respectively [58]. More recently, direct corticospinal projections modulating light touch sensitivity and allodynia have been identified [59].

Together, the complexity of the dorsal horn underlies its importance as a locus of somatosensory processing. However, its complexity also makes its functional network prone to perturbation in pathogenic states. When cutaneous receptors and their downstream circuitry are working properly, the somatosensory system carries information from cutaneous periphery to cortex with incredible fidelity and speed. However, pathogenic states of somatosensory circuitry can have disastrous sensory consequences.

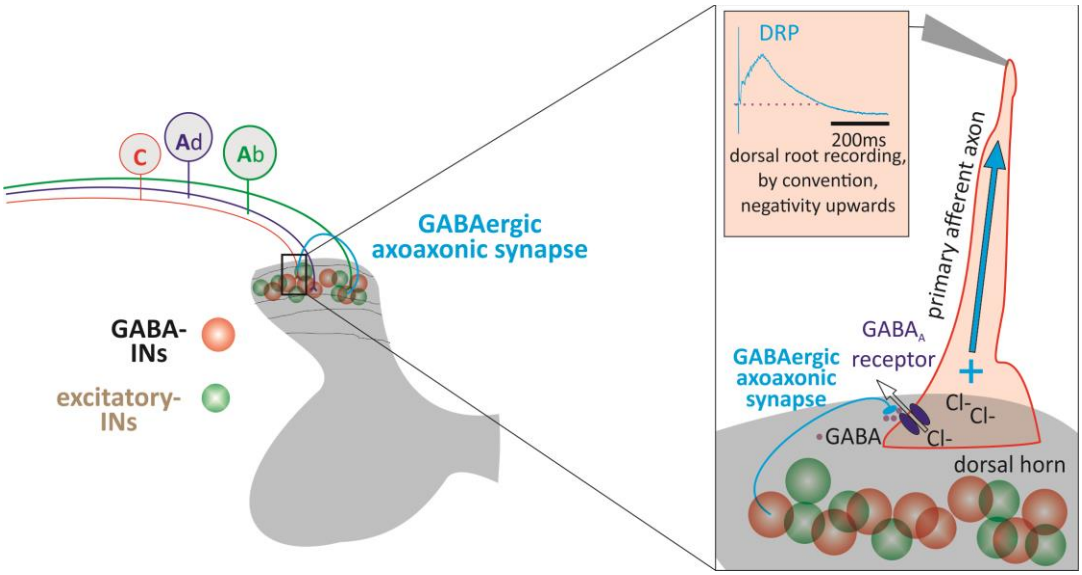

Figure 1-3: Circuitry underlying PAD

***Left**: Subpopulations of interneurons form axoaxonic reciprocal connections onto primary afferent spinal projections [30, 53, 60-62], where they mediate PAD, largely through depolarizing but inhibitory GABAergic synaptic signaling, which is recorded extracellularly as a DRP. **Right**: Axoaxonic synapses from GABAergic interneurons evoke depolarization in primary afferent spinal projections through $GABA_A$ receptor-induced extrusion of chloride ions. Depolarization propagates peripherally, where it can be recorded as a DRP. Right figure adapted conceptually from [41].*

1.5 SCI and Neuropathic pain

According to the International Association for the Study of Pain (IASP), neuropathic pain is, by definition, "…pain that arises as a direct consequence of a lesion or diseases affecting the somatosensory system." [63]. In this work, I will focus on SCI as a cause of neuropathic pain. It is approximated that 80% of SCI patients develop neuropathic pain at some point post-injury, often months or years after the initial event [64-66]. SCI causes damage not only to neurons at the site of injury but also large-scale systemic changes that can lead to long-term aberrant sensory states. Increasingly, aberrant post-injury plasticity in the somatosensory and other systems has been implicated as a key cause of neuropathic pain after SCI [67-70].

SCI and neuropathic pain are both extraordinarily heterogenous conditions. Neuropathic pain is known to occur through mechanisms such as wind-up, spontaneous firing of nociceptors, disinhibition, and activation of microglia, each of which can be generated through a number of sensory insults [70-76]. Clinically, these causes for pain occur through different mechanisms and can present differently in patients through diagnostic testing including electrophysiology, quantitative sensory testing, nerve and skin biopsy, and fMRI [77]. For example, patients known to be experiencing spontaneous chronic pain demonstrate spontaneous C-fiber firing in the absence of somatosensory stimulation as observed with microneurography [78]. At the core, hyperexcitability in peripheral and central circuits has been implicated as a critical driver of the pain etiological mechanisms above. In sensory circuits, this hyperexcitability manifests as spontaneous firing (likely experienced as spontaneous pain) or increased firing in response to low threshold stimuli (indicative of allodynia).

In the US, SCI most commonly damages cervical and lower thoracolumbar levels and occurs as a result of automobile accidents [79]. A plurality (43%) of patients in this population experienced

American Spinal Injury Associated (AISA) grade A SCI, indicating that the impairment was complete (no sensory or motor function below the level of injury), with the remaining patients retaining some level of sensory or motor function. These results are consistent with retrospective injury studies performed in other countries [80, 81]. SCI patient populations commonly describe pain as one of their most significant concerns after injury, with ~80% of SCI patients experiencing some sort of neuropathic pain after injury, with onset usually months-years after time of injury. [64, 66]. Perhaps surprisingly, there is little relationship between the completeness of SCI and the experience of neuropathic pain after injury [65, 66, 82-85]. SCI neuropathic pain patients most commonly experience diffuse pain at and below the level of injury and often describe the pain as “deep”, “shooting”, “electric shock-like”, “lancinating” and “burning” [66, 86, 87]. It is worth emphasizing that patients only develop pain at the same level as their injury (at-level) and below-level pain. While chronic intractable pain is in and of itself a massive concern, it also commonly results in secondary issues such as depression, insomnia, anxiety, social isolation, and extended recovery times [88, 89]. The current treatments for SCI-induce include behavioral therapy, electrical stimulation therapy, or pharmacological therapy with gabapentin, pregabalin, opioids anticonvulsants, or the tricyclic antidepressant amitriptyline. [90]. Interestingly, recent studies have suggested that anticonvulsants are particularly effective in the treatment of neuropathic pain, especially when compared to traditional analgesics like opioids [91-94]. Non-pharmacological interventions, such as dorsal root ganglia stimulation [95] or spinal cord stimulation [96-99], are highly effective in a subset of cases, but their mechanisms of action are not fully understood [99]. While the prognosis for these surgical interventions is often promising, these treatments are largely reserved for cases of particularly severe refractory neuropathic pain due to their invasiveness. Overall, the prognosis

for chronic neuropathic pain is relatively poor, largely due to the shortcomings in our understanding of how neuropathic pain develops and manifests. Attempting to address some of these shortcomings, this work focuses on SCI-induced dysfunction of primary afferents and the dorsal spinal cord: the sites of transduction and initial processing of somatosensory information. Specifically, I will draw comparisons between post-SCI neuropathic pain and epileptic activity in order to suggest a new way of looking at post-injury sensory reorganization.

1.6 Animal models of SCI neuropathic pain

Numerous animal models have been exhaustively developed to study various etiologies and aspects of neuropathic pain, most commonly using mouse or rat as a model organism [100, 101]. This is a perpetually evolving body of literature in which investigators are constantly trying to match clinical presentations and other aspects of pain [102, 103] with injury models and behavioral measurements. The current work will later make brief mention of several specific neuropathic pain model methodologies including peripheral nerve injury and inflammation, but the focus is on manifestations of dorsal horn hyperexcitability SCI.

In general, years of work with neuropathic pain animal models have established that neuropathic pain after SCI can result from dysfunction throughout the somatosensory system, including peripheral nociceptor hyperexcitability [104, 105], alterations in dorsal horn circuity function [75, 106-110], and ascending tract/cortical dysfunction [111, 112]. Recent animal work has used complex genetic toolkits to begin to understand how cutaneous peripheral receptors, spinal cord circuitry, and the brain work together to interpret the different facts underlying pain as an experience [18, 21, 70, 107, 113-117]. The current work focuses on mechanisms of dorsal horn hyperexcitability after SCI, specifically lower thoracic contusion injury, which best matches many clinical features of SCI [118].

While animal models have elucidated much about neuropathic pain and how to treat it, one major shortcoming in the field is a reliable way to measure non-evoked spontaneous neuropathic pain [119], although it is by far the most widely reported form of neuropathic pain. In one study, it was reported that 93% of neuropathic pain patients with below-level pain reported spontaneous pain and only 35% reported allodynia (pain from non-painful stimuli) [120]. In chapter 5, I will discuss the potential of this work to provide new methods for identifying biomarkers of ongoing spontaneous pain.

1.7 Hypotheses explaining allodynia after SCI

While the main goal of this work is to elucidate mechanisms of SCI neuropathic pain, I will focus on low threshold mechanoreceptors and the interneuronal circuits they target in the superficial dorsal horn. It may seem intuitive that pain would be encoded by nociceptive primary afferents, but this is not always the case in neuropathic pain states. As such, it can arise from dysfunction in the peripheral nerves, the spinal cord, or the brain. We understand little about the etiology of individual presentations of neuropathic pain, particularly after SCI. Hypotheses explaining SCI pain involve enhanced microglia expression, astrocytic dysfunction, ongoing immune response, peripheral sensitization, and central sensitization through numerous mechanisms [102, 110, 121, 122]. Here, I will focus on hypotheses involving neural circuit plasticity of spinal circuitry. Broadly, hypotheses explaining spinal circuit's role in allodynia after SCI can be split into two categories: 1) peripheral hyperexcitability including receptor hypersensitivity and sustained spontaneous activity in primary afferent dorsal root ganglia and 2) central hyperexcitability including dorsal horn network hyperexcitability and unmasking of silent circuitry in the dorsal horn.

The first body of work, which focuses on peripheral hyperexcitability, has implicated spontaneous activity in nociceptor cell bodies after SCI in the experience of neuropathic pain [104, 123]. In these experiments, increased repetitive spontaneous activity in putative nociceptors in DRG correlated with behavioral indicators of mechanical and thermal allodynia. Mechanistically, upregulation of the sodium channel Nav1.8 in primary afferent cell bodies has been implicated as responsible for the emergence of spontaneous activity [71, 124] and downregulation of the potassium channel Kv3.4 is thought to underly repetitive firing [125, 126]. Together, this works implicate ongoing nociceptive afferent input as a key driver of pain circuit activation and therefore pain perception and emphasizes that SCI is a systemic injury that results in maladaptive properties throughout the somatosensory system [69, 123, 127].

The second body of work, focusing on central hyperexcitability after injury, has focused on hyperexcitability of dorsal horn interneurons and projection neurons and unmasking of normally silent circuitry in the dorsal horn. At a basic level, these forms of hyperexcitability can manifest as increased firing rates in both wide WDR and nociceptive projection neurons (often presenting as hyperalgesia), activation of nociceptive projection neurons by normally innocuous stimulation (often presenting as allodynia) [128, 129], or spontaneous activity in any of these populations or wider circuitry (presenting as spontaneous ongoing pain). These SCI-induced changes are associated with alterations in voltage-gated sodium channels in dorsal horn neurons [121, 130] and voltage-gated potassium channel function in DRG [126], as well as perturbations in intracellular chloride homeostasis in the dorsal horn [131-133], all of which support increases in sensory circuit excitability. Alterations in dorsal horn intracellular chloride homeostasis [134] can induce circuit hyperexcitability through loss or degradation of GABAergic inhibition, which manifests in several injury models [135, 136]. Another proposed mechanism by which the dorsal

horn becomes hyperexcitable after SCI is aberrant sprouting of afferents, which allows activation of networks previously inaccessible by those afferents and increased excitatory drive to spinal networks [137, 138].

While some mechanisms of neuropathic pain, such as afferent and sympathetic sprouting, afferent hyperexcitability, and dysregulation of intracellular chloride homeostasis, are critical in peripheral nerve injury as well as SCI [139-145], others are unique to SCI. One unique feature of SCI particularly relevant to the present work is that loss of descending systems unmasks synchronous multisegmental DRPs including as suprathreshold bursts [146-148]. As discussed earlier, descending input plays a critical modulatory role in all levels of sensory computation in the spinal cord, from primary afferent action potential propagation to dorsal horn computation. Loss of this descending input, along with other mechanisms of hyperexcitability, make SCI a perturbation that can manifest massive spinal hyperexcitability and subsequent somatosensory dysfunction.

Overall, existing literature has effectively explored post-SCI changes at the macro and micro levels – examining human symptoms, animal evoked behavioral phenotypes, and single-cell changes quite effectively. What is lacking is an examination of the circuits driving specific pain phenotypes, especially in the SCI field. Dorsal horn somatosensory connectivity is complex and further exploring measurable circuits will allow us to better understand how it can dysfunction to produce pain. In this spirit, this work will examine circuit-level changes in dorsal horn function after SCI to better understand the underlying causes behind post-injury neuropathic pain.

1.8 Similarities between epilepsy and neuropathic pain

In this work, I will be highlighting the mechanistic and functional similarities between SCI neuropathic pain and the various epileptic conditions. I will make the case that different sensory circuitries (cortex and dorsal horn) experience similar failures in inhibition to achieve pathogenesis and that the conditions could share more than has been previously suggested. Here, I will introduce epilepsy and a few basic features it shares with neuropathic pain.

Epilepsy is a group of conditions marked by the experience of seizures, or bouts of excessive synchronous neural activity in the brain [149]. Much like SCI and neuropathic pain, epileptic conditions are heterogenous but generally thought to arise from an imbalance in excitatory and inhibitory input within a neural network [150]. As described, neuropathic pain, through clinical description and animal model study, is known to be related to the expression of hyperexcitability in somatosensory circuitry. Discussed methods of hyperexcitability include alterations in voltage-gated sodium and potassium channel expression, loss of GABAergic inhibition, and alterations in intracellular chloride homeostasis. Excessive circuit level excitability through each of these mechanisms is also a prominent feature in the various epilepsies and it is possible that SCI -induced increases in sensory circuit excitability also manifests epilepsy-like (**epileptiform**) activity [151-154]. Consistent with this possibility is the observation that the convulsant 4-aminopyridine (4-AP) leads to epileptiform activity in spinal dorsal horn circuits [155] that can subsequently be depressed preferentially by anticonvulsants, and that anticonvulsants may be the most effective treatment for SCI neuropathic pain [94]. In general, **epileptiform circuits** exhibit the following characteristics: they 1) consist of episodes of stereotyped bursting activity, 2) exhibit synchrony between normally independent circuits, 3) can be triggered by sensory input , 4) exhibit a prolonged refractory period during which another episode cannot be evoked, and 5)

result from changes in circuit functional reorganization of synaptic networks [92, 155-158]. This work used these criteria to determine whether SCI network activity was epileptiform.

1.9 Pain and the brain

This work focuses entirely on the cutaneous periphery and spinal cord dorsal horn, but it is impossible to discuss pain without mentioning its cortical processing and representation. As mentioned earlier, after initial processing in the spinal cord, somatosensory information passes through either 1) the dorsal column medial-lemniscus (DCML) system, 2) the anterolateral (also called spinothalamic) system, or the spinocerebellar system [21]. Each of these pathways is responsible for transmitting a different subtype of somatosensory information. In brief, the DCML system is responsible for conveying the sensations of fine touch, vibration, two-point discrimination, and proprioception to the primary somatosensory cortex; the anterolateral system is responsible for conveying pain, temperature, and crude touch to the thalamus; and the spinocerebellar tract is responsible for relaying proprioceptive information from the trunk and lower limbs to the cerebellum [159]. Of these, this work focuses on spinal circuitry whose outputs are projection neurons of the anterolateral and DCML systems. As far as the representations of pain in the brain, we are still uncovering the exact circuitry responsible for the conscious and unconscious perceptions associated with painful stimuli, but are beginning to unravel neural ensembles responsible for perceiving facets of pain [113, 160]. We do know, however, that lesioning the anterolateral tract is sufficient to cause neuropathic pain in animal models, which matches observations in humans [161]. Furthermore, neuropathic pain can occur after stroke, suggesting that damage to the brain alone can be sufficient to cause neuropathic pain symptoms [162-165].Overall, neuropathic pain can arise from damage to peripheral nerves, to the spinal cord, to the brain, or any combination of these perturbations [163]. While all

mechanisms deserve careful study, the present work will focus on SCI-induced dysfunction of peripheral and spinal signaling.

1.10 Summary and goals

Here, I have outlined the organization of peripheral and spinal somatosensory circuitry, highlighting their sensitivity to expression of aberrantly hyperexcitable circuit behavior after an injury like SCI. SCI neuropathic pain remains a significant clinical issue, in large part due to an incomplete understanding of its etiology. Given the mechanistic similarities between SCI-induced spinal hyperexcitability and epileptic hyperexcitability, including the success of treating SCI neuropathic pain with anticonvulsant drugs, I propose that there may be unappreciated similarities between the two conditions. Here, I use an ex vivo adult mouse intact spinal cord preparation to explore the expression of hyperexcitable somatosensory circuit states after SCI. This preparation is an extremely powerful tool with which to study rostrocaudally distributed dorsal horn circuit systems, as will be investigated in this work. This dissertation sought to determine whether dorsal horn circuit-driven afferent bursting was epileptiform in nature (Chapter 2) and explore essential questions regarding the composition of this circuitry, including afferent identity, synaptic connectivity of involved interneurons, and the extent of burst propagation to the periphery (Chapter 3). In the concluding chapter, I will describe potential implications of this work and suggest future directions that could further our understanding of somatosensory processing and its corruption after perturbation. A series of appendices will provide discussion of software I developed in Python to facilitate analysis of bursting behavior and discuss additional results and limitations of the skin-nerve preparation.

Chapter 2: Epileptiform bursting after SCI

2.1 Abstract

Spinal cord injury (**SCI**) leads to sensory dysfunction including neuropathic pain associated with increased sensory afferent spontaneous activity and hyperexcitability in spinal dorsal horn networks. As epileptiform circuits emerge from hyperexcitable circuitry, we sought to determine whether epileptiform circuit activity is expressed in a thoracic SCI contusion model of neuropathic pain. Using an isolated spinal cord that enables recordings from attached sensory axons in multiple segmental dorsal roots (**DRs**), SCI led to increased expression and frequency of spontaneous ectopic burst spiking in recorded afferents that synchronized across multiple adjacent DRs. Bursting required recruitment of $GABA_A$ receptors, presumably via conversion of GABAergic presynaptic afferent drive from subthreshold inhibitory to suprathreshold spiking among other potential dorsal horn synapses. Afferent stimulation also recruited and reciprocally interacted with ongoing bursting with consistent prolonged post-burst refractory period (500-750ms). Overall, SCI-induced hyperexcitability led to emergence of bursting with distinguishing traits of epileptiform circuit including stereotyped bursting activity that exhibited hypersynchrony, post-burst refractory period, sensory input activation, and reorganization of connectivity. Emergent features of bursting after SCI could be reproduced in naïve animals with the convulsants 4-aminopyridine (4-AP) and tetraethylammonium (TEA), the KCC2 blocker VU0240551, and simply over time in some preparations, suggesting degeneracy in development of hyperexcitable burst circuitry. Degeneracy refers to the capability of a circuit to generate the same activity pattern through multiple mechanisms; in this case, dorsal horn circuitry achieves hyperexcitability and subsequent ectopic bursting through multiple perturbations. As further evidence of degeneracy, 4-AP and VU0240551 increased burst frequency, but not synchrony, in

SCI mice, implicating actions on common circuits. Ectopic bursting in afferents can propagate bidirectionally to have reentrant (projecting back into the spinal cord) central and antidromic peripheral actions; thus, SCI induced emergence of epileptiform activity could identify a novel circuitry driving sensory dysfunction after SCI.

2.2 Introduction

An estimated 80% of patients develop neuropathic pain after spinal cord injury (**SCI**) [65, 66, 81]. Our understanding of the etiology of neuropathic pain, and subsequently, treatment prognoses, remains relatively poor [73]. Previous work identifying the mechanisms of post-SCI neuropathic pain has focused largely on spontaneous activity in dorsal root ganglia (**DRG**) [104, 105] and unmasking of circuitry and crosstalk in the somatosensory dorsal horn [132, 166, 167].

These SCI-induced changes are associated with alterations in voltage-gated sodium [130] and voltage-gated potassium channel function in DRG [126], as well as perturbations in intracellular chloride homeostasis and loss of GABAergic tone in the dorsal horn [131-133], all of which support increases in sensory circuit excitability. Excessive circuit level excitability through these mechanisms is also a prominent feature in the various epilepsies, and it is possible that SCI - induced increases in sensory circuit excitability also manifests epileptiform activity via recruitment of characteristic mechanisms [151-153, 167, 168]. “Epileptiform” refers to observed electrophysiological activity that exhibits key characteristics of epilepsy (see below for further description). Consistent with the possibility that post-SCI spinal hyperexcitability is epileptiform is the observation that the convulsant 4-aminopyridine (**4-AP**) leads to epileptiform activity in spinal dorsal horn circuits [155] that can subsequently be depressed preferentially by $GABA_A$ receptor antagonists and anticonvulsants, and that anticonvulsants may effectively treat SCI

neuropathic pain [94]. These similarities led us to investigate manifestations of spinal cord dorsal horn hyperexcitability after SCI.

In the spinal cord dorsal horn, primary afferents synapse onto excitatory glutamatergic and inhibitory GABAergic interneurons [42, 108, 169-175]. Subpopulations of GABAergic interneurons form presynaptic axoaxonic synapses onto intraspinal afferent projections, canonically mediating a critical form of negative feedback control [17, 53, 176, 177] (also see [178]). As primary afferents express the chloride-extruding Na-K-Cl transporter KCC2 at extremely low levels [179], their intracellular chloride concentrations are high, and actions through $GABA_A$ receptors are depolarizing. However, PAD inhibits afferent neurotransmitter release through multiple mechanisms and decreases afferent action potential amplitude through shunting, resulting in potent presynaptic inhibition [38, 44, 61]. Under normal conditions, PAD is a critical inhibitory mechanism of pain control [18, 40]. In pathogenic circumstances, DRP depolarization can summate to evoke dorsal root reflexes (**DRRs**), or ectopic action potentials. Suprathreshold ectopic spiking events have been observed in peripheral injury pain models [45, 180, 181].

Compared to peripheral nerve injury-induced spinal sensory excitability, a unique feature of SCI is that loss of descending systems unmasks synchronous multisegmental DRPs including as suprathreshold bursts [147, 148, 182, 183]. Similar suprathreshold ectopic spiking events have been observed in peripheral injury pain models [45, 180]. Ectopic spikes would travel bidirectionally: reentrant spikes would act on central circuits while antidromic actions could propagate to cell bodies in DRG and peripheral innervation sites and alter function [49, 181, 184, 185]. Whether ectopic spikes emerge after SCI-induced hyperexcitability and associated neuropathic pain remains unstudied.

Given the mechanistic similarities in hyperexcitability between neuropathic pain and epileptic conditions, we sought to determine whether epileptiform activity is seen after SCI. Epileptiform circuits would be expected to: 1) consist of episodes of stereotyped bursting activity, 2) exhibit synchrony between normally independent circuits, 3) be triggered by sensory input , 4) exhibit a refractory (post-ictal) period during which another episode cannot be evoked, and 5) result from functional reorganization of circuitry [92, 155-158].

Here, we used the isolated whole spinal cord in a lower thoracic contusion model of neuropathic pain [186] to study sensory hyperexcitability [118, 187-190]. We undertake a series of experiments to assess the role of spinal circuit dysfunction consistent with hyperexcitability leading to recruitment of epileptiform circuits that generate ectopic burst firing in afferents.

This work has been published in part as poster presentations (SFN 2021, SFN 2022, IEEE EMBS Conference on Neural Engineering 2023) and as a short report in ELife. Results previously reported in these works included data from a single wild-type SCI (n = 10) and sham (n = 7) cohort. Data discussed in this chapter pools this data with results from a second SCI (n = 5) and sham (n = 4) cohort of Vglut3-ChR2 mice.

2.3 Methods

2.3.1 Animals

All procedures were approved by the Emory University Institutional Animal Care and Use Committee. Data from this chapter includes multiple cohorts of surgical and naïve mice. The first surgical cohort included SCI (n = 10) and sham (n=7) wild-type C57/Bl6 females, aged between 110 and 130 days at time of surgery, and between 310 and 561 days at time of terminal experiments. The wide range of ages at terminal experimentation is due to delays associated with

the COVID19 pandemic. A second surgical cohort included SCI (n = 5) and sham (n = 4) Vglut3-ChR2 males and females aged between P60 and P150 at surgery and between P120 and P210 at time of terminal experiments. Sample sizes were too low to determine sex differences, although nearly all SCI studies are performed in female animals. Spontaneous ectopic bursting was expressed preferentially by SCI animals in both surgical cohorts. Data were pooled in this chapter to assess the electrophysiological behavior of SCI spinal cords as a singular, although heterogenous, population. Differences between the cohorts will be discussed at the beginning of chapter 4. Naïve mice used for pharmacological experiments (n = 6) were male (n=4) and female (n=2) Vglut3-IRES2-Cre-D (Jax 028534) :: Ai32(RCL-ChR29H134R)/EYFP (R26-ChR2-eYFP)(Jax 024109) aged between 100 and 150 days at time of terminal experiments. Naïve mice used for c-fos experiments (n=6) were male Nk1R (*Tacr1*$^{tm1.1(cre/ERT2)Sros}$/J) (Jax 035046) :: B6;129S6-*Gt(ROSA)26Sor*$^{tm14(CAG-tdTomato)Hze}$/J (Jax 007908) aged between 100 and 150 days at time of terminal experiments. Naïve mice used by Shaquia Idlett for experiments and re-examined for spontaneous emergence of bursting activity were 14 males and 8 females aged between 90 and 150 days at terminal experimentation.

2.3.2 Spinal Cord Injury

Contusion injuries were performed as previously described using the Infinite Horizon spinal cord impactor device [186]. Briefly, mice were anesthetized with 5% inhaled isoflurane, then a midline incision performed, and a dorsal laminectomy performed at T10-T12 based on distance from cord apex. The mouse was moved to the impactor and the exposed cord impacted at 50kD with 0 dwell time. Mice were given 2 mg/kg meloxicam (Cayman Chemical Company) the day of surgery and the next day, as well as 0.5 mg/kg Enrofoxacin (Baytril, Bayer) daily following surgery. Sham mice underwent surgical and post-surgical procedures other than impact. Mice in

the first SCI cohort underwent Von Frey testing and home cage recording for 2 weeks [191] before injury, as well as after injury to confirm development of allodynia and monitor activity levels. Mice in the second (Vglut3-ChR2) cohort underwent thermal preference testing and home cage recording of respiratory rate variability [191] after surgical recovery. Post-surgery, animals were housed in isolated cages with a maximum of two animals per cage.

2.3.3 Measurement of mechanical allodynia

Mechanical hypersensitivity was measured using Chaplan's up-down protocol for von Frey filaments [192]. Briefly, animals were acclimated to the von Frey filaments (0.4, 0.6, 1.4, and 2.0 grams), cages, and mesh floor for several days prior to testing. Mechanical sensitivity was assessed in both hind paws three times prior to surgery and once weekly afterwards for 10 weeks. The 50% paw withdrawal threshold (PWT) was quantified for SCI and sham groups. This metric is defined as the stimulus intensity (in grams) required to produce a withdrawal response 50% of the time and is a common measure of mechanical allodynia in both human and animal populations [193, 194]. As expected, SCI animals in this work developed mechanical hypersensitivity as previously described (**Figure 2-1A**).

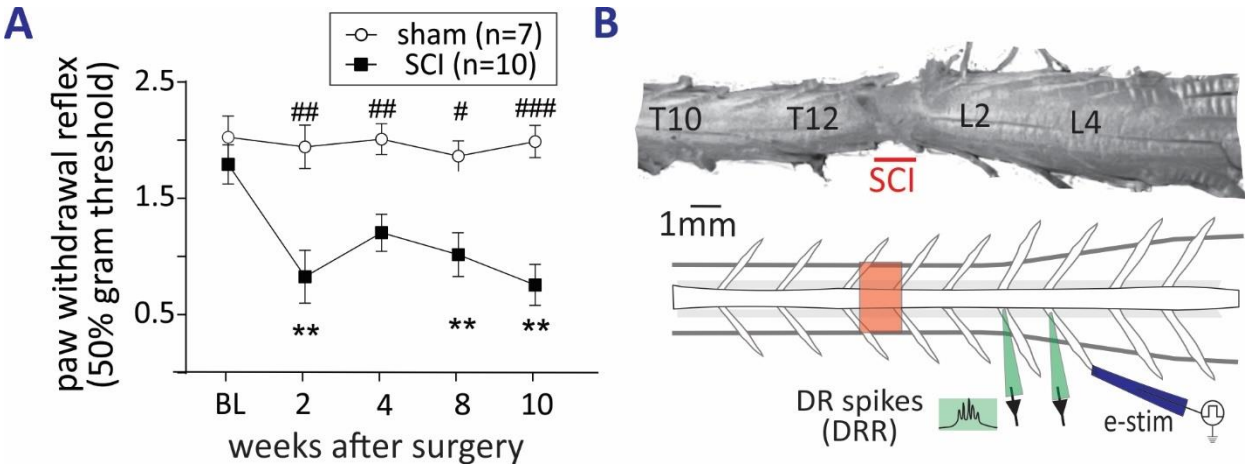

Figure 2-1: Von Frey testing results and ex-vivo recording configuration

(A) *As expected, the SCI population developed mechanical hypersensitivity consistent with allodynia (t-test *p<0.05, **p<0.01, ***p<0.001; # compares sham and SCI measures weekly; *compares weekly SCI measure to baseline SCI measure).* ***(B)****Top: Representative example of ex-vivo spinal cord with T12 contusion injury. Bottom: Diagram of recording configuration. Suction electrodes are attached to dorsal roots and dorsal root entry zones to enable recording and electrical stimulation. Some recordings including recordings from Lissauer's Tract (LT) and/or electric field potential (EFP) recordings from superficial dorsal horn subjacent to LT.*

2.3.4 Dissections

Ex-vivo intact spinal cord preparation

Mice were lightly anesthetized with inhaled isoflurane then injected intraperitoneally with 300µL 50% urethane for deep anesthesia. To induce hypothermia, dorsal skin overlying the vertebral column was removed and mice were submerged in ice-cold ACSF until respiration rate slowed (2-3 minutes). Animals were removed from ACSF, decapitated, and the whole spinal cord dissected with a ventral approach as previously described [195]. The spinal cord dissection was performed in ice cold Recovery ACSF [196] oxygenated with 95% O_2-5%CO_2. The isolated cord was then equilibrated to room temperature for 1 h in modified HEPES holding solution [196] oxygenated with 95% O_2-5%CO_2, and then pinned dorsal side up in a Sylgard-lined recording chamber while superfused with an oxygenated aCSF containing (in mM) 128 NaCl, 1.9 KCl, 1.3 $MgSO_4$, 2.4 $CaCl_2$, 1.2 KH_2PO_4, 10 glucose, and 26 $NaHCO_3$ at ~40 ml/min. All experiments were undertaken at room temperature.

In-vivo dorsal cutaneous neve recording

Mice were deeply anesthetized with inhaled isoflurane: anesthesia was induced with inhalation of 5% isoflurane and maintained with 2-4% isoflurane based on monitoring of respiration and

heart rate. Body temperature was maintained with a circulating bath heated to 36˚C by a Peltier device built by Bill Goolsby. Once anesthesia was stable, a midline incision was made in the dorsal truncal skin and DCNs were dissected from one side of the animal. Animals were administered 0.2 mg/kg 4-AP to induce bursting.

2.3.5 Electrophysiology

Suction electrodes were fabricated from 1.65/0.75 (OD/ID, Dagan Corp) glass capillary tubes electrodes, pulled using Narishige PC-100 electrode puller with tips broken back to achieve internal tip diameters of a tip size of 100-200 µm. Electrodes were placed to suction various dorsal root entry zones, distal dorsal roots, or Lissauer's Tract (LT) **(Figure 2-1B)** along the cord. Electrical stimulation was delivered using constant current stimuli [197] by suction electrodes attached to the distal ends of dorsal roots. Roots were selected based on intact structure after dissection. Targeted recording of LT was accomplished by positioning a glass microelectrode in gray matter lateral to the dorsal column (DC), in between dorsal root entry zones. All recorded data were digitized at 10 kHz (Digidata 1322A 16 Bit DAQ, Molecular Devices, U.S.A.) with pClamp acquisition software (v. 10.7 Molecular Devices). Recorded signals were amplified (10000x) and low-pass filtered at 3 kHz using in-house amplifiers. Electrical stimulation was delivered by suction electrodes attached to the distal ends of nerve roots and optogenetic stimulation was delivered in a manner that ensured that only roots and not cord were stimulated. Optogenetic stimulation was delivered through laser diode boxes built and calibrated by Bill Goolsby.

2.3.6 Models of sensory hyperexcitability

A broad-spectrum voltage-gated K^+ (K_v) channel blocker, 4-aminopyridine (**4-AP**) (1-100 µM, Spectrum), was used to generate a model of sensory circuit hyperexcitability in the *ex vivo* intact

spinal cord preparation and injected IP *in-vivo* (0.2 mg/kg) during dorsal cutaneous nerve recordings. 4-AP exerts its clinically relevant effects through fast potassium conductances [198], broadening action potentials and inducing burst firing in some neurons [199, 200]. 4-AP has been demonstrated to increase the excitability of neurons and the likelihood of action potential propagation in preclinical and clinical studies [201, 202]. It is currently used as a treatment for improving locomotion after the demyelinating disease multiple sclerosis [203] and for improving locomotion and sensory function after SCI [204, 205]. However, it has also been shown to recruit spinal nociception-encoding circuitry consistent with the emergence of spontaneous neuropathic pain [155, 206]. It is also commonly used as a pharmacological model of epilepsy in cortex [207, 208]. To characterize the dose-response relationship of the model, 4-AP was bath applied at increasing concentrations (1-150µM) during recording of dorsal roots. A second broad spectrum voltage-gated K^+ channel blocker, tetraethylammonium **(TEA)**, which reduces the action potential afterhyperpolarization without broadening the action potential itself [198], was also used to induce hyperexcitability. TEA exhibits differing affinities for K_v channels than 4-AP, resulting in its capacity to modulate repetitive firing. TEA is also used as an epilepsy model [209]. The KCC2 inhibitor VU0240551 (50 µM, Cayman Chemical Company) was used to model increased intracellular chloride concentration as noted after SCI [210, 211]. KCC2 is known to be reduced after SCI and has been implicated in various epileptic conditions [153, 212, 213]

2.3.7 Blockade of synaptic activity

AMPA and NMDA glutamatergic receptor block was achieved with cyanquixaline (**CNQX**, 40 µM, RBI) and D-2-Amino-5-phosphonovaleric acid (**APV**, 100 µM, Tocris) respectively. Several $GABA_A$ receptor antagonists were used in this chapter: bicuculline (10 µM, Enzo Life

Sciences), picrotoxin (25 µM, Sigma-Aldrich), and gabazine (1 µM, EMD Millipore). As all $GABA_A$ antagonists had comparable effects on bursting, their results have been pooled where appropriate (see figure legends).

2.3.8 Data and statistical analysis

Data was recorded using Clampex, initially visualized in Clampfit, and then analyzed and visualized using Spike2 and custom-written scripts and applications in Python and R (see code accessibility section for access and chapter 3 for in-depth description of Python analysis program). Recorded roots were selected for analysis based on the presence of bursting either at baseline or after addition of 4-AP. To study below-level plasticity, roots T13-L4 were considered for analysis. Any roots that did not show bursting after 4-AP addition were excluded from analysis as it was not possible to determine whether this was due to destruction of the root during dissection. Roots with signal to noise ratios too poor to reliably differentiate bursts from background noise were also excluded from analysis. For refractory period analysis involving stimulation, all electrical stimulus strengths that resulted in a burst (not direct afferent volley) were considered as a single population. Statistical significance of data was determined via ANOVA, Spearman's correlation, Wilcoxon rank-sum test when appropriate (as determined by Shapiro-Wilks test), or two-tailed t-test, depending on the normality and scedasticity of the data. Relationships were considered significant at $p < 0.05$. See figure legends for individual statistical tests and outcomes. Values in plots with error bars are presented as mean ± standard deviation (sd) unless otherwise specified.

Bursts were identified and quantified with custom-written Python software. See Appendix A for further details. Briefly, peaks were identified with a peak threshold set at 3.5x RMS noise. Recordings were considered to contain bursting activity when the standard deviation of inter-

spike intervals was greater than the mean inter-spike interval of all peaks. Inter-spike interval was also used to characterize packets of peaks as bursts (peaks were binned together when they were <20 ms apart and only groups of 5 or more peaks were considered a burst). Once bursts were identified, they were quantified (amplitude, duration, etc.) and cross-correlations were processed with combinations of channels taken 2 at a time. When cross-correlation is not specified, burst synchrony was determined by comparing burst times (from start to end of burst) across channels. If channels shared >50% of burst times, they were considered to exhibit synchrony.

2.3.9 Code accessibility

Custom-written Python application for burst analysis available at https://github.com/mbryso4/2023_Burst_Analysis. Available versions are the same that were used for analysis of this work. Updated versions will be maintained elsewhere. See Appendix A for discussion of analysis program.

2.4 Results

2.4.1 Injured mice preferentially exhibit spontaneous and stereotyped bursting in primary afferents.

Sensory circuit hyperexcitability was assessed in an ex-vivo spinal cord preparation with access to multiple segmental dorsal roots (DRs) for stimulation and recording of primary afferents [214]. Occasional bouts of spontaneous ectopic bursting were seen in all preparations. Bursts appeared both independently in single roots and synchronously across multiple roots **(Figure 2-2A).** Individual bursts had similar and stereotyped appearance and duration **(Figure 2-2A, 2-2B$_1$)**, suggesting common circuit recruitment. However, compared to naïve and sham, bursts had

larger amplitude **(Figure 2-2B$_2$)** and higher frequency in SCI mice **(2-2B$_3$)**, suggesting more frequent and powerful recruitment of afferents. Overall, burst frequency showed moderate correlation with paw mechanosensitivity (↓ paw withdrawal reflex threshold [PWT]; **Figure 2-2C**). In all conditions, bursts occurred both independently in individual roots and at the same time across roots, which we termed synchronous bursting.

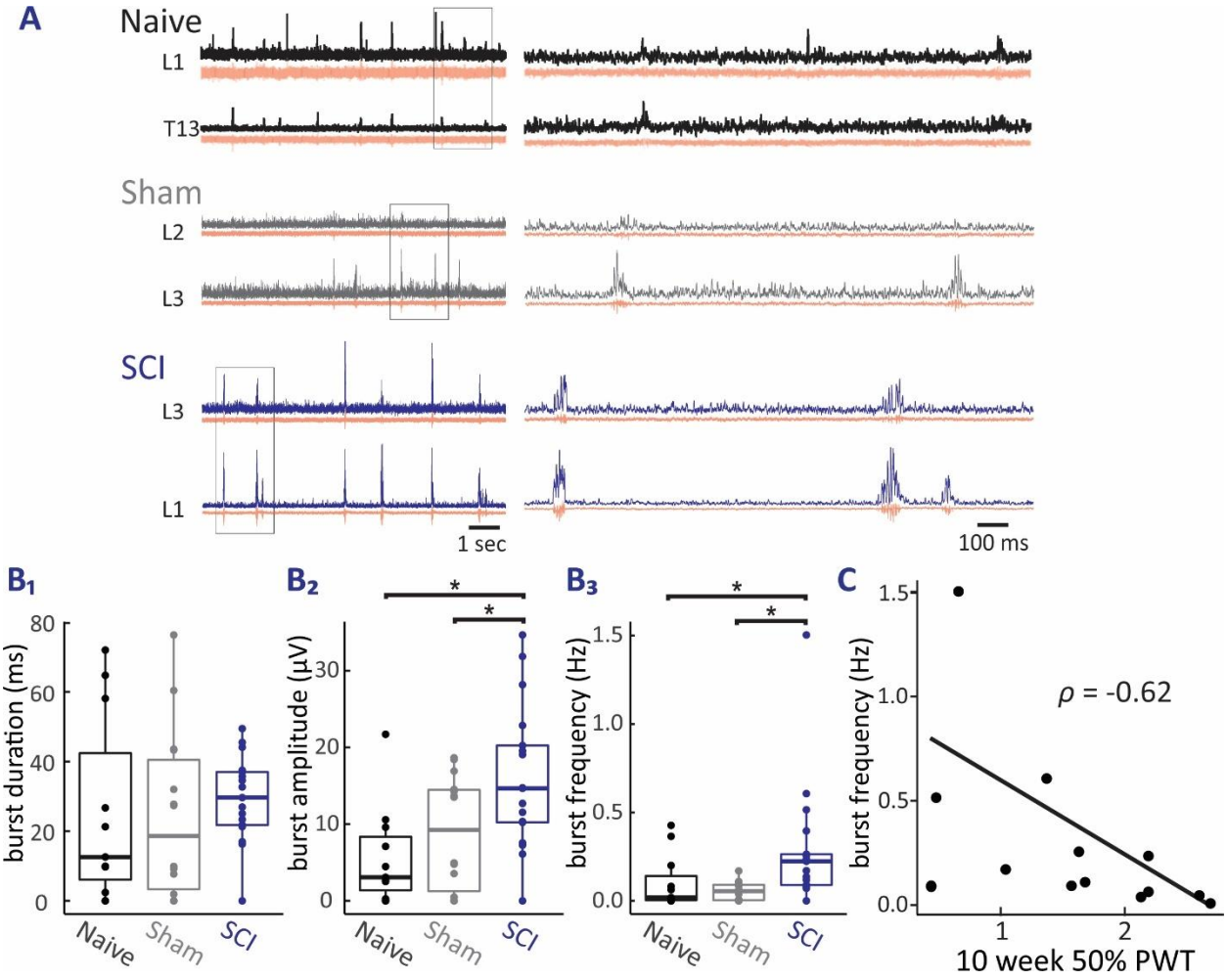

Figure 2-2: Spontaneous bursting is preferentially expressed in SCI cord preparations

(A)** Representative spontaneous bursting activity recorded from one naïve, one sham, and one SCI preparation. Boxes denote region of magnification in lower panels. Bottom traces are raw dorsal root recordings. Top traces are RMS amplitude filtered with a 1 ms time constant. **(B$_1$)

Bursts between conditions showed no significant difference in burst duration (ANOVA F(2, 39) = 0.245, p = 0.78). ***(B$_2$)*** *Bursts in SCI cords expressed higher amplitude than those in sham cords (Wilcoxon rank-sum test W = 67.5, p-value = 0.04; n = 17 SCI, 14 sham) and those in naïve cords (Wilcoxon rank-sum test W = 31, p-value = 0.003; n = 17 SCI, 11 naïve).* ***(B$_3$)*** *Mean burst frequency of SCI preparations was greater than that of sham preparations. (Wilcoxon rank-sum test W = 36.5, p-value = 0.001; n = 17 SCI, 14 sham) and that of naïve preparations (Wilcoxon rank-sum test W = 44, p-value = 0.02; n = 17 SCI, 11 naïve).* ***(C)*** *Paw withdrawal threshold at 10 weeks is negatively correlated with preparations' mean burst frequency, suggesting a relationship between extent of allodynia and bursting (Spearman's rho = -0.62, p-value = 0.02). Data consist of recordings from a single cohort of surgical animals (n=14).*

2.4.2 Burst synchrony arises from unilateral burst generators that can synchronize contralaterally

Ongoing regular bursting was a predominant feature in SCI, where the percentage of roots expressing synchrony with another root was increased **(Figure 2-3A)**. Cross-root synchronous bursting exhibited distinct temporal correlations. Synchronous bursts were common within adjacent ipsilateral DRs while correlated activity at more distant segments or contralaterally showed both lag and lead times indicating no clear primary locus of origin **(Figure 2-3B$_1$, 2-3C$_1$),** demonstrating that networks driving bursting within a root could initiate or be recruited by networks driving bursts elsewhere **(Figure 2-3B2$_2$, 2-3C$_2$)**. To quantify the relationship between roots, cross-correlations were calculated for recordings with synchronous bursting **(Figure 2-3B$_3$, 2-3C$_3$)**. At the level of the entire SCI population, ipsilateral bursts synchronized with no lag, supporting improvement by a common drive. However, contralateral bursting networks showed

bidirectional relationships supporting interactions between bursting networks **(Figure 2-3D)**. Overall, observed temporal relationships demonstrate the capacity for coupling between discrete and overlapping burst generating networks, with at least a single burst generator on each side of the cord at the levels examined. These ipsilateral burst generators expressed broad rostrocaudal distribution and could synchronize with contralateral burst generators.

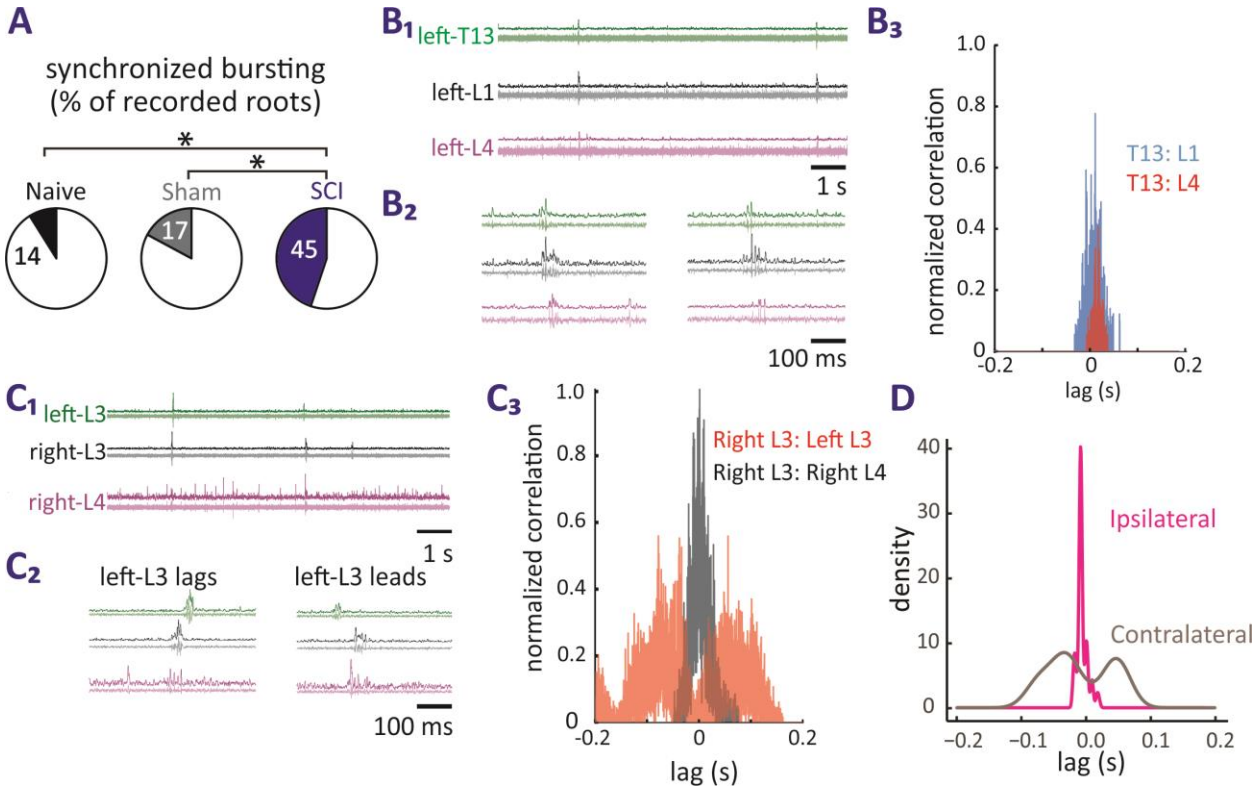

Figure 2-3: Bursts originate from ipsilateral burst generating networks that can synchronize.

***(A)** SCI preparations exhibited a significantly higher percentage of roots with synchronous bursting than did sham preparations or naïve preparations (*Chi-square p-value < 0.05). **(B$_1$)** Example bursting activity in three ipsilateral dorsal roots from another preparation – two roots are adjacent thoracic (T13 and L1) with other several segments caudal at L4. (B2) Magnified timescale examples. (B3) Cross-correlograms of T13 and L1 (shown in blue) and T13 and L4*

(shown in red) illustrate that burst arrives almost simultaneously in all roots, with T13 slightly leading L4. ***(C$_1$)*** *Example recording of bursting activity in three dorsal roots – two adjacent and one contralateral lumbar (L) root. Both raw and RMS amplitude filtered waveforms are shown.* ***(C$_2$)*** *Magnified timescale examples of differing relationships between bursts shown above. In both cases, right L3 and right L4 occur near-simultaneously while contralateral left either L3 lags (left panel) or leads (right panel) bursting on right side.* ***(C$_3$)*** *Cross-correlograms visualizing 300 seconds of recordings reduced to only identified bursts with all background noise removed. Right L3 and right L4 (shown in black) and right L3 and left L3 (shown in red) illustrate that the differences exemplified in B1,2 are consistently present throughout the entire recording.* ***(D)*** *Density plot (smoothed histogram) of the top 5 lag values from cross-correlations across all SCI preparations reveals that coordinated bursts occur with lead/lag when sampled roots were contralateral and simultaneously when roots were ipsilateral. Cross-correlations were calculated for all permutations of SCI roots with bursting in multiple roots (n = 8 preparations).*

2.4.3 SCI Bursts can be evoked by afferent stimulation after a refractory period

Spontaneous bursts typically exhibited a > 500 ms inter-burst interval. When spontaneous bursting was seen, high-intensity afferent electrical stimuli (recruiting Aβ, Aδ and C fibers) always also evoked bursts with comparable appearance to spontaneous bursts (n = 11/11 preparations) **(Figure 2-4A$_1$)**. To probe burst refractory state, we compared bidirectional interactions between spontaneous and evoked bursts. Afferent stimuli almost always failed to evoke a burst if a spontaneous burst occurred sooner than ~700 ms before stimulation **(Figure 2-4A$_2$**, 2 examples shown of 14 SCI preparations tested; other preparations exhibited similar peaks

for both relationships between 0.75 and 2s**)**. Similarly, spontaneous bursts following stimulus-evoked bursts rarely occurred sooner than ~500 ms after stimulation **(Figure 2-4A$_2$)**.

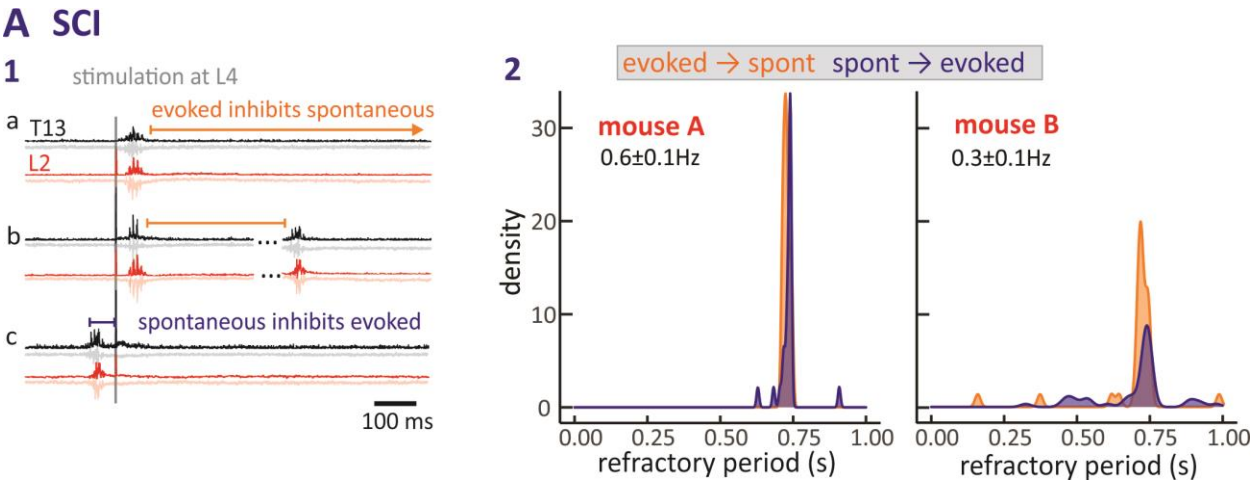

Figure 2-4: Relationships between SCI spontaneous and evoked bursts

(A$_1$) *Representative recordings from two roots of SCI preparation during stimulation. If a spontaneous burst preceded stimulation, stimulation failed to evoke a burst. Inversely, spontaneous events rarely occurred following an evoked burst.* ***(A$_2$)*** *Density plots (smoothed histograms) quantifying the bidirectional distribution of burst refractory periods between spontaneous and evoked bursts in two SCI mice with 0.6 and 0.3 Hz spontaneous burst frequencies. Burst circuit refractory period was prominent for several hundred ms (bursts plotted: mouse A evoked to spont = 111, spont to evoked = 289; mouse B evoked to spont = 87, spont to evoked = 189).*

2.4.4 Ectopic bursting can be recapitulated with the convulsant 4-AP

As burst synchrony and refractory periods are features of epileptiform circuits, we compared SCI bursting with that seen after administration of 4-aminopyridine (4-AP), a convulsant used in animal models of epilepsy [215]. 4-AP has been shown to generate epileptiform activity in spinal

dorsal horn neurons *in vitro* in transverse and longitudinal slices in the juvenile rat [155]. 4-AP has also been shown to drive synchronous bursting in primary afferents *in vivo* [216]. In our experiments, 4-AP was able to recruit spontaneous bursting activity in all naïve preparations (n=6/6) **(Figure 2-5A$_1$)** with a dose-dependent effect on burst frequency **(Figure 2-5A$_1$)**. Above a small dose of 4-AP, burst amplitude and duration plateaued and was comparable with that seen in SCI mice **(Figure 2-5A$_2$)**. Strikingly, burst synchrony dramatically increased after 4-AP administration in sham but not in SCI preparations **(Figure 2-5B)**, suggesting that 4-AP is recruiting the same bursting circuitry as SCI.

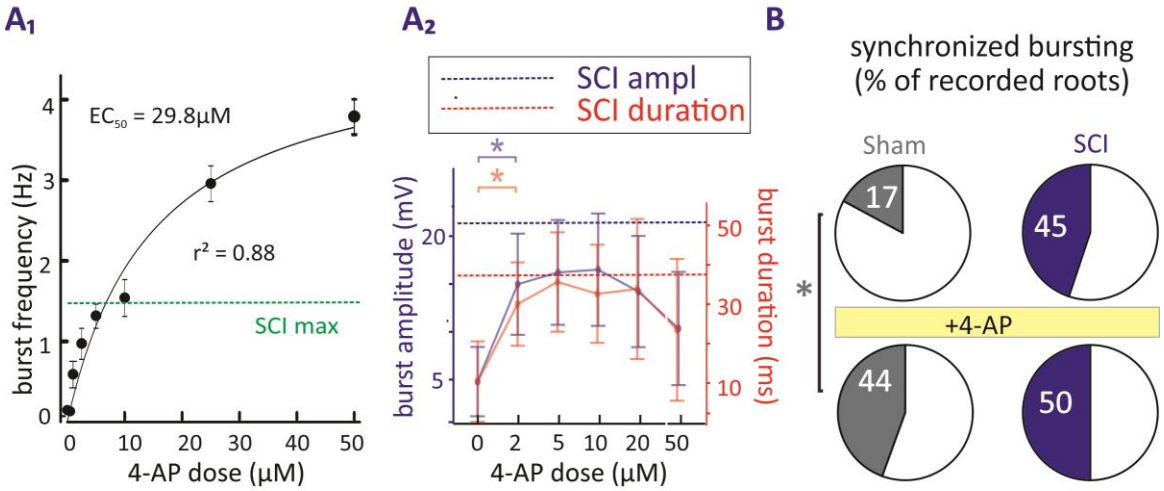

Figure 2-5: 4-AP evokes spontaneous bursting in a dose-dependent manner

***(A$_1$)** Effect of 4-AP dose on emergent burst frequency. Values shown are means ± standard error. Fit r2 = 0.88, EC50 = 29.8 µM. Dotted green line identifies SCI mouse with highest recorded burst frequency, which compares to frequencies obtained ~20µM 4-AP (n=6). **(A$_2$)** Burst amplitude and duration values were comparable at 4-AP doses between 2-20µM. Dotted lines representing mean amplitude and duration values from the SCI population show comparable values (Welch's t-test *p < 0.05, n=6). **(B)** 4-AP (10µM) significantly increased the*

percentage of synchronously bursting roots in sham (Chi-square; p=0.02; n=7), but not SCI preparations (Chi-square; p=0.4; n=10).

To compare the refractory period of SCI and 4-AP preparations, I analyzed the same bidirectional interactions between electrical stimulation and spontaneous bursts. Spontaneous burst waveform, inter-burst interval, and recruitment by afferent stimulation were comparable between 4-AP and SCI preparations, suggesting similar hyperexcitability in the two conditions **(Figure 2-6A$_1$-2-6A$_2$**, 2 preparations shown of 14 preparations tested; other preparations exhibited similar peaks for both relationships between 0.75 and 2s**)**. The greater width of these distributions and slightly earlier peak times (particularly in the blue distribution) can likely be attributed to greater excitability in the 4-AP condition. Burst frequencies in these preparations were greater than those in the comparable SCI preparations (1.3±0.5Hz and 1.0±0.2Hz after 4-AP vs 0.6±0.1Hz and 0.3±1Hz in the SCI preparations). However, despite the faster bursting, the 4-AP and SCI share common features of refractoriness consistent with recruitment of similar dorsal horn circuitry.

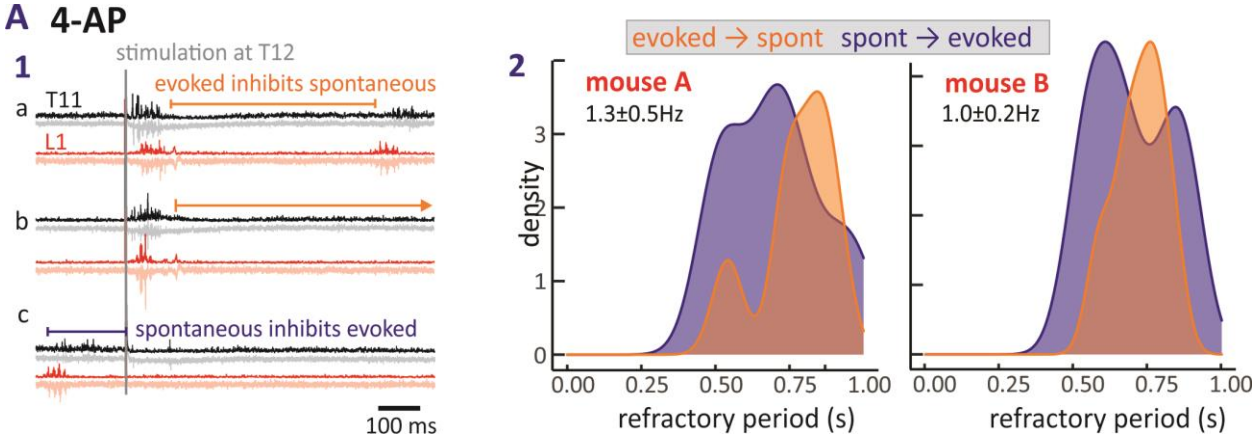

Figure 2-6: Mutually inhibitory interactions between spontaneous and evoked bursts identify burst refractory period after 4-AP in naïve mice.

(A$_1$) *Example recording showing that spontaneous events are not seen for several hundred milliseconds after an evoked burst (panels a, b), and spontaneous bursts similarly prevent subsequent expression of evoked bursts (panel c).* ***(A$_2$)*** *Density plots quantifying the bidirectional distribution of burst refractory periods between spontaneous and evoked bursts in two mice undergoing 4-AP (10μM) induced bursting with 1.3 and 1.0 spontaneous burst frequencies. Note that refractory period duration was shorter than in SCI mice (possibly related to higher burst frequencies) (bursts plotted: mouse A evoked to spont = 127, spont to evoked = 296; mouse B evoked to spont = 53, spont to evoked = 292).*

2.4.5 Burst circuitry can be unmasked by 4-AP, TEA, SCI, time, and KCC2 block, suggesting degeneracy in burst-evoking dorsal horn hyperexcitability

As 4-AP acted as an effective acute pharmacological tool to induce bursting in naïve preparations, I next sought to understand whether other acute perturbations could lead to similar emergence of bursting. If so, then spinal hyperexcitability and subsequent unmasking of bursting circuitry could be understood to exhibit degeneracy: a characteristic such that a circuit state can be reached through a variety of mechanisms, in this case injury-induced or pharmacological perturbations, each independently sufficient to cause the same shift in circuit state. Recent work has highlighted the significance of degeneracy in afferent hyperexcitability in neuropathic pain and in cortical circuit hyperexcitability in epilepsy [158, 217], forms of neural dysfunction that are both relevant to the circuitry discussed here. In the case of neuropathic pain, decreasing K_V1 conductance and increasing $Na_V1.3$ conductance were both independently sufficient to confer afferent hyperexcitability in modeling and electrophysiology experiments [218]. Inversely, in the same study, increasing K_V1 and decreasing $Na_V1.3$ conductance in neurons already expressing hyperexcitability after spinal nerve ligation were each independently sufficient to rescue normal

hyperexcitability, suggesting that different mechanisms can cause excitability changes in either direction. I sought to determine whether epileptiform bursting circuitry similarly expressed degeneracy and could be generated through multiple mechanisms.

The first piece of evidence suggesting degeneracy in dorsal horn burst circuitry was that 4-AP increased burst synchrony in sham, but not SCI preparations (n=10, **Figure 2-5B**). The drug increased burst frequency in all, including SCI, preparations. However, it failed to increase burst synchrony in SCI preparations, suggesting that SCI and 4-AP induce bursting in similar dorsal horn circuitry through different mechanisms and indicating that blockade of K_V channels is sufficient to induce bursting in naïve preparations.

In addition to this result, bursting could be unmasked with SCI (**Figure 2-7A;** n = 16/17 SCI preparations), administration of 4-AP (**Figure 2-7B;** SCI n=8/8, naïve n=6/6, and sham n=7/7 preparations), administration of TEA (**Figure 2-7C;** n = 2/2 preparations), simply over time (2-3 hours) in a minority of naïve preparations (**Figure 2-7D;** n = 3/24 preparations with bursting [re-examination of naïve preparations used for experiments by Shaquia Idlett]), and administration of VU0240551 (**Figure 2-7E;** 3/6 naïve preparations). In all cases, this bursting occurred spontaneously with predictable and similar waveform across conditions, could be evoked with afferent stimulation after a refractory period, and exhibited synchrony between roots – all critical characteristics of epileptiform activity. In support of the spontaneous emergence of bursting in naïve preparations, previous work in the hamster *ex-vivo* spinal cord indicated that DRRs can be unmasked spontaneously over time as the preparation rests for ~2 hours [146, 219].

Furthermore, in SCI preparations, much like 4-AP, blockade of KCC2 with VU0240551 increased burst frequency (**Figure 2-7F$_1$;** n = 4/4), but not synchrony (**Figure 2-7F$_2$;** n = 3/3) (recordings from one preparation allowed comparison of frequency but not synchrony). These

results suggest that KCC2 blockade and subsequent intracellular chloride perturbation lead to hyperexcitability through unmasking of the same circuits as SCI and 4-AP, albeit through different mechanisms. While the downstream mechanisms leading to burst emergence after each of these perturbations are yet to be uncovered, the fact that they all individually induce dorsal horn hyperexcitability that manifests as bursting suggests that this circuit hyperexcitability does indeed exhibit degeneracy and that multiple perturbations are each sufficient to induce hyperexcitability and bursting through different mechanisms.

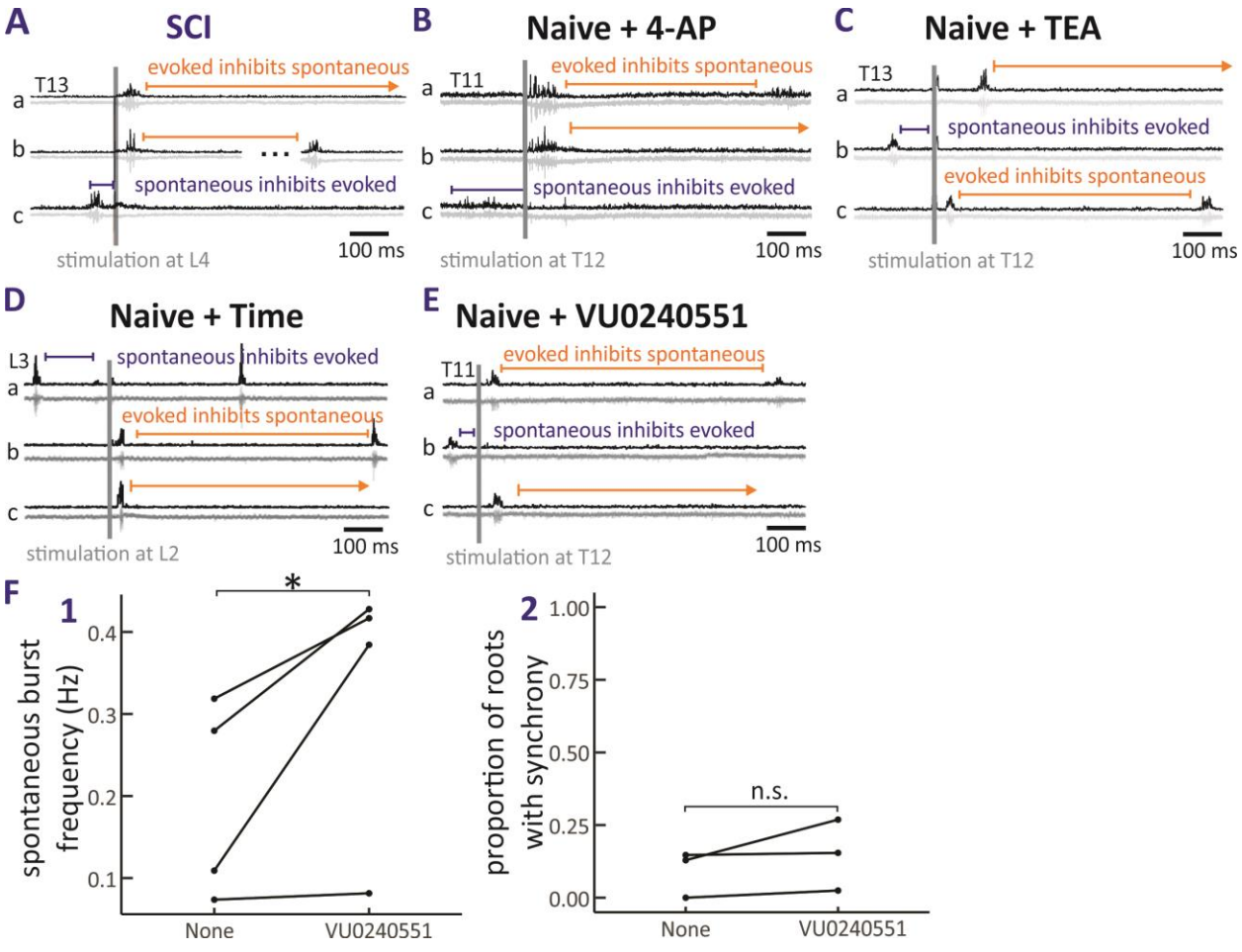

Figure 2-7: Bursting circuitry exhibits degeneracy in mechanisms of generation.

In each example shown, bursting occurs spontaneously with a stereotyped waveform, can be evoked by afferent stimulation, and exhibits a refractory period during which spontaneous and evoked bursts inhibit one another bidirectionally. Number of preparations analyzed in each condition are included in text. ***(A)*** *Example trace of SCI-evoked bursting.* ***(B)*** *Example trace of bursting evoked in a naïve preparation by administration of 10µM 4-AP.* ***(C)*** *Example trace of bursting evoked in a naïve preparation by administration of 100µM TEA.* ***(D)*** *Example trace of bursting in a naïve preparation after 2 hours without perturbation or drug administration.* ***(E)*** *Example of bursting in a naïve preparation after administration of 50µM VU0240551.* ***(F) 1:*** *Addition of VU0240551 to 4 SCI preparations increased spontaneous burst frequency in each preparation (paired t-test *p<0.05).* ***2:*** *Addition of VU0240551 to 3 SCI preparations had no effect on percentage of recorded roots expressing synchrony with another root. Preparations were only considered for this analysis if bursting effects clearly resulted from VU0240551 administration, not time or mixed effects of other drugs in the bath.*

2.4.6 Burst frequency is reduced by the anticonvulsant retigabine

Given that bursting expressed epileptiform characteristics (episodes of stereotyped bursting activity, synchrony between normally independent circuits, triggering by afferents , refractory period) and correlated with mechanical hypersensitivity, I sought to determine whether epileptiform activity could be modulated by an anti-epileptic drug, specifically, retigabine, an anticonvulsant KCNQ/K_v7 channel opener (enhances M current to reduce firing rate) with known anti-hyperalgesic and anti-epileptic effects [220-222]. Retigabine (50µM) was added to a subset of preparations with 4-AP-induced bursting (n = 3). In all preparations, retigabine reduced burst frequency, but interestingly also slightly altered the waveform of spontaneous bursts **(Figure 2-8A, 2-8B$_1$)**. Specifically, the drug increased the number of spikes per burst **(Figure 2-**

8B$_3$), indicating that although bursts were less frequent, each burst recruited a greater number of spikes in afferents. Despite this, the mean amplitude of burst spiking was unchanged by the drug. Burst duration appears longer in raw traces, but the difference was not statistically significant, potentially due to low sample size **(Figure 2-8B$_2$).** Overall, retigabine's capacity to reduce bursting while also altering burst waveform is consistent with actions on both dorsal horn and afferent KCNQ channels, as waveform alterations would be expected to be due actions on afferent ion channels.

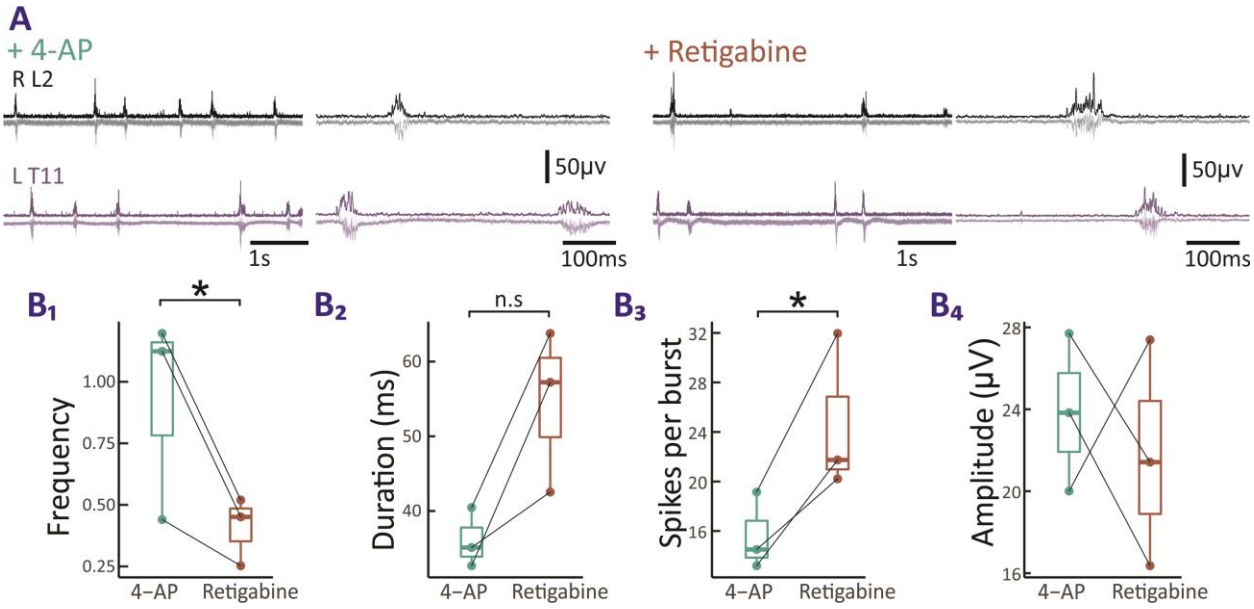

Figure 2-8: Burst frequency is reduced by Retigabine and waveforms are altered.

***(A)** Left: Example traces of 4-AP induced bursting with zoomed inset shown to right. Right: Example traces of the same preparation and roots after addition of 50µM retigabine. **(B$_1$)** Retigabine significantly reduced spontaneous burst frequency (paired t-test t = 7.9, df=2, p-value = 0.015; n = 3, 4-AP = 0.8±0.45 Hz; Retigabine = 0.38±0.15 Hz, [mean ± sd]). **(B$_2$)** Retigabine visibly increased burst duration, but the relationship was not significant (paired t-test t= -3.3, df=2, p-value = 0.079; n = 3; 4-AP = 35.8±10.3 ms; Retigabine = 53.9±14.4 ms, [mean*

*± sd]). **(B_3)** Retigabine increased the number of spikes per burst, measured as the total number of peaks above threshold during the burst event divided by 2 (see appendix A for details) (paired t-test t = -4.3681, df = 2, p-value = 0.049; n = 3; 4-AP = 15.84±10.3 spikes; Retigabine =24.5±8.2 spikes, [mean ± sd]). **(B_4)** Retigabine had no effect on burst amplitude, measured as the mean amplitude of all peaks occurring during a given burst (see appendix A for details) (paired t-test t = 0.4456, df = 2, p-value = 0.6994; n = 3; 3; 4-AP = 24.3±11.0 µV; Retigabine = 21.2±5.6 µV, [mean ± sd]).*

2.4.7 Bursting is dependent on $GABA_A$ receptors

Normally, dorsal root stimulation evokes subthreshold DRP responses as a form of negative feedback presynaptic inhibition due to activation of axoaxonic synapses on primary afferents. DRPs are canonically GABAergic, but can rely on NMDA [42], non-NMDA [223], 5-HT_3 receptors [224], and presumably nicotinic receptors [41]. Subthreshold-evoked DRPs are shown here in a cord without bursting, with conversion to excitatory bursting action after 4-AP (**Figure 2-9A**). Spontaneous and evoked bursts were completely blocked and DRP amplitude severely reduced in amplitude after $GABA_A$ block with bicuculline, further suggesting that bursts are mediated through GABAergic PAD (n = 4) (**Figure 2-9A**). In all mice, 4-AP initiated or increased burst frequency **(Figure 2-9B)**. Spontaneous bursting was always completely blocked following application of $GABA_A$ receptor antagonists. This was seen in 2/2 SCI preparations not given 4-AP **(Figure 2-9C)** and all preparations subsequent to 4-AP application (SCI n=8; naïve n=2; and sham n=7) **(Figure 2-9B)**. Consistent with the effect shown in **Figure 2-9A**, application of $GABA_A$ receptor antagonists also blocked evoked bursting in all conditions tested.

To compare the effects of glutamatergic and GABAergic blockade, frequency was measured in 11 preparations expressing either SCI or 4-AP bursting **(**burst frequency = 0.8±0.5Hz; **Figure 2-**

9D) that received glutamate receptor block, $GABA_A$ receptor block, or both. Glutamate receptor blockade with CNQX+APV reduced burst frequency in 6/6 preparations but did not eliminate bursting in any **(**burst frequency = 0.4±0.3Hz; **Figure 2-9D)**. Bursting was blocked in all preparations by subsequent or initial application of $GABA_A$ antagonists (burst frequency = 0 Hz; n = 11/11) **(Figure 2-9D)**. Similar to glutamate receptor block's effect on burst frequency, addition of CNQX + APV to bursting preparations reduced, but did not ablate burst synchrony between roots **(Figure 2-9E)**, suggesting that glutamatergic interneurons or afferents support synchronization of bursts across roots. That both SCI- and 4-AP-induced ectopic bursting require activation of $GABA_A$ receptors, presumably driven by common interneurons, further highlighted that SCI and 4-AP activate similar or overlapping circuits to induce bursting.

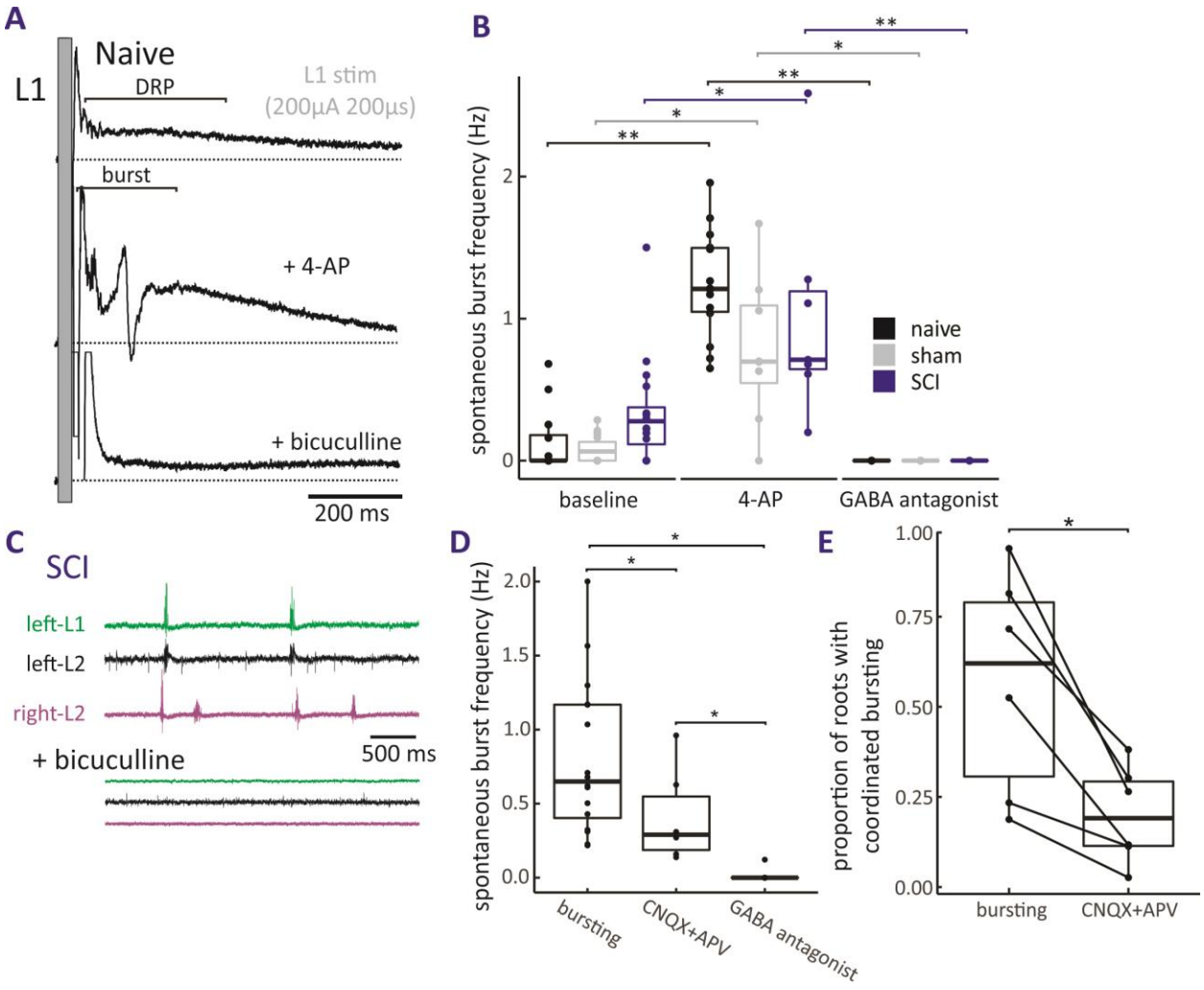

Figure 2-9: Evidence of burst dependence on GABA interneurons

(A) *Example of DR stimulation-evoked subthreshold dorsal root potential (DRP) in a naïve preparation (top) After addition of 10µM 4-AP, DRP is increased in amplitude and a suprathreshold volley is also present (middle). Evoked bursting and DRP are blocked by bicuculline (bottom) (n = 4). Colored traces represent averages of individual traces shown in background (10 per condition).* ***(B)*** *Effect of 4-AP and bicuculline on spontaneous burst frequency in naïve (n=2), sham (n=2-7 per drug condition), and SCI (n=6-10 per drug condition) preparations. Spontaneous bursting is induced or increased in frequency by 4-AP*

*(10μM). Bursting is subsequently completely or near-completely and blocked in similar fashion with GABAA antagonists bicuculline (n = 5), picrotoxin(n=3), and gabazine(n=4) so results are pooled. (Welch's t-test *p < 0.05, **p<0.01, ***p<0.001; n=2-10 depending on drug and injury condition; values show mean +/- standard deviation).* ***(C)*** *Example of bicuculline abolishing spontaneous bursting.* ***(D)*** *"Bursting" category includes burst frequency measurements from SCI and 10μM 4-AP conditions, 11 preparations (mean* ± sd = *0.85*±0.38Hz*). Glutamatergic blockade with CNQX + APV reduces but does not fully eliminate bursting in 6 of those preparations that were administered at least 10μM CNQX + 20 μM APV (maximum dose = 40μM CNQX + 100 μM APV, burst frequency = 0.3 Hz after administration) (mean* ± sd = *0.41*±0.32Hz*). $GABA_A$ receptor antagonists ablated all bursting activity in 11/11 preparations shown *(Welch's t-test p < 0.05, n = 11).* ***(E)*** *Addition of CNQX (10μM) + APV (20μM) to bursting preparations significantly reduced, but did not ablate, synchrony of bursts across roots (paired t-test t = 4.3, p-value = 0.01, n = 6 preparations [4 SCI, 2 naïve + 10μM 4-AP]; bursting = 0.51±0.3, CNQX+APV = 0.21±0.16 [mean ±sd])*

2.5 Discussion

Sensory changes occurring after SCI are complex and notoriously difficult to quantify in animal models, especially given the heterogeneity of injury [225, 226]. Here, in a contusion model of SCI, I describe post-injury functional changes in spinal somatosensory circuitry that are characteristically epileptiform and correlate with the extent of mechanical hypersensitivity. These epileptiform characteristics include episodes of stereotyped bursting activity, hypersynchrony, sensory triggering by afferent stimulation, post-burst refractory period, and functional circuit reorganization (**Figure 2-10A**). While previous work has established the epileptiform capacity of dorsal horn neurons [155], this study is the first to link epileptiform

afferent activity to SCI and a behavioral measure of neuropathic pain. This work links SCI to ectopic epileptiform DRRs and supports previous studies linking DRRs to disinhibition of dorsal horn circuitry [45, 180, 227], as well as provides evidence that spinal epileptiform circuitry exhibits degeneracy, allowing it to be expressed through a variety of cellular mechanisms **(Figure 2-10B)**, a further demonstration of similarity of emergence to known circuits generating epilepsy [158, 217, 218].

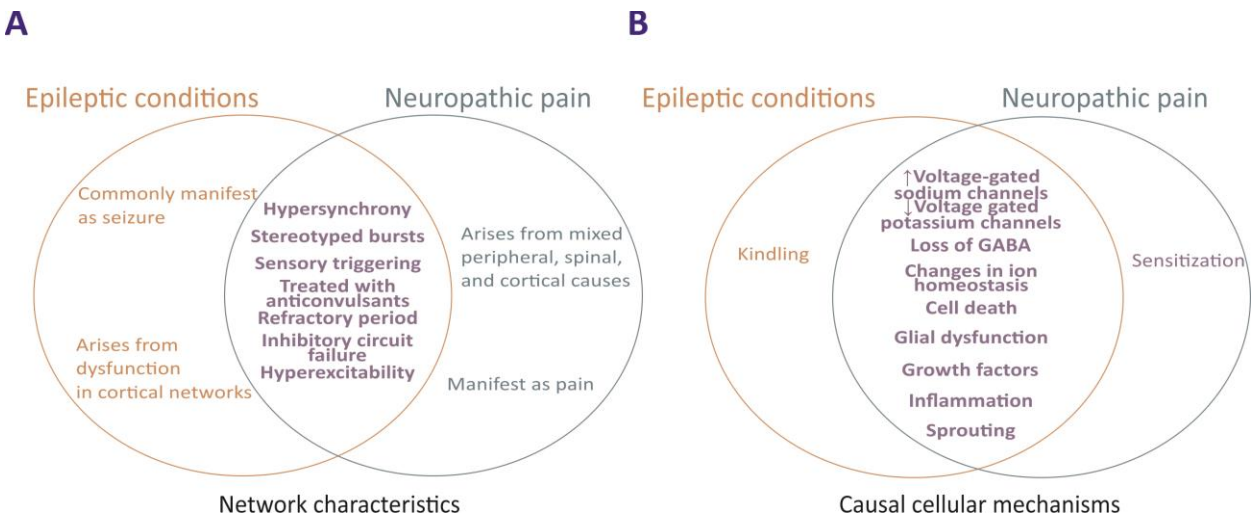

Figure 2-10: Network and cellular-level similarities between epilepsy and neuropathic pain

***(A)** Network characteristics shared between epileptic conditions and neuropathic pain demonstrated in this chapter. **(B)** Known cellular mechanisms shared between epileptic conditions and neuropathic pain [91, 92, 151-154, 157, 158, 166, 168, 213, 228-231].*

Ectopic bursting is driven by normally inhibited dorsal horn circuitry

A previous group focusing on spontaneous spinal bursting in hamster found that the ex-vivo isolated spinal cord develops comparable spontaneous afferent bursting over time [146, 232]. The ability to recapitulate SCI -induced epileptiform bursting with 4-AP suggests that dorsal horn circuitry driving bursting is always present but normally suppressed. Reexamination of

naïve mice in an earlier study [214] showed time-dependent development of spontaneous activity in 3/24 mice. It therefore seems likely that circuit hyperexcitability is driven by SCI -induced loss of descending modulatory tone whose absence facilitates synchrony of GABAergic interneuronal actions on afferents [147]. This is consistent with previous observations of dorsal horn population bursting in naïve and paw-inflamed mice [146, 233]. Perhaps known loss of voltage-gated K+ channel function observed after SCI [211] is reproduced acutely with 4-AP, as both SCI and 4-AP lead to epileptiform bursting in primary afferents, allowing ectopic circuit activation.

Bursting is dependent on GABAergic interneurons

We hypothesize that last order presynaptic GABAergic axoaxonic function transitions from negative feedback (PAD) (**Figure 2-11A$_1$**) to aberrant amplification and spontaneous recruitment of afferent activity (ectopic bursting) (**Figure 2-11A$_2$**) due to increased synaptic drive. Feasibly, the generation of larger DRPs due to stronger GABAergic depolarization could convert subthreshold DRPs to suprathreshold bursting (**Figure 2-9A**) as depolarization toward EGABA in afferents, thought to be ~ -30mV [234], should be above spike threshold, thus enabling suprathreshold spiking. This conversion [32, 42] represents a fundamental functional perturbation in sensory system control. Epileptiform ectopic spiking is expected to influence system excitability via reentrant central collaterals as well as peripheral projections (**Figure 2-11A$_3$**). Bilateral propagation of bursting will be further explored in Chapter 3.

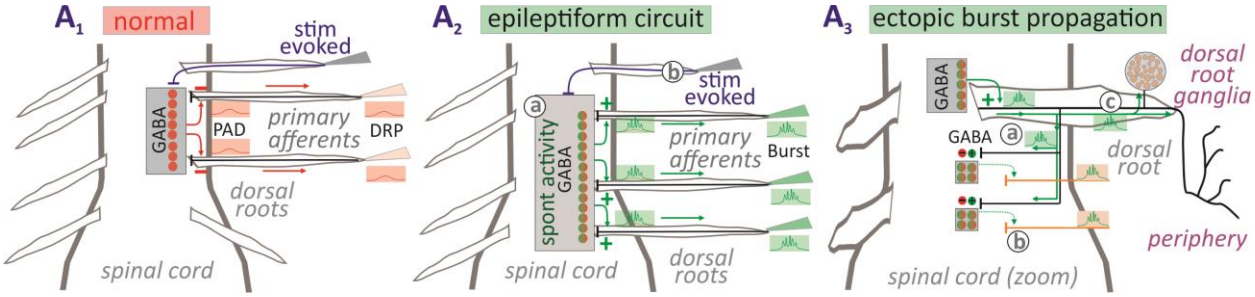

Figure 2-11: Diagram of proposed bursting circuitry

(A$_1$) *Normally, afferent input acts on interposed GABA interneurons to provide negative feedback presynaptic inhibition via subthreshold afferent membrane depolarization (PAD) recorded as dorsal root potential (DRP) (orange boxes).* ***(A$_2$)*** *SCI or 4-AP supports multisegmental synchronization of GABAergic PAD circuits.* ***(A$_{2a}$)*** *Emergent spontaneous synchronized GABAergic drive increases PAD via suprathreshold excitatory actions across multiple spinal segments (green boxes).* ***(A$_{2b}$)*** *Afferent stimulation can recruit the same circuitry.* ***(A$_3$)*** *Ectopic bursting can propagate bidirectionally.* ***(A$_{3a}$)*** *Reentrant propagation along afferent collateral projections lead to activation of spinal circuits.* ***(A$_{3b}$)*** *Antidromically-propagating bursts project to cell bodies in dorsal root ganglia and peripheral terminal fields. Figure adapted from figure by Dr. Shawn Hochman.*

Based on the bursts' sensitivity to GABAergic blockade, the data presented here implicates alteration in the circuit function of GABAergic interneurons, presumably those with axo-axonic synapses [32, 42], as a key driver of bursting. The current work includes recordings of bursting recruited by GABAergic dorsal horn interneuron actions on primary afferent $GABA_A$ receptors. Other work has similarly found that 4-AP induced bursting in dorsal horn interneurons is blocked with bicuculline [155], indicating that $GABA_A$ receptor activity may also be an essential component of the underlying burst circuitry in our system, not just at the afferent axoaxonic synapse. While PAD in cutaneous somatosensory afferents can be mediated by non-GABAergic

mechanisms [39, 41, 42, 223, 224], ectopic bursting's dependence on GABAergic synaptic signaling, disability to continue in the absence of GABAergic synaptic transmission **(Figure 2-9B)**, and ability to continue spontaneously in the absence of glutamatergic input **(Figure 2-9D)** suggests that GABAergic interneurons are necessary to drive spontaneous ectopic bursting. However, the reduction in burst frequency and synchrony associated with glutamate receptor blockade with CNQX + APV indicates that glutamatergic transmission plays an important facilitatory role in spontaneous burst generation and synchronization across segments, likely through afferent projections and excitatory interneurons.

Recent work has identified GABAergic parvalbumin$^+$ and cadherin$^+$ inhibitory interneurons as subpopulations responsible for GABAergic PAD [17, 235, 236], implicating them as potential drivers of the ectopic bursting discussed here. Given the known capacity for hyperactive PAD to generate ectopic DRRs [45], it is likely that these PAD-driving GABAergic interneurons are the last-order interneurons behind afferent spiking. In fact, parvalbumin$^+$ inhibitory interneurons, which fall under the umbrella of islet cells [17, 18], are known to exhibit tonic firing properties and extensive rostrocaudal projections [237]. While bursting evoked by these interneurons would explain the widespread ipsilateral rostrocaudal synchrony of ipsilateral bursts, phase coupling of contralateral bursts is more puzzling. Given recent work describing a population of afferents that project bilaterally and experience hyperexcitability-driven unmasking [238], it is plausible that ectopic afferent bursts on one side of the cord propagate through reentrant actions to activate burst circuits on the other side of the cord. Alternatively, bilateral coupling could arise from recruitment of interneurons with contralateral projections to bursting circuits [239]. Future work should focus on confirming the identity of last-order neurons responsible for afferent burst spiking and quantifying their electrophysiological behavior during bursting.

However, a key question remains how dorsal horn GABAergic interneuron circuitry loses inhibitory capacity such that DRRs are organized into periods of periodic bursting that can occur even in the absence of glutamatergic input. One hypothesis consistent with 4-AP's capacity to evoke afferent bursting is that changes in voltage-gated potassium channel expression after SCI [125, 126] allow a critical subset of interneurons to convert to a bursting phenotype that drives afferent bursts even in the absence of excitatory input. This conversion to a bursting phenotype is known to occur in both Lamina I GABAergic neurons and deep dorsal horn motor system neurons after SCI [240, 241]. Feasibly, the same could occur in a critical population of lamina II interneurons. One hypothesis regarding synchrony of GABAergic circuitry after 4-AP administration is that chloride loading of cells with $GABA_A$ receptors reduces GABAergic inhibition, potentially to the point of paradoxical GABA-based depolarization. As GABAergic synaptic inhibition is activity-dependent and becomes less hyperpolarizing, or even depolarizing in states of increased activity [242, 243], this mechanism could cause synchrony through 4-AP induced bursting, even without dysfunction in NKCC1/KCC2. Regarding the last-order GABAergic interneurons implicated in this work, inhibitory parvalbumin$^+$ interneurons are known to be tonic firing in the presence of depolarizing current [17] and cadherin$^+$ interneurons exhibit a mix of firing phenotypes including predominantly gap and regular spiking [17]. The firing rates of both populations are proportional to the degree of depolarizing input, and they do not normally experience rebound firing after cessation of hyperpolarizing current [244]. It could be the case that their firing rate properties change after SCI [240, 241] due to changes in various ion channel activities. For example, acquiring a capacity for rebound firing could allow them to fire bursts during pauses of inhibitory input, especially if inhibitory neurons providing input to burst generators exhibit a phasic firing pattern. In support of this hypothesis, recent optogenetic

work in cortex suggests that GABAergic neurons may play a direct role in seizure generation through mechanisms such as post-inhibitory rebound excitation and synchronization [230]. A similar dorsal horn circuitry based on rebound firing upon release from inhibition from other local inhibitory GABAergic interneurons could cause intermittent burst firing in last-order GABAergic interneurons, which would result in direct burst recruitment of DRRs as seen here.

Another mechanism that likely contributes to interneuron-driven bursting is that SCI induces shifts in dorsal horn intracellular chloride gradients such that GABA's inhibitory capacity is reduced [136, 212, 245]. Evidence of KCC2 dysregulation after chronic constriction injury suggests that intracellular chloride concentration can even be shifted such that GABA becomes depolarizing rather than hyperpolarizing, resulting in excitation rather than inhibition (in this case in lamina I neurons) [242]. Evidence of NKCC1 and KCC1 downregulation after SCI [44, 131, 133, 212] would explain reduced GABAergic inhibition in the dorsal horn. There is also evidence of death of GABAergic interneurons after SCI [246-248]. Loss of GABAergic tone implies that glutamate might underly hyperexcitability. However, considering the evidence that bursting can still be spontaneously generated in the presence of glutamate receptor block **(Figure 2-9D)**, the most likely explanation of ectopic bursting is that burst-generating interneurons themselves are disinhibited to the point of being spontaneously active and subsequently recruiting suprathreshold spiking in afferents through axo-axonic synapses. As activity-dependent Cl^- buildup can outpace KCC2's Cl^- extrusion capacity [243, 249], particularly in cases like SCI where KCC2 function is perturbed, inhibitory neurons could synchronize during periods where intracellular Cl^- accumulates to the point that GABA becomes excitatory, as is known to occur during epileptiform synchronization in cortex [for review see: [250]]. Given the complexity and interconnectivity of dorsal horn circuitry, relatively minor changes in

NKCC1/KCC2 expression can significantly alter inhibitory tone and potentially directly induce synchrony, both of which manifest significant perturbations in circuit function. Perhaps unsurprisingly, perturbations in NKCC1 and KCC2 expression have been implicated in a variety of hyperexcitability-based disruptions including epilepsy and neuropathic pain [132, 166, 211].

Yet another possibility is that dorsal horn interneuron networks can synchronize through gap junction-based coupling after SCI or administration of 4-AP. Neuronal gap junctions are known to be expressed at dorsal horn excitatory synapses [251], have been implicated in central sensitization [252], and are known to exhibit altered expression profiles after SCI [253]. The role of gap junctions in pain conditions including SCI has been well-established, although most evidence implicates alterations in glial networks that alter inflammatory and apoptotic signaling pathways [253-256]. Overall, uncovering the mechanisms by which bursting synchronizes should be a key goal in the future of this work.

4-AP acutely recapitulates epileptiform bursting

4-AP successfully induced GABA-driven afferent spiking that recapitulated key features of the epileptiform bursting recorded from SCI preparations. The drug has long been used as a model of cortical epilepsy [207, 208] and has previously been shown to induce epileptiform bursting in dorsal horn [155], furthering the connection between SCI-induced hyperexcitability and epilepsy. As a non-selective voltage-gated potassium channel (K_V) blocker with primary targets in the K_V1, K_V2, K_V3, and K_V4 potassium channel families, 4-AP is known to broaden action potentials and induce burst firing in subpopulations of neurons based on their K_V expression [199, 202]. Given that its capacity to broaden action potentials, it was approved in 2012 to be used to improve locomotor function by enhancing axonal conduction in multiple sclerosis, a demyelinating condition [203]. Its similar use has also been investigated for post-SCI recovery of

locomotor function, with relatively promising results [204, 205, 257]. Perhaps unsurprisingly given the 4-AP data presented here, common side effects of treatment are spasm, pain, and paresthesia [258].

TEA was used as a secondary K_V channel blocker, as it targets a slightly different constellation of K_V channels, as well as some K_{Ca} channels, ablating the action potential afterhyperpolarization rather than broadening action potentials [198, 200]. Despite these differences, TEA is also used as a model of cortical epilepsy [209] and induces cellular hyperexcitability. While 4-AP's and TEA's acute mechanisms of action are likely not identical to the cellular mechanisms of SCI-induced hyperexcitability, ability to induce spinal epileptiform behavior with K_V perturbation makes it an attractive pharmacological model of epileptiform circuit behavior. Furthermore 4-AP's capacity to increase burst frequency, but not synchrony, in SCI preparations provided important evidence that epileptiform circuitry expressed degeneracy. The occlusion of 4-AP's ability to increase synchrony in the SCI population suggested that SCI-induced hyperexcitability was reached through a mechanism distinct from 4-AP's K_V block, but that bursting arose from the same underlying circuit behavior.

The ability of the anticonvulsant retigabine to reduce burst frequency, as it acts by opening KCNQ channels [221, 222, 259], further supports the hypothesis that bursting circuitry is sensitive to excitability changes following a perturbation of a multitude of ion channels. While retigabine reduced burst frequency, it paradoxically increased the number of spikes per burst, potentially suggesting that a greater number of afferents were excited by dorsal horn interneuron input. More likely given the reduction in burst frequency, a similar number of afferents were excited over a broader period of time, allowing individual spikes to appear more clearly in the burst waveform.

Degeneracy in epileptiform circuit induction

Degeneracy refers to the concept that a particular outcome can be achieved through numerous causal mechanisms. The concept is applicable in both cellular settings, where disparate ion channel constellations can produce similar neuronal function [260], as well as in circuits, where disparate inputs can produce similar circuit-wide function [261]. Recent work has highlighted the importance of degeneracy in enhanced afferent excitability in neuropathic pain [217, 218] and in enhanced cortical circuit excitability in epilepsy [158], indicating that both of these states can arise from various perturbations in their respective underlying circuitries. As the bursting circuitry implicated in this work exhibited key epileptiform characteristics and arose from afferent and dorsal horn hyperexcitability, I sought to determine whether it also exhibited degeneracy.

As epileptiform bursting was able to be induced through blockade of K_V channels with 4-AP and TEA, perturbation of intracellular chloride concentration by KCC2 block with VU0240551, and Chronic SCI, I argue that hyperexcitable burst circuitry can indeed be considered to exhibit degeneracy. In addition to these diverse methods to induce ectopic bursting, previous work focusing on the hamster found that the ex-vivo spinal cord develops spontaneous afferent bursting over time [146, 219, 262]. Recent work has also demonstrated that ectopic bursting is associated with peripheral inflammation. [233, 263]. Taken together, it is clear that the circuitry underlying ectopic bursting can be unmasked through a wide variety of perturbations. Considering these results, as well as those presented in this work, epileptiform bursting almost certainly exhibits degeneracy: circuit hyperexcitability and subsequent bursting can be achieved through different perturbations, each inducing hyperexcitability through slightly different mechanisms. Recent computational work has established the degenerate nature of neuropathic

pain, highlighting that ablation of inhibitory GABAergic input, loss of inhibition through changes in chloride regulation and changes in K_A channel expression can all induce circuit changes consistent with the expression of neuropathic pain [264].

Evidence of degeneracy in epileptiform circuitry suggests that the previously discussed perturbations induced by SCI: increase in Na_V expression, decrease in K_V expression, disruption of cellular chloride homeostasis, and loss of GABAergic inhibition, could each be sufficient to generate hyperexcitable dorsal horn circuitry and epileptiform bursting. As the experiments presented here focused on K_V and KCC2 function, future work should focus on defining the sufficiency and interaction between other known post-SCI cellular perturbations. As discussed by other authors [218], the concept of degeneracy should influence how we view neuropathic pain conditions and associated hyperexcitability, emphasizing that circuitry can develop a hyperexcitable steady state through a variety of perturbations.

2.6 Conclusions

These results demonstrate that epileptiform bursts emerge after SCI and after a variety of other acute perturbations, suggesting degeneracy in burst circuitry. Ectopic bursting's epileptiform characteristics include episodes of stereotyped bursting activity, hypersynchrony, sensory triggering by afferent stimulation, post-burst refractory period, and functional circuit reorganization. Identifying this activity as epileptiform and degenerate could change the way we look at circuit-level properties of neuropathic pain. Overall, these results support a conceptually novel understanding of SCI -induced sensory dysfunction and associated neuropathic pain driven by epileptiform behavior **(Figure 2-11)**. In this model of sensory dysfunction, GABAergic interneurons normally responsible for PAD also recruit suprathreshold bursts of spiking in afferents across multiple spinal segments. These bursts occur spontaneously and can be evoked

by afferents through the same circuitry. Segmentally propagating bursts are consistent with common descriptions of propagating neuropathic pain (e.g. shooting, stabbing, lancinating) [87] and may serve as an index of hyperexcitability associated with these pain descriptions. Overall, given the long timeline, animal welfare concerns, and experimental difficulty of SCI experiments, a pharmacological model like 4-AP is a promising tool for future work. The concept of degeneracy further emphasizes the usefulness of pharmacological tools like 4-AP or TEA.

2.7 Research Contributions

Contusion surgeries were performed by Karmarcha Martin and Matthew Bryson. Behavioral data were acquired by Heidi Kloefkorn-Adams and Don Noble. Electrophysiology data were acquired by Matthew Bryson and Shawn Hochman. Data quantification and analysis were performed by Matthew Bryson (see appendix A for details on quantification program). Matthew Bryson authored the chapter with collaboration from Dr. Shawn Hochman and Dr. Peter Wenner.

Chapter 3: Spinal circuits and burst propagation

3.1 Abstract

When driven to hyperexcitability, as after SCI, dorsal horn circuitry can generate spontaneous epileptiform activity that recruits ectopic bursting in primary afferents. This bursting is putatively driven by GABAergic interneuron networks and also can be recruited by sensory input, presumably by recruitment of the same interneurons normally responsible for PAD. Here, I used approaches in the ex vivo intact spinal cord to explore the relationship between bursting circuits and the afferents recruiting or recruited by them. Higher stimulus intensities that recruited Aδ and C fibers always recruited bursting in cords expressing spontaneous bursting, as did selective recruitment of Aδ- and C-LTMRs with optogenetic stimulation. Electrical stimulation evoking selective recruitment of Aβ fibers was also able to recruit burst circuitry on several occasions. Conversely, via collision testing, ectopic bursting was observed to occur in Aδ- and C-LTMRs. Ectopic bursts were shown to propagate along central branches to have reentrant orthodromic synaptic actions on superficial dorsal horn circuits as well as antidromic actions in cutaneous afferents. Collectively, bursting circuits at least receive input from Aβ fibers and Aδ- and C-LTMRs while acting on at least Aδ- and C-LTMRs. After SCI, bursting was shown to be expressed along a spectrum of excitability with increases in burst synchrony associating with higher frequency, amplitude, and duration of bursts. Using alterations in extracellular [Mg^{+}] and [Ca^{2+}] to limit transmission largely to monosynaptic actions reduced but did not block ectopic bursting, suggesting that last-order GABAergic actions are sufficient to generate bursts, while loss after $GABA_A$ receptor block demonstrated that they are necessary. That afferent stimulation could still evoke bursts suggests that afferents have strong monosynaptic actions on last-order GABAergic interneurons to generate evoked bursts

disynaptically. Bursting frequency was modulated by extrasynaptic $GABA_A$ receptors, which are known to play a key role in modulating propagation at axonal branchpoints. Together, these results further elucidate the afferent populations and dorsal horn networks involved in evoked and spontaneous burst generation.

3.2 Introduction

In chapter 2, I demonstrated that spinal ectopic DRR bursting can be generated by dorsal horn hyperexcitability such as occurs after SCI. Here, this hyperexcitability manifests as spontaneous and afferent stimulation evoked ectopic bursting in primary afferents. This bursting is epileptiform in nature and activity in afferents requires $GABA_A$ receptor activity, ostensibly from a subpopulation GABAergic interneurons responsible for PAD through axoaxonic contacts with a wide variety of innocuous and nociceptive primary afferents [17, 27, 39, 42]. As such, bursting likely consists of DRRs driven by hyperactivation of axoaxonic synapses normally responsible for PAD [34]. As DRRs can propagate orthodromically [35, 47, 265] and antidromically [45, 49, 52, 181, 227], it is critical to understand which afferent populations can recruit bursting circuitry, as well as which afferent populations and networks of spinal neurons are recruited during the ectopic burst event. If nociceptive circuits are recruited during bursting, as is suggested by 4-AP data presented in chapter 2, then bursts could underly emergent spontaneous and evoked neuropathic pain through spontaneous and cross-modal activation of pain circuitry, respectively [40, 266].

Through PAD, non-nociceptive afferents provide presynaptic inhibitory control over peripheral afferent signaling to the dorsal horn [44], which can be lost in cases where afferent $GABA_A$ receptor activation evokes repetitive afferent spiking [267]. PAD can be evoked by multiple afferent and descending fiber types with converging polysynaptic modulation over a single

afferent fiber population [41]. For example, nociceptive C-fibers projecting directly to lamina I pain projection neurons receive inhibitory tone in the form of PAD from Aβ, Aδ, and C fibers [27]. If bursting exhibited similar convergence of afferent types, it could provide a spinal substrate for explaining symptoms like allodynia: non-nociceptive fibers that normally inhibit painful afferents through PAD would now evoke ectopic bursts in them instead through the conversion from presynaptic inhibition to aberrant excitation demonstrated in chapter 2.

Aδ- and C-LTMRs are exclusively non-nociceptive afferents known to provide polysynaptic input to dorsal horn interneuron circuitry, including to postsynaptic dorsal column tract cells of the DCML [17, 42]. While Aδ-LTMR afferent input can directly evoke PAD, previous work has failed to generate PAD with C-LTMR input [42]. However, C-LTMRs are known to provide polysynaptic input to lamina 1 spinothalamic tract projection neurons [268, 269], providing them indirect access to pain projection neurons. This connectivity demonstrates that these populations play a role in maintaining high fidelity somatosensation through canonical and non-canonical modulation of multiple projection networks [270-272]. As might be expected, LTMR afferents with this polysynaptic capacity to influence nociceptive circuitry could excite rather than inhibit it, such as is the case with C-LTMR (C tactile afferent) driven allodynia in humans [13, 273-275]. Similarly, in mice, C-LTMR input is sufficient to cause affective pain after SCI [276]. Aδ-LTMR's directional mechanosensitivity is driven by BDNF signaling [277], and BDNF signaling perturbations facilitate nociceptive effects after SCI [278]. Thus, SCI could alter LTMR encoding properties to promote nociception. Given this evidence, I sought to determine both whether these afferents can generate bursting through their interneuron synapses and whether they are recruited during bursting.

To this end, I performed a series of experiments with two transgenic mouse lines selective for channelrhodopsin expression in these non-nociception encoding afferent populations. The first line, Vglut3-ChR2, selectively expresses channelrhodopsin in C-LTMRs, responsible for the affective component of light touch [279, 280] (see chapter 1 for more detailed description). The second line, TrkB-ChR2, expresses channelrhodopsin in Aδ-LTMRs, which are responsible for the sensory-discriminative components of light directional touch [277] (see chapter 1 for more detail). Together, along with Aβ hair follicle receptors, these afferents form a functional unit of light touch reception in hairy skin and terminate in distinct lamina of the dorsal horn, forming the LTMR recipient zone (**LTMR-RZ**) [19, 281, 282]. Given the complexity and interconnectivity of somatosensory processing in the LTMR-RZ, there are numerous mechanisms by which these innocuous afferents and the interneuron networks they contact can perturb somatosensation [24, 283-285].

In this chapter, I will discuss a series of experiments designed to elucidate the afferents and dorsal horn circuits involved in burst generation. Specifically, I will describe evidence that Aβ fibers are minimally involved in burst propagation, define the role of Aδ- and C-LTMRs in evoking and propagating bursts, and explore the circuitry underlying bursting with a series of ion manipulation and pharmacology experiments.

3.3 Methods

3.3.1 Animals

All procedures were approved by the Emory University Institutional Animal Care and Use Committee. Naïve Vglut3-ChR2 mice (n = 28) were male and female Vglut3-IRES2-Cre-D (Jax 028534) :: Ai32(RCL-ChR229H134R)/EYFP (R26-ChR2-eYFP)(Jax 024109) aged between

100 and 150 days at time of terminal experiments. Naïve mice used for Aδ-LTMR experiments (n = 6) were male and female B6.129S6(Cg)-Ntrk2tm3.1(cre/ERT2)Ddg/J (Jax 027214) :: Ai32(RCL-ChR29H134R)/EYFP (R26-ChR2-eYFP)(Jax 024109) aged between 100 and 150 days at time of terminal experiments. Both SCI cohorts discussed in chapter 2 were also included here, with the first cohort consisting of SCI (n = 10) and sham (n = 7) C57/Bl6 females aged between 110 and 130 days at time of surgery, and between 310 and 640 days at time of terminal experiments, and the second cohort consisting of SCI (n = 5) and sham (n = 4) Vglut3-ChR2 males and females with a mean age of P100 at surgery and between P120 and P210 at time of terminal experiments. Naïve mice used for skin-nerve preparation antidromic stimulation experiments (n=4) were male and female Vglut3-IRES2-Cre-D (Jax 028534) :: Ai32(RCL-ChR29H134R)/EYFP (R26-ChR2-eYFP)(Jax 024109) aged between 100 and 150 days at time of terminal experiments. Post-surgery, animals were housed in isolated cages with a maximum of two animals per cage.

Table 3-1: Transgenic animal lines used for optogenetic experiments

Strain name in this work	**Afferent type**	**Jax #**	**Physiological function**
Vglut3/Vg3	C-low threshold mechanoreptor (C-LTMR)	028534	Affective component of light touch
TrkB	Aδ-low threshold mechanoreceptor (Aδ-LTMR)	027214	Discriminatory component of light directional touch

3.3.2 Spinal Cord Injury

Contusion injuries were performed as previously described using the Infinite Horizon spinal cord impactor device [186]. Briefly, mice were anesthetized with 5% inhaled isoflurane, then a midline incision performed, and a dorsal laminectomy performed at T10-T12 based on distance from cord apex. The mouse was moved to the impactor and the exposed cord impacted at 50kD with 0 dwell time. Mice were given 2 mg/kg meloxicam (Cayman Chemical Company) the day of surgery and the next day, as well as 0.5 mg/kg Enrofoxacin (Baytril, Bayer) daily following surgery. Sham mice underwent surgical and post-surgical procedures other than impact. Mice in the first SCI cohort underwent Von Frey testing and home cage recording for 2 weeks [191] before injury, as well as after injury to confirm development of allodynia and monitor activity levels. Mice in the second (Vglut3-ChR2) cohort underwent thermal preference testing and home cage recording of respiratory rate variability [191] after surgical recovery. Post-surgery, animals were housed in isolated cages with a maximum of two animals per cage.

3.3.3 Models of sensory hyperexcitability

A voltage-gated K^+ channel blocker, 4-aminopyridine (**4-AP**) (1-100 µM, Spectrum), was used to generate a model of sensory circuit hyperexcitability in the *ex vivo* intact spinal cord preparation. 4-AP has been demonstrated to increase the excitability of neurons in preclinical and clinical studies [201, 202] and recruits spinal nociception-encoding circuitry consistent with the emergence of spontaneous neuropathic pain [155, 206] **(Figure 2-1B).**

3.3.4 Dissections

Intact spinal cord preparation

Mice were lightly anesthetized with inhaled isoflurane then injected intraperitoneally with 300µL 50% urethane for deep anesthesia. To induce hypothermia, dorsal skin overlying the vertebral

column was removed and mice were submerged in ice-cold artificial cerebrospinal fluid (aCSF) until respiration rate slowed (2-3 minutes). Animals were then removed, decapitated, and the whole spinal cord dissected with a ventral approach as previously described [214]. The spinal cord dissection was performed in ice cold recovery aCSF oxygenated with 95% O2-5%CO2. The isolated cord was then equilibrated to room temperature for 1 h in modified HEPES holding solution [286] oxygenated with 95% O2-5%CO2, and then pinned dorsal side up in a Sylgaard-lined recording chamber while superfused with an oxygenated aCSF containing (in mM) 128 NaCl, 1.9 KCl, 1.3 MgSO4, 2.4 CaCl2, 1.2 KH2PO4, 10 glucose, and 26 NaHCO3 at ~40 ml/min. All experiments were undertaken at room temperature.

Experiments assessing synaptic relationships included recordings with alternate aCSF including 1) *high-*Mg^{2+}*/low-*Ca^{2+} artificial cerebral spinal fluid (aCSF) containing (in mM), [NaCl 128, KCl 1.9, $MgSO_4$ 13.3, $CaCl_2$ 1.1, KH_2PO_4 1.2, glucose 10, $NaHCO_3$ 26] and 2) *high-*Mg^{2+}*/high-*Ca^{2+} artificial cerebral spinal fluid (aCSF) containing (in mM), [NaCl 128, KCl 1.9, $MgSO_4$ 13.3, $CaCl_2$ 3.8, KH_2PO_4 1.2, glucose 10, $NaHCO_3$ 26]. I will refer to these solutions as *high-*Mg^{2+}*/low-*Ca^{2+} and *high-*Mg^{2+}*/high-*Ca^{2+}solutions, respectively, throughout this chapter.

Skin-nerve preparation

Mice were lightly anesthetized with inhaled isoflurane then injected with 70µL 50% urethane for deep anesthesia. Trunk skin with intact T8-T13 dorsal cutaneous nerves was removed as quickly as possible as previously described [287]. Briefly, a ventral midline incision was performed, skin separated from the body cavity and removed until DCNs were visible, then DCNs partially dissected, and the trunk skin removed. Dissected skin was transferred to a dish containing room temperature oxygenated Kings ACSF, then mounted onto a custom-made dish for recording (**Figure 3-1A**). Here, dorsal cutaneous nerves (DCNs) were further dissected: the surrounding

fascia was removed and the nerves themselves de-sheathed to allow electrode placement at multiple locations along nerves.

In-vivo DCN recording

Mice were deeply anesthetized with inhaled isoflurane: anesthesia was induced with inhalation of 5% isoflurane and maintained with 2-4% isoflurane based on monitoring of respiration and heart rate. Body temperature was maintained with a circulating bath heated to 36˚C by a Peltier device built by Bill Goolsby. Once anesthesia was stable, a midline incision was made in the dorsal truncal skin and DCNs were dissected from one side of the animal. Animals were administered 0.2 mg/kg 4-AP to induce bursting. In some experiments, a suction electrode was attached to multiple DCNs to monitor ongoing bursting. In others, a single suction electrode was attached to a DCN to monitor bursting and a sharp electrode was inserted into various cutaneous regions to attempt to record bursting.

3.3.5 Intact spinal cord preparation electrophysiology

Suction electrodes were fabricated from 1.65/0.75 (OD/ID) glass capillary tubes (Dagan Corp) using Narishige PC-100 electrode puller with tips broken back to achieve internal tip diameters of 100-200 µm. Electrodes were placed on dorsal root entry zones and distal dorsal roots between T6 and L6 for recording and stimulation. Most commonly, electrical stimulation was delivered using constant current stimuli [197] to the distal ends of dorsal roots. Where noted, Lissauer's Tract (LT) recordings were undertaken with small diameter (50µm) extracellular electrodes and LT/DH recordings were undertaken with glass capillary tubes (WPI, 1.0mm OD) pulled to 1-2µm tip diameter (3-5MΩ). Electric field potentials (EFPs) (also called local field potentials of LFPs) typically reflect local subthreshold population synaptic activity. EFPs were recorded by inserting the 1-2µm tip electrodes into the dorsal horn at known depths, focusing on

lamina II (~90µm below LT). In this case, EFPs in lamina II represent synchronous subthreshold synaptic actions on interneurons [214]. Suction electrode LT recordings recorded EFPs from subjacent superficial dorsal horn in some recordings, but focused on spiking in axons of small diameter afferent collaterals and interneuron axonal projections [288, 289]. Electrical stimulation was delivered by suction electrodes attached to the distal ends of nerve roots and optogenetic stimulation was delivered in a manner that ensured that only roots and not cord were stimulated. Roots were selected based on intact structure after dissection. Optogenetic stimulation was performed with laser diode boxes built by Bill Goolsby. All recorded data were digitized at 10 kHz (Digidata 1322A 16 Bit DAQ, Molecular Devices, U.S.A.) with pClamp acquisition software (v. 10.7 Molecular Devices). Recorded signals were amplified (10000x) and low-pass filtered at 3 kHz using in-house amplifiers. In all data presented, the number of animals utilized for analysis is represented by the noted n value. For each animal, a representative value was determined by averaging the evoked response from multiple trials within that animal (a minimum of 5) or by analyzing a minimum of 5 minutes of spontaneous gap-free recording.

3.3.6 Skin-nerve preparation electrophysiology

Recording dish

The skin nerve preparation was placed epidermal side down on the bottom of the dish, covering a hole just smaller than the section of skin such that the skin forms a seal with the dish **(Figure 3-1A)**. The epidermal side of the skin remains accessible for stimulation. A computer-controlled MP-225 micromanipulator is positioned beneath the opening and is outfitted with a fiber optic cable for optogenetic stimulation and a tube for air pressure mechanical stimulation. The robotic arm is programmable to move in µm increments within an x, y, and z plane. This feature was developed for precise receptive field characterization, and to deploy mechanical stimulation

while moving across the skin. The inside of the skin, and attached dorsal cutaneous nerves, face up, and the dish were filled with recirculating, temperature controlled, oxygenated (95/5) Kings ACSF containing (in mM), [NaCl 128, KCl 1.9, $MgSO_4$ 1.3, $CaCl_2$ 2.4, KH_2PO_4 1.2, glucose 10, $NaHCO_3$ 26], at ˜40ml/minute to maintain viability of the nerves throughout the recording session.

Electrode preparation and recording configurations

Suction electrodes were fabricated from 1.65/0.75 (OD/ID) glass capillary tubes (Dagan Corp) using Narishige PC-100 electrode puller with tips broken back to achieve internal tip diameters of 150-200 µm. For in-vivo cutaneous recordings, sharp electrodes (pulled to 1-2 µm tip diameter) were fabricated from 1.0/0.75 (OD/ID) glass capillary tubes (World Precision Instruments) using a Narishige PC-100 electrode puller and inserted into dorsal cutaneous hairy skin or hindpaw hairy skin. Spontaneous and evoked potentials from T8-T12 dorsal cutaneous nerves were recorded simultaneously during optogenetic and/or mechanical stimulation. In antidromic stimulation trials, a stimulating electrode was placed en-passant between DCN cutaneous terminations and the recording electrode. Antidromic electrical stimulation parameters were based on recordings of spontaneous activity from the ex-vivo spinal cord preparation (100 Hz 200 µs 200 µA electrical stimulation to preferentially activate Aδ fibers). Electrical stimulation was performed at the end of cut DCNs and volleys recorded en-passant between the nerve end and skin. Mechanical stimulation was performed with air pulses from an air controller built by Bill Goolsby and controlled through Clampex (voltage range 0-10V corresponding to 0-20mN, **Figure 3-1B**). All recorded data were digitized at 10 kHz (Digidata 1322A 16 Bit DAQ, Molecular Devices, U.S.A.) with pClamp acquisition software (v. 10.7 Molecular Devices). Recorded signals were amplified (2000x) and low-pass filtered at 3 kHz It was not used for the

purposes of this project. Glass suction electrodes were mounted on an electrode holder associated with a 3D micromanipulator that allowed for accurate mechanical positioning and flexible movement. To map receptive fields, an MP225 micromanipulator controller was modified by Bill Goolsby to be controllable through LabView software. Stimulators were attached to the manipulator and moved through scripted X and Y coordinates, which were later mapped back to the layout of the skin-nerve preparation. Evoked responses were normalized and mapped using X and Y coordinates.

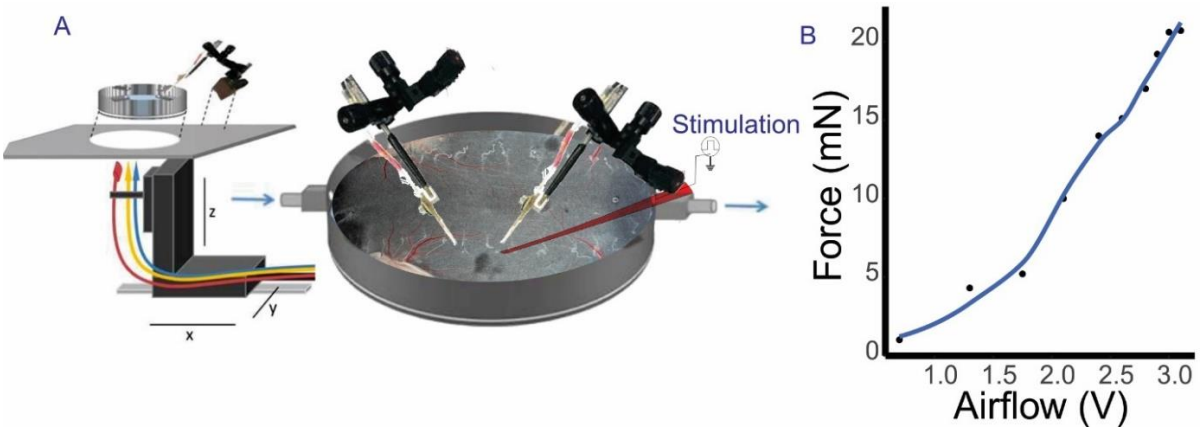

Figure 3-1: Skin-nerve preparation recording dish and air pulse calibration

(A) *Diagram of skin-nerve preparation. A computer-controlled robotic arm is positioned beneath the opening and is outfitted with a fiber optic cable for optogenetic stimulation and a tube for air pressure mechanical stimulation. The robotic arm is programmable to move in µm increments in the x, y, and z planes to automatically map receptive fields. Dissected DCNs are recorded and stimulated with glass suction electrodes.* ***(B)*** *Calibration curve of airflow device airflow output reading vs. force in mN. This curve was used to convert output voltage readings to mN for figures in this chapter.*

3.3.7 Conduction velocity and collision testing recording configurations

The conduction velocity of antidromically propagating bursts was measured by recording from two sites along the same dorsal roots during spontaneous bursting, which travelled antidromically along the DR. Distance between recording electrodes was measured with a micrometer and difference in burst timing (based on arrival of earliest identifiable burst component) was measured in Spike2 after DC removal, rectification, and RMS filtering with a time constant of 0.005s in order to best identify the first component of bursts. Bursts were measured based on the earliest arriving identifiable spike. Collision testing was performed by electrically evoking a burst while recording distally from a heteronymous root with optical stimulation aimed at a site between the cord and the end of this root to evoke and record an antidromic Aδ- or C-LTMR volley. If the burst recruited spiking in the given afferent subtype, the propagating burst would ablate or greatly reduce the amplitude of the optically evoked antidromic volley, as these fibers would be in a refractory period at the time of optical stimulation. In some cases, especially with C-LTMR selective optical stimulation, optically evoked volleys consisted of multiple peaks. In this case, the clearest peak that could be tracked between sweeps was measured. Even when the volley consisted of multiple identifiable components, this single amplitude measure captured the effects of collision with burst. Amplitude measurements were taken manually with Clampfit. The minimum number of technical replicates per collision testing configuration (number of files with moving electrical stimulation collision testing performed) for an individual preparation was 2).

3.3.8 Fos labeling

To obtain histological evidence of 4-AP induced activation of nociceptive circuitry in the dorsal horn, we stained spinal cord slices for *c-fos* protooncogene activation of the protein Fos - an

indirect metabolic marker for neuronal activity [290]. For the studies in this work, a Neurokinin 1 Receptor (Nk1R)-TdTomato cross was used to assess c-fos activation in Nk1R superficial dorsal horn neurons, which are critical for spinoparabrachial pain pathway signal propagation [291, 292]. For the 4-AP conditions, we applied 10μM 4AP for 10 mins, followed by a wash out and 2-hour incubation period. Negative control cords had stimulation electrode attached for 10 minutes (no stimulation delivered) then removed for the 2-hour incubation period. All c-fos experiments were conducted at 27 °C, as Fos-immunoreactivity (Fos-ir) was previously demonstrated to be temperature-dependent [293]. Following experimentation, the cord was then removed from the recording chamber and fixed in 4% paraformaldehyde for 2 hours. After fixation the cord was placed in 20% sucrose in phosphate buffered saline (PBS) until sectioning. The following processing methods were adapted from Alexander et. al. 2015 [294].Transverse sections 20 μm thick were cut through the lumbar cord on a freezing microtome and mounted on slides. Sections were washed in 0.01 M PBS with 0.1% Triton X-100 (PBS-T), blocked for 1 h in 5% normal goat serum in PBS-T, and incubated at room temperature overnight in rabbit antiFos antibody (1:250; Santa Cruz Biotechnology) in PBS-T with 2% goat serum. Sections were washed in 3×PBS-T and incubated with donkey anti-rabbit conjugated to Cyanine Cy3 (1:250; Jackson Immunoresearch) for 2 h at room temperature. Sections were then washed in PBS three times and coverslipped. Fos-ir in the spinal cord was quantified by visual counting of cells in the dorsal horn showing nuclear staining. Positive staining cells were counted separately in dorsal horns ipsilateral and contralateral to the stimulated root. Counts were pooled to calculate an average and standard deviation of the number of dorsal horn cells expressing Fos protein.

3.3.9 Data and statistical analysis

Data was recorded using Clampex, initially visualized in Clampfit, and then analyzed and visualized using Spike2 and custom-written scripts and applications in Python and R (see code accessibility section for access and chapter 3 for in-depth description of Python analysis program). In the spinal cord preparation, recorded roots were selected for analysis based on the presence of bursting either at baseline or after addition of 4-AP. To study below-level plasticity, roots T13-L4 were considered for analysis. Any roots that did not show bursting after 4-AP addition were excluded from analysis as it was not possible to determine whether this was due to destruction of the root during dissection. Roots with signal to noise ratios too poor to reliably differentiate bursts from background noise were also excluded from analysis. For the skin-nerve preparation, dorsal cutaneous nerves T8-T12 were recorded if they exhibited robust response to air pulse stimulation. Roots lacking a response were excluded from experimentation and analysis.

Statistical significance of data was determined via ANOVA, Spearman's correlation, Wilcoxon rank-sum test when appropriate (as determined by Shapiro-Wilks test), or two-tailed t-test, depending on the normality and scedasticity of the data. Relationships were considered significant at $p < 0.05$. See figure legends for individual statistical tests and outcomes. Values in plots with error bars are presented as mean ± standard deviation (sd) unless otherwise specified.

Bursts were identified and quantified with custom-written Python software. See Appendix A for further details. Briefly, peaks were identified with a peak threshold set at 3.5x RMS noise. Recordings were considered to contain bursting activity when the standard deviation of inter-spike intervals was greater than the mean inter-spike interval of all peaks. Inter-spike interval was also used to characterize packets of peaks as bursts (peaks were binned together when they

were <20 ms apart and only groups of 5 or more peaks were considered a burst). Once bursts were identified, they were quantified (amplitude, duration, etc.) and cross-correlations were processed with combinations of channels taken 2 at a time. When cross-correlation is not specified, burst synchrony was determined by comparing burst times (from start to end of burst) across channels. If channels shared >50% of burst times, they were considered to exhibit synchrony.

3.3.10 Code accessibility

Custom-written Python application for burst analysis available at https://github.com/mbryso4/2023_Burst_Analysis. Available versions are the same that were used for analysis of this work. Updated versions will be maintained elsewhere. See Appendix A for discussion of analysis program.

3.4 Results

3.4.1 Bursts are evoked by Aβ, Aδ, and C fiber electrical stimulation

To determine which afferents propagated burst spiking, I obtained conduction velocity (CV) measurements by recording from a proximal and a distal site on the same DR during bursting (**Figure 3-2**). These recordings indicated that bursts always propagated from the spinal cord to the periphery. Conduction velocity measurements were made based on the first clear spike of the burst in each channel (shown by arrows in **Figure 3-2**). These measurement indicated that bursts propagated in fibers slower than Aβ, implicating conduction through Aδ and C fibers (mean CV = 0.92 ± 0.8 m/s at 22˚C, n = 3; 1 SCI, 1 naïve + VU0240551, 1 naïve + VU0240551 + 4-AP) [9, 295] (**Figure 3-2**).

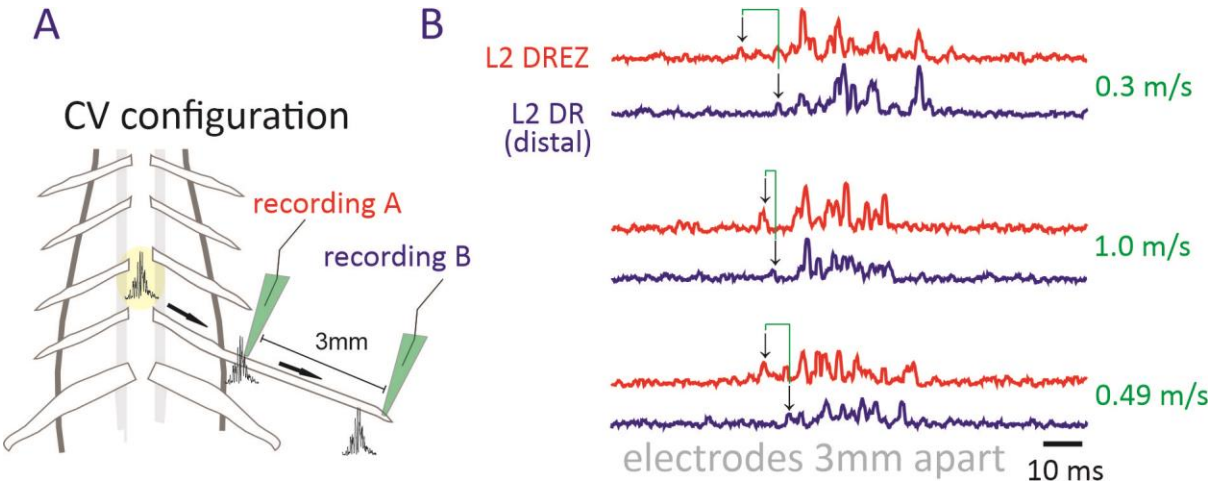

Figure 3-2: Conduction velocity recording configuration and results.

***(A)**: Diagram of recording configuration for conduction velocity measurements. **(B)** Example of conduction velocity measurements based on differences in spike timing between two recording sites: one at the DREZ proximal to the cord (shown in red) and one at the end of the dorsal root distal to the cord (shown in blue). Arrows indicate the first clearly arriving spike of the burst in each channel with the green line indicating the temporal difference between arrival time in the proximal and distal channel. Bursts propagated in the Aδ-C conduction velocity at room temperature (n = 3, mean CV = 0.92 ± 0.8 m/s at 22˚C) [9, 296]. Burst waveforms were rectified and RMS filtered with a time constant of 0.005s to best identify earliest burst component.*

To determine which afferent subpopulations evoked bursting, electrical stimulation at varying intensities (50µs 50µA, 200µs 200µA, and 500µs 500µA) was delivered to distal DRs while recording from homonymous and heteronymous DREZs. Bursts in SCI and naïve/sham 4-AP preparations were always evoked with electrical stimulation that recruited Aβ, Aδ, and C fibers (n = 28/28 tested preparations; SCI n = 11; sham + 4-AP n = 6; naïve + 4-AP n = 11; 200µs, 200µA and 500µs, 500µA [214]). Electrical stimulation that preferentially recruited Aβ or Aβ and Aδ fibers (50µs 50µA) evoked bursting in 61% (17/28) tested preparations exhibiting burst

recruitment at this lower stimulus intensity with clear evidence of burst recruitment having Aβ but no Aδ volley. Burst recruitment at this low intensity was observed in 9/11 SCI preparations, 3/6 sham + 4-AP preparations, and 6/11 naïve + 4-AP preparations. Incidence between preparations was not statistically significant (Chi-Square (2, n = 28) = 2.5, p-value = 0.29).

As electrical stimulation was performed with constant values (50µs, 50µA; 200µs, 200µA; and 500µs, 500µA) rather than with afferent volley-based thresholding, it was somewhat difficult to accurately interpret results regarding afferents recruited by low intensity stimulation (Aβ fibers). Furthermore, based on recording configuration and the focus on DREZ rootlets, most stimulation experiments did not include recordings from the same DR and thereby lacked afferent volleys by which to judge afferent recruitment. It is possible that some Aδ fibers were recruited by 50µs, 50µA stimulation and equally possible that poor suction quality prevented 50µs, 50µA from recruiting any fibers in the trials where no bursts were evoked at this stimulus intensity. Despite these shortcomings, a subset of preparation demonstrated bursting recruited by exclusively Aβ fibers (n = 3). **(Figure 3-3A)**. Examination of high intensity stimulation in the same preparation and recording configuration confirmed exclusive Aβ recruitment by 50µs, 50µA stimulation, as Aδ and C volleys are clearly visible in the same preparation and recording configuration at higher stimulation intensity **(Figure 3-3B)**.

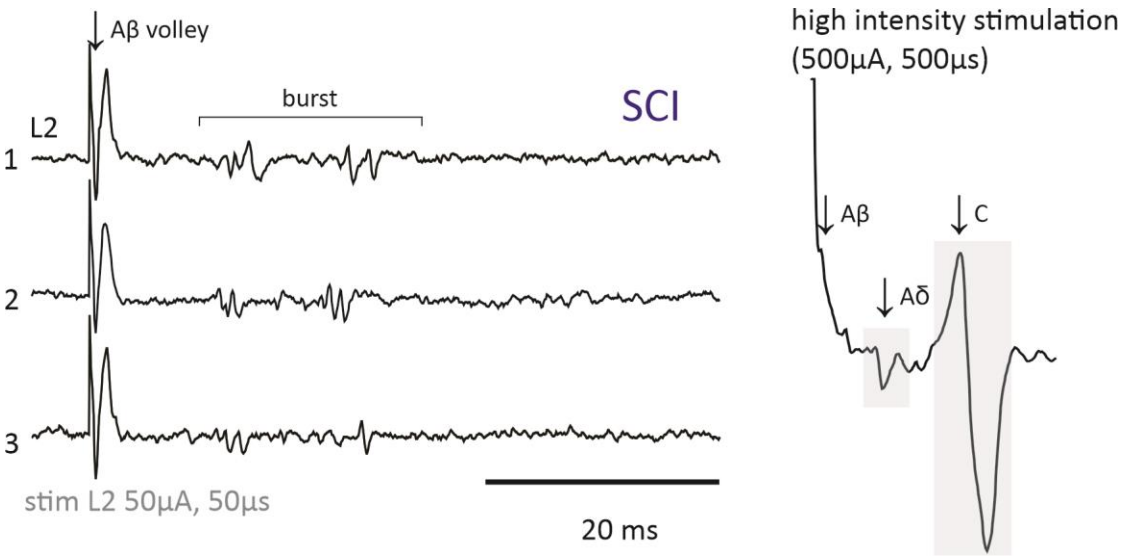

Figure 3-3: Aβ electrical stimulation can evoke bursts

***(A)** Representative traces of low intensity (50µs, 50µA) stimulation recruiting Aβ fibers, as demonstrated by afferent volley. Aβ stimulation evoked bursting. **(B)** Representative example of high intensity stimulation in the same preparation and recording configuration. Electrical stimulation at this intensity recruited Aβ, Aδ, and C fibers, confirming that 50µs, 50µA recruited Aβ fibers. Highlights indicate compound action potentials of labeled afferent fiber types. Time scale is the same as in traces shown to the left.*

3.4.2 Epileptiform bursting occurs along a continuum of hyperexcitability

Next, I sought to determine if Aδ-LTMRs and C-LTMRs could evoke bursts. To study the role of C-LTMRs in SCI bursting, I performed T10 contusion surgeries on a cohort of transgenic Vglut3-ChR2 mice. In this cohort, spontaneous bursting was present in 4/5 SCI preparations and 0/4 sham preparations. The waveform of ectopic bursting was broadly like that seen in the WT cohort reported in Chapter 2 (**Figure 3-4A**). The WT population's spontaneous burst frequency (0.37±0.28 Hz) was like that of the Vglut3-ChR2 population (0.20±0.15Hz), with no statistical

difference between the groups (**Figure 3-4B$_1$**), although some preparations in the WT cohort exhibited notably higher burst frequency and the WT population exhibited a far wider variability in burst frequency (**Figure 3-4B$_1$**). Burst amplitude (**Figure 3-4B$_2$**) and burst duration (**Figure 3-4B$_3$**) were also higher in the WT SCI population compared to the Vglut3-ChR2 population, suggesting greater excitation of afferents during bursts in the WT population. This difference could be reflective of differences in injury severity or location, as I performed Vglut3-ChR2 T10 contusion surgeries and Karmarcha Martin performed T12 contusion surgeries for the initial WT cohort. Although the same contusion impact parameters (50 kD, 0s dwell time) were used, inter-individual differences in surgical technique could account for different outcomes.

Alternatively, differences could be related to the age of the animals at the time of terminal experimentation: the WT cohort animals were aged P310-P640 at time of terminal experiments, while the Vglut3-ChR2 cohort animals were aged P120-P210. In support of age affecting development of bursting, one sham animal from the WT cohort developed mechanical hypersensitivity over time despite a lack of injury (50% PWT of 0.23g at P640 with a baseline 50% PWT of 2.6g at P180) and its spinal cord expressed synchronous bursting (0.12±0.1Hz). While bursting behavior was variable both within and between cohorts, it was always preferentially expressed in SCI animals over sham and naïve animals, suggesting increased spinal hyperexcitability in those animals.

Assessing all SCI and sham preparations with bursting (in the absence of 4-AP or other drug administration) together, there was a moderate correlation between burst frequency and the mean number of spikes per burst (Spearman's Rho = 0.55, p-value = 0.001; n = 33) (**Figure 3-4C$_1$**. Similar correlations existed between burst frequency and amplitude (Spearman's Rho = 0.45, p-value = 0.01; n = 33) (**Figure 3-4C$_2$**) and between burst frequency and duration (Spearman's

Rho = 0.65, p-value < 0.001; n = 33) (**Figure 3-4C$_3$**). These interrelated positive correlations are all consistent with bursting circuitry expressing a gradient of response magnitude associated with varying levels of spinal hyperexcitability, in the present cohorts likely influenced by a combination of injury severity and age.

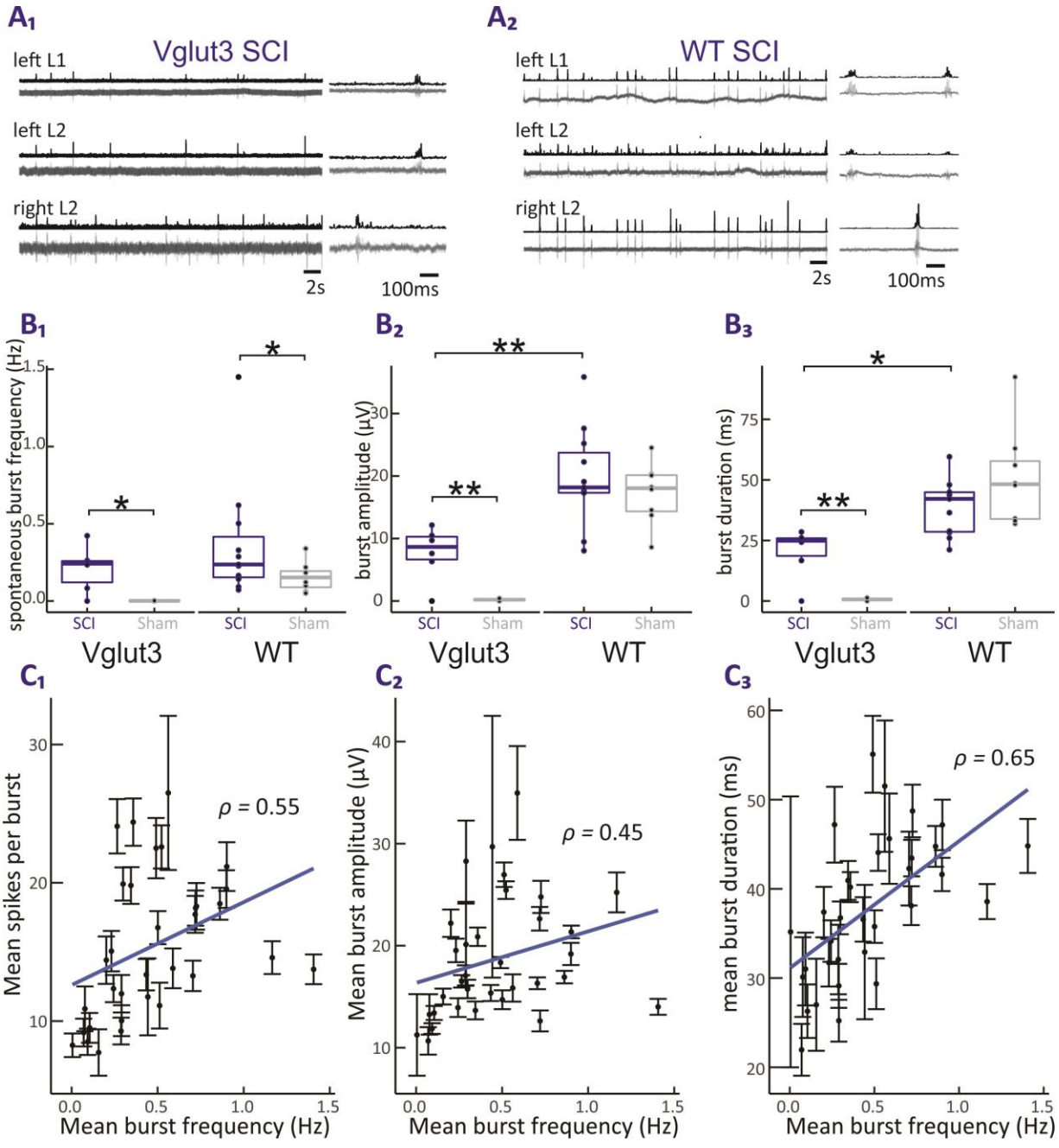

Figure 3-4: Comparison between WT and Vglut:ChR2 SCI cohorts

(A$_1$) *Representative traces from Vglut3-ChR2 preparation. As shown in chapter 2, bursts occurred both independently and synchronously across roots.* ***(A$_2$)*** *Representative traces from WT SCI preparation.* ***(B$_1$)*** *In both cohorts, burst frequency was higher in SCI than sham preparations (Welch's t-test *p<0.05; WT SCI n = 10, WT sham n = 7; Vglut3 SCI n = 5, Vglut3 sham n = 4). There was no significant difference in burst frequency between SCI preparations of each cohort (Wilcoxon rank-sum test p = 0.43)* ***(B$_2$)*** *Burst amplitude was higher in the WT SCI population (18.5 ± 8 µV) than the Vglut3-ChR2 population (7.6 ±4.2 µV). As none of the Vglut3-ChR2 sham preparations exhibited bursting, the SCI burst amplitude was significantly greater than 0 (Welch's t-test **p<0.01).* ***(B$_3$)*** *Burst Duration was higher in the WT SCI population (36 ± 13ms) than in the Vglut3-ChR2 SCI population (20 ± 10ms) (Welch's t-test *p<0.05, **p<0.01). As none of the Vglut3-ChR2 sham preparations exhibited bursting, the SCI burst duration was significantly greater than 0 (Welch's t-test **p<0.01).* ***(C)*** *Correlation plots include sham and SCI animals from both WT and Vglut3 cohorts.* ***(C$_1$)*** *There was a significant correlation between spontaneous burst frequency and the number of individual spike events per burst (Spearmans rho = 0.55, p-value = 0.001; n = 33).* ***(C$_2$)*** *There was a significant correlation between spontaneous burst frequency and burst amplitude (Spearmans rho = 0.45, p-value = 0.01; n = 33).* ***(C$_3$)*** *There was a significant correlation between spontaneous burst frequency and burst duration (Spearmans rho = 0.65, p-value < 0.001; n = 33). Correlation plots in* ***C*** *are shown as mean ± SEM.*

3.4.3 C-LTMR afferent stimulation recruits bursting networks

With the Vglut3-ChR2 SCI cohort, I sought to determine whether C-LTMRs could evoke bursts after SCI. Indeed, when spontaneous bursting was seen after SCI, optical stimulation of Vglut3-ChR2 preparations evoked bursts with comparable appearance to spontaneous bursts (n = 3/3

SCI preparations [some animals in the Vglut3-ChR2 SCI cohort were channelrhodopsin negative] (**Figure 3-5A$_1$**). Similarly, optical stimulation of C-LTMRs evoked bursts after SCI resembled those seen in naïve Vglut3-ChR2 mice given 4-AP (n = 22/22 naïve + 4-AP preparations) or seen spontaneously in this cohort (n=6/6) **(Figure 3-5A$_2$).** In all cases tested, both C-LTMR evoked bursting and coinciding spontaneous bursting was blocked by $GABA_A$ antagonists when tested (n = 12/12), including gabazine as shown in this example (**Figure 3-5A$_2$**).

To probe burst refractory state, I compared bidirectional interactions between spontaneous and evoked bursts after SCI or administration of 10μM 4-AP. Like results with electrical stimulation presented in Chapter 2, optically-evoked stimulation exhibited a bidirectional relationship with spontaneous bursts. (**Figure 3-5B$_1$**). The temporal relationship between evoked bursts and the next spontaneous burst was like that observed with electrical stimulation in Chapter 2, with spontaneous bursting exhibiting a clear refractory period following C-LTMR stimulation (500-700ms) **(Figure 3-5B$_2$,** shown in orange**).** The ability of spontaneous bursts to prevent expression of evoked bursts was limited compared to that seen with electrical stimulation in chapter 2 **(Figure 3-5B$_2$,** shown in blue**)**. These relationships were consistent across all analyzed preparations (n=4). One plausible interpretation of these results is that C-LTMRs evoke bursts through an overlapping, but not identical network to electrical stimulation. Another similar interpretation is that multiple overlapping burst generators receive afferent input and can generate bursts. As subtype-specific optical stimulation would recruit a smaller pool of afferents than electrical stimulation, this would suggest that the electrical stimulation refractory period is based on the overall refractory state of all overlapping burst generators. Evoking a burst with electrical stimulation and following the evoked burst with optical stimulation 50ms later failed to

evoke an optically evoked burst, demonstrating that optical and electrical stimulation share access to common or overlapping burst-generating circuitry with a refractory period (n = 2/2). Taken together, these results support the hypothesis bursts can be recruited through similar and/or overlapping circuitry by various afferent fiber types and modalities.

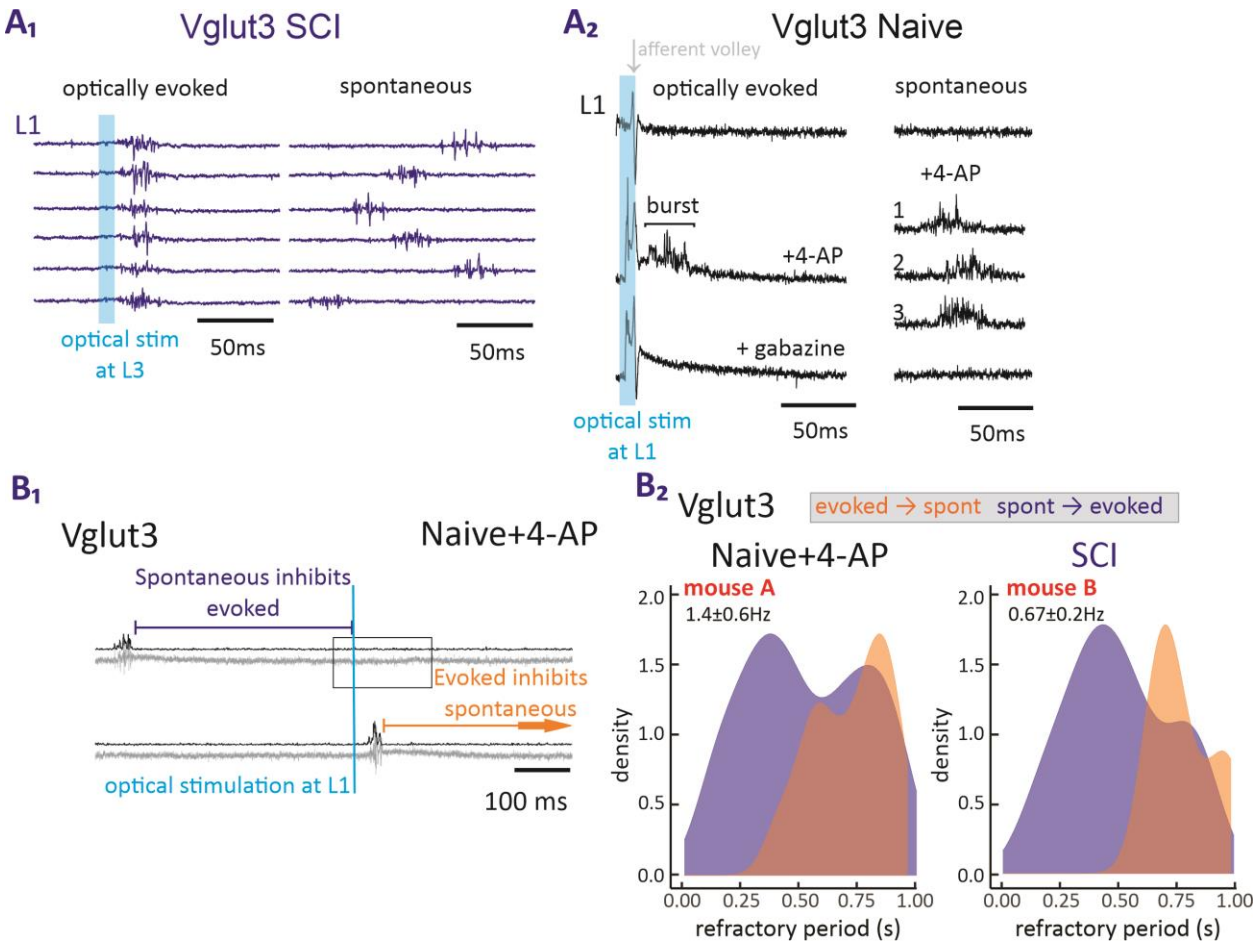

Figure 3-5: Optogenetic stimulation of C-LTMRs evokes bursts.

***(A₁)** Representative recordings from root of SCI Vglut3-ChR2 preparation demonstrates that optically evoked and spontaneous bursts share a stereotyped waveform. Representative example shown of n=3. **(A₂)** Example homonymous optical stimulation of Vglut3-ChR2 naïve preparation at baseline, after 10µM 4-AP, and after 1µM gabazine. At baseline, optical stimulation evoked*

an afferent volley, but no DRP or burst. After 4-AP, optogenetic stimulation evokes bursts and associated DRPs (n = 22). 3 separate examples of spontaneous bursts are shown to the right to compare spontaneous and evoked waveforms. Administration of 1µM gabazine abolished bursting and underlying evoked DRP in this example. Similar blockade was achieved with other GABA receptor antagonists across experiments. (n = 9 bicuculline [10µM], n = 2 picrotoxin [25µM], n = 3 gabazine [1µM]).]). Differing afferent volleys can be attributed to slight changes in optical ferrule positioning during recording. ***(B$_1$)*** *Representative recordings from root of Vglut3-ChR2 preparation after administration of 10µM 4-AP during optical stimulation Relationships between optically evoked and spontaneous bursts are like those observed with electrical stimulation, with spontaneous and evoked bursts reciprocally inhibiting one another within a refractory period.* ***(B$_2$)*** *Density plots quantifying the bidirectional distribution of burst refractory periods between spontaneous and evoked bursts in two mice undergoing 4-AP (10µM) induced bursting with 1.4 and 1.3 spontaneous burst frequencies (bursts plotted: mouse A evoked to spont = 77, spont to evoked = 99; mouse B evoked to spont = 75, spont to evoked = 98).*

3.4.4 Aδ-LTMR afferent stimulation recruits bursting networks

As with C-LTMRs, optical stimulation of Aδ-LTMRs in 4-AP evoked bursts resembling spontaneous bursts after administration of 4-AP (n = 5) (**Figure 3-6A$_1$**). Also similarly, Aδ-LTMR evoked and spontaneous bursts shared a common and stereotyped waveform. Comparing bidirectional interactions between spontaneous and evoked bursts after administration of 10µM 4-AP (n=4) **(Figure 3-6A$_2$,** shown in orange**)**, the temporal relationship between evoked bursts and the next spontaneous burst was similar to that observed with electrical stimulation in Chapter 2 (500-700ms) and to that observed between C-LTMR evoked and spontaneous bursts **(Figure 3-6A$_3$**, shown in blue**).** As with C-LTMR stimulation, the effect of spontaneous bursts on

subsequent evoked bursts exhibited a broader distribution than seen with electrical stimulation, demonstrating that Aδ-LTMR stimulation may also be able evoke bursts earlier than electrical stimulation following a spontaneous burst. Together, these results suggest that Aδ-LTMR and C-LTMR afferent stimulation evoked bursts have a stronger effect on the spontaneous bursting network than the network has on Aδ-LTMR and C-LTMR afferent stimulation evoked bursts. Both tested LTMR populations, as well as general Aδ and C fiber populations as tested with electrical stimulation **(Figures 2-4 and 2-6)**, share access to burst-generating interneuron circuitry, but demonstrate differing interactivity with spontaneous bursting, suggesting that perhaps bursts are evoked by discrete but overlapping generator networks.

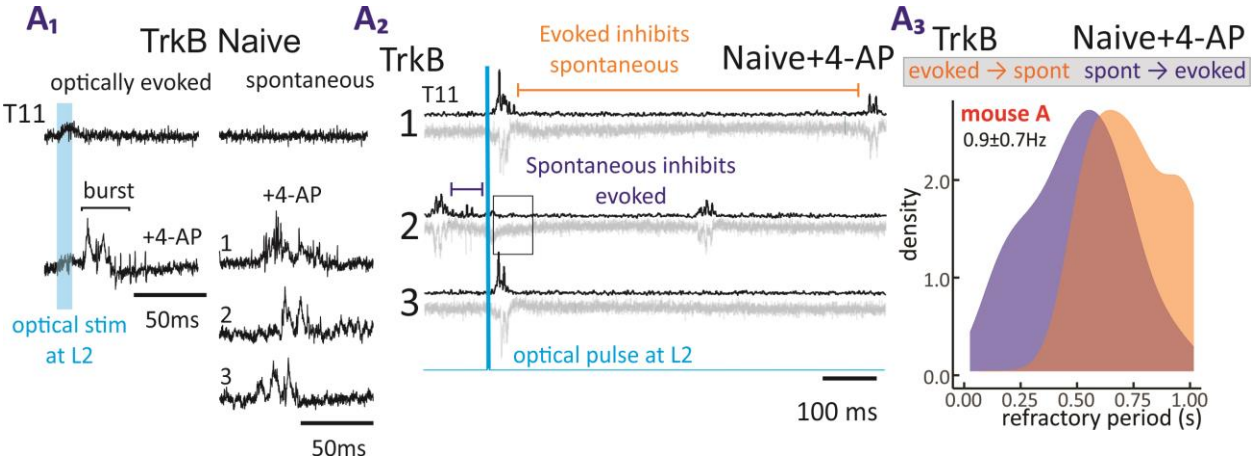

Figure 3-6: Aδ-LTMRs recruit burst circuitry.

***(A₁)** Representative recordings from root of TrkB-ChR2 preparation after administration of 10μM 4-AP. Three separate examples of spontaneous bursts are shown to the right to compare spontaneous and evoked waveforms and demonstrate variability between waveforms. **(A₂)** Relationships between optically evoked and spontaneous bursts are like those observed with electrical stimulation, with spontaneous and evoked bursts reciprocally inhibiting one another within a refractory period. Numbers differentiate traces and do not correspond to numbers in A₁.*

(A_3) *Density plots quantifying the bidirectional distribution of burst refractory periods between spontaneous and evoked bursts in one mouse undergoing 4-AP (10μM) induced bursting with 0.9Hz spontaneous burst frequency (bursts plotted: mouse A evoked to spont = 102, spont to evoked = 27).*

3.4.5 Bursting recruits spiking in C-LTMR and Aδ-LTMR afferents

After establishing that Aδ- and C-LTMR optical stimulation could evoked bursts, I sought to determine whether bursts propagated through these afferents. To assess whether these LTMRs were recruited by bursts, I performed a series of collision experiments with Vglut3-ChR2 (n = 3) and TrkB-ChR2 (n = 2) transgenic animals. Experiments were performed either in SCI animals with bursting or by inducing bursting with 10μM 4-AP. Briefly, optically evoked afferent volley amplitude was measured while bursting was evoked by electrical stimulation of an adjacent root. Optical stimulation time was invariant, while burst-evoking stimulation was given with varying timing. With proper timing and involvement of C-LTMR or Aδ-LTMR fibers in the burst, the optical volley would occur during the burst refractory period, resulting in a reduced or ablated afferent volley in response to optical stimulation **(Figure 3-7A).** The difference in timing between burst and optically evoked afferent volley was measured as the difference between the onset of the evoked burst and the time of optical stimulation (a value of 0 indicates perfect alignment between burst start and optical stimulation).

Trials were considered to exhibit collision when the measured afferent volley amplitude was less than 75% of the maximum amplitude measured during the same recording. This cutoff was based on control baseline recordings where consecutive optical stimuli were given without electrical stimulation (**Figure 3-7B$_{1,2}$**). With proper timing between burst generation and optical

stimulation, optically evoked afferent volleys were successfully reduced in amplitude, demonstrating that Aδ-LTMR **(Figure 3-7C$_1$**, n = 2 preparations, 7 technical replicates**)** and C-LTMR **(Figure 3-7C$_2$**, n = 3 preparations, 8 technical replicates**)** afferents are directly recruited by evoked bursts. The variation in successful collision timing between experiments can likely be accounted for by differences in DR lengths and variations in conduction velocity **(Figure 3-7D$_{1,2}$)**, especially in C-LTMR experiments, as they are slowly conducting. Note that x-axis values in these plots represent the time of burst onset, not the time of stimulation. Negative values indicate that the optically evoked volley occurred during the burst. These results indicate that bursts recruit both Aδ-LTMRs and C-LTMRs, suggesting that bursts are propagating Aδ- and C-LTMRs.

A limitation of this approach is that it only allowed analysis of interactions between electrically evoked and optically evoked bursts. The afferent makeup of spontaneous bursts is unaddressed by this technique, although the refractory period between electrically-evoked bursts and spontaneous bursts suggests similarity in at least underlying burst generation circuitry. Although it would take many trials of recording to achieve proper timing, future work should attempt to use collision testing to determine whether spontaneous bursts also recruit Aδ-LTMRs and C-LTMRs.

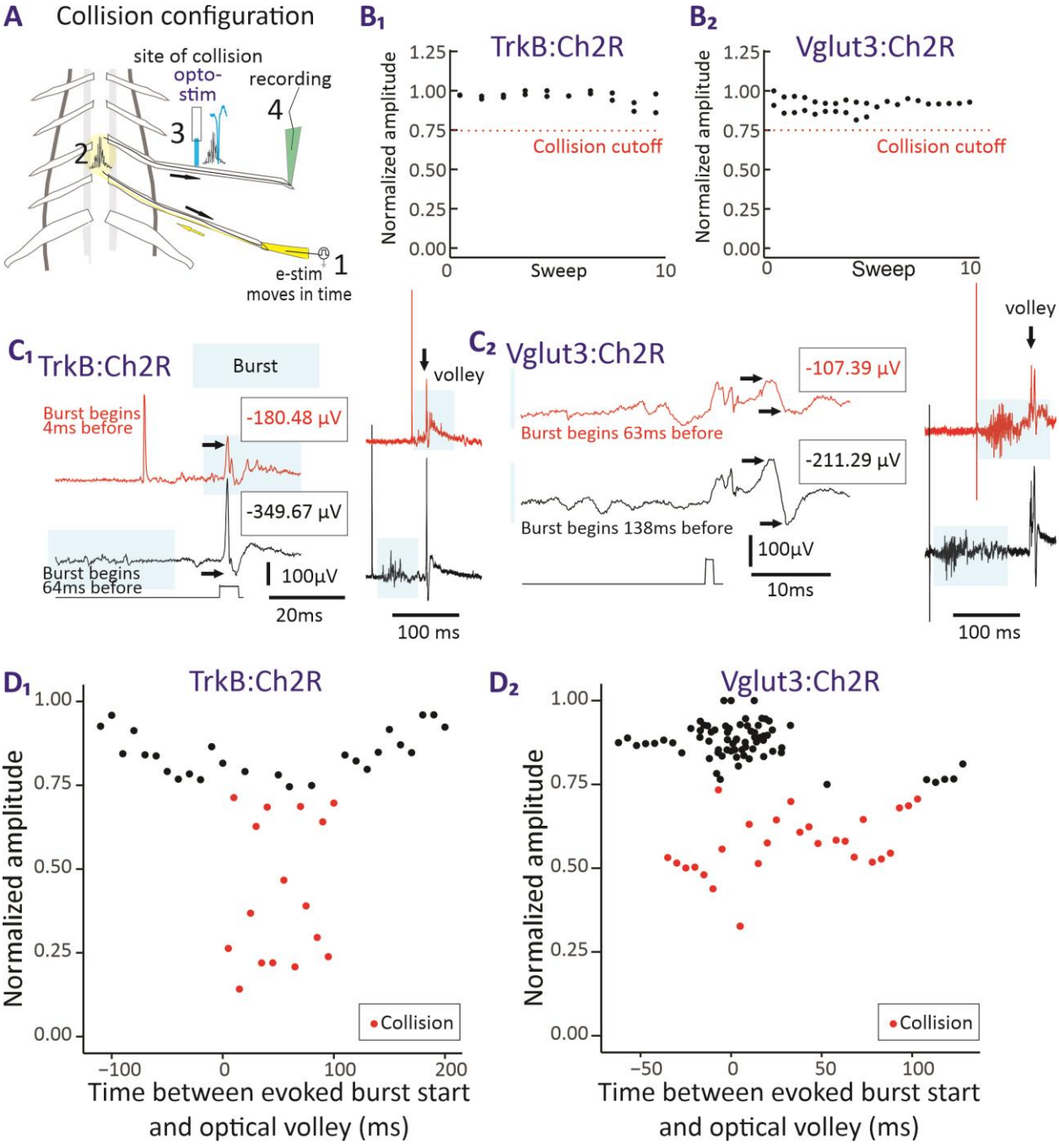

Figure 3-7: Collision testing results

***(A)** Diagram of recording configuration for collision testing. Electrical stimulation on a root **(1)** evokes a burst that propagates to nearby roots **(2)**. Laser optical stimulation is placed on a root heteronymous to stimulation **(3)** between the cord and a recording electrode placed at the distal*

*end of this root **(4)**, which records antidromic volleys evoked by optical stimulation. Optical stimulation is given at a constant time while electrical stimulation evokes a burst with varying timing. With proper timing, optical stimulation occurs during the refractory period induced by an electrically evoked burst and the antidromic volley is smaller in size. **(B_1)** Optogenetic stimulation of TrkB:-ChR2 preparations at the same frequency as collision testing shows little variation in optically-evoked volley (minimum normalized volley amplitude = 0.86, or 14% lower amplitude than maximum amplitude). Control was repeated for each preparation. **(B_2)** Similarly, optically evoked volleys in Vglut3-ChR2 preparations show little variation over time (minimum normalized volley amplitude = 0.81, or 19% lower than maximum amplitude). Control was repeated for each preparation. **(C_1)** Example of collision in a TrkB:-ChR2 animal. Right: compressed view of burst and volley demonstrates burst waveform and relative arrival time. **(C_2)** Example of collision recording in a Vglut3:-ChR2 animal. Note that in both cases, bursting occurs earlier in the trace than is shown. Right: compressed view of burst and volley demonstrates burst waveform and relative arrival time. **(D_1)** Collision timing in TrkB-ChR2 experiments (n = 2 preparations, 7 trials). Times represent time between start of burst and optical stimulation. **(D_2)** Collision timing in Vglut3-ChR2 experiments (n = 3 preparations, 8 trials). Times represent time between onset of burst (not time of electrical stimulation) and optical stimulation.*

3.4.6 Insights into synaptic organization of burst generation

Earlier experiments with glutamate receptor and $GABA_A$ receptor block demonstrated the necessity of synaptic transmission through $GABA_A$ receptors and the facilitatory role of glutamate receptors in bursting. To elucidate the more general synaptic interconnectivity necessary for spontaneous and afferent evoked bursting. I used a *high* Mg^{2+}/*high* Ca^{2+} [Mg^{2+}

13.3mM] [Ca^{2+} 3.8mm]) [297] to suppress di- and tri-synaptic transmission and a high *Mg^{2+}/low Ca^{2+}* ([Mg^{2+} 13.3mM] [Ca^{2+} 1.1mM]) solution to suppress all synaptic transmission [41].

Interestingly, the *high Mg^{2+}/high Ca^{2+}* solution greatly reduced 4-AP burst frequency (n=4/4), but did not abolish bursting, except in one preparation (n=1/4) (**Figure 3-8A$_{1,2}$**). Additionally, bursts could still be evoked by electrical stimulation in the preparations where bursting was not completely abolished (n=3/4). **(Figure 3-8A$_3$)**. One interpretation of these results is that interneurons underlying bursting receive sufficient monosynaptic input from primary afferents to evoke bursting by a non-synaptic mechanism [60]. More likely, evoked burst circuitry is minimally monosynaptic, with synchronous afferent input onto interneurons offering sufficient drive to be capable of recruiting GABAergic interneurons, which in turn have sufficient drive to evoke bursting by monosynaptic actions on afferents. Direct reciprocal connectivity could still enable disynaptic actions [60]. The most plausible explanation of spontaneous bursting is that ectopic bursts arise monosynaptically from bursting GABA interneurons. The reduction of burst frequency in *high Mg^{2+}/high Ca^{2+}* solution is consistent with burst-generating interneurons receiving additional drive from polysynaptic pathways, which, given the known reduction in bursting with glutamatergic blockers, would include excitatory glutamatergic transmission. This is consistent with the reduction in burst frequency and synchrony following glutamatergic block in Chapter 2 **(Figure 2-9)**. Unfortunately, available recordings did not allow analysis of burst synchrony in *high Mg^{2+}/high Ca^{2+}* solution due to low n (n = 2).

A *high Mg^{2+}/low Ca^{2+}* solution was used to suppress synaptic transmission [60, 214]. Using this solution, all spontaneous and evoked bursting was blocked (n=4/4) (**Figure 3-8$_{B1,2}$**), demonstrating that synaptic transmission is necessary for burst generation, consistent with the

previously shown reliance on GABAergic synaptic transmission (Chapter 2). A graphical summary of these results can be found in the discussion section of this chapter.

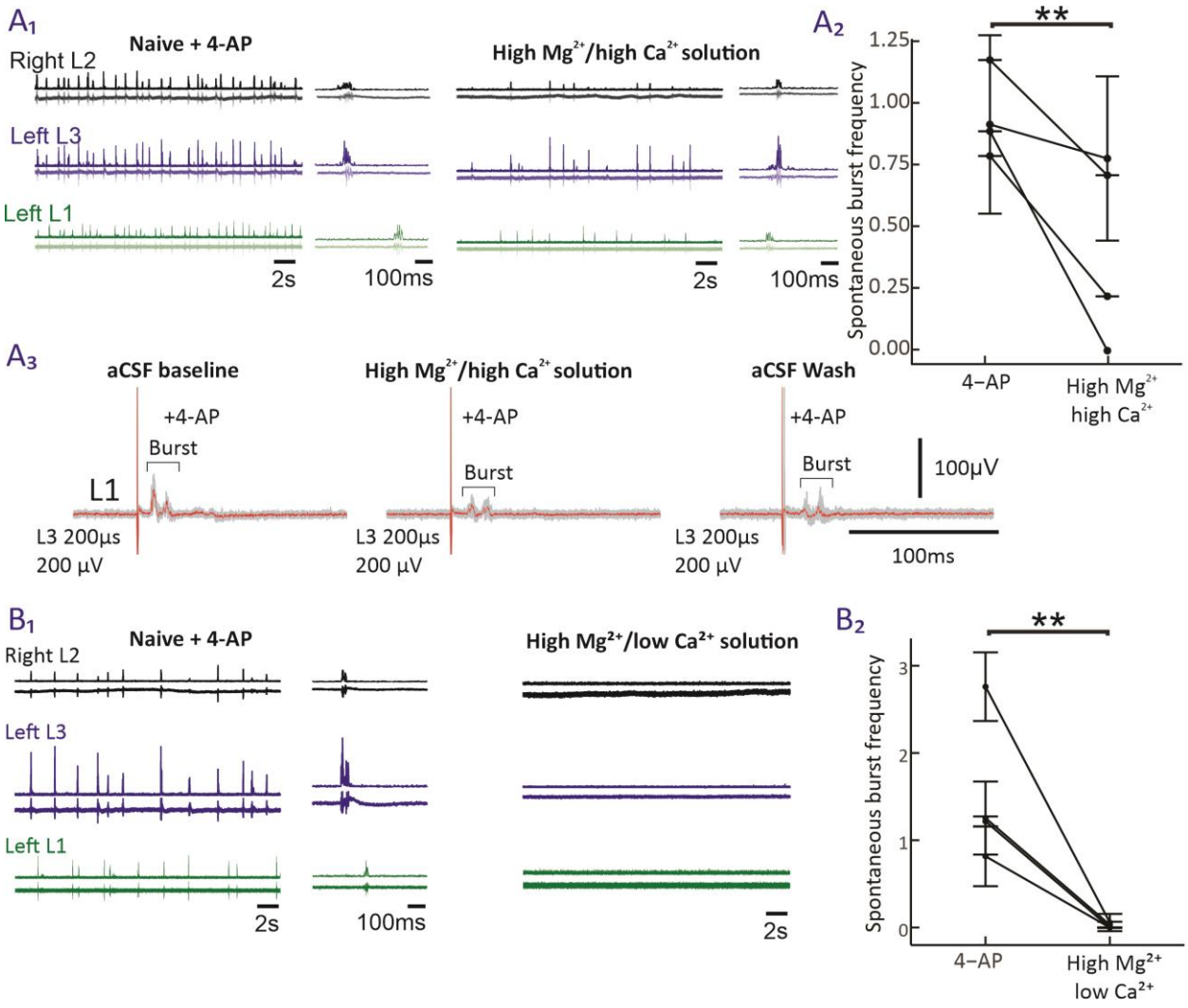

Figure 3-8: Evidence of monosynaptic burst generation

***(A₁)** After administration of 10µM 4-AP to induce bursting, replacement of aCSF with high Mg^{2+} high Ca^{2+} solution reduces burst frequency but does not abolish bursting. **(A₂)** high Mg^{2+} high Ca^{2+} solution significantly reduces burst frequency (Paired t-test p-value = 0.009, n = 4; 4-AP = 0.88±0.15 Hz, high Mg^{2+} high Ca^{2+} solution = 0.4±0.45 Hz [mean ±sd]). **(A₃)** While in high Mg^{2+} high Ca^{2+} solution, bursts can still be evoked by electrical stimulation multiple roots away*

from recording site (stimulation at L3, recording at L1). ***(B$_1$)*** *After administration of 4-AP to induce bursting, replacement of aCSF with high Mg^{2+} low Ca^{2+} solution solution completely abolishes bursting.* ***(B$_2$)*** *Bursting is abolished by high Mg^{2+} low Ca^{2+} solution (Paired t-test p-value = 0.009; 4-AP = 1.5±0.8 Hz, high Mg^{2+} low Ca^{2+} solution = 0.02±0.02 Hz [mean ±sd]). Data from ¾ animals was recorded by Shaquia Idlett.*

3.4.7 Extrasynaptic GABAergic modulation

Given the demonstrated critical role of $GABA_A$ receptors in burst generation, I sought to determine whether the role of GABA was entirely synaptic or included extrasynaptic components. The $GABA_A$ α-5 subunit is expressed at extrasynaptic sites in the dorsal horn and primary afferents and modulates tonic GABAergic tone [39, 298, 299]. The $GABA_A$ α-5 subunit selective channel blocker L655, 708 (an inverse agonist) moderately but significantly reduced burst frequency, but not amplitude, in 5/6 preparations tested **(Figure 3-9A$_1$, 3-9A$_2$)**. The lack of change in burst amplitude is not consistent with recent work suggesting that tonic extrasynaptic GABA receptors facilitate Aβ afferent transmission across branchpoints [178]. That L655, 708 decreased frequency is consistent with a role of decreasing the excitability of GABAergic burst-evoking interneurons. Overall, these results suggest that extrasynaptic $GABA_A$ receptors are not critical for burst generation but can play a role in frequency modulation through actions on spinal interneurons.

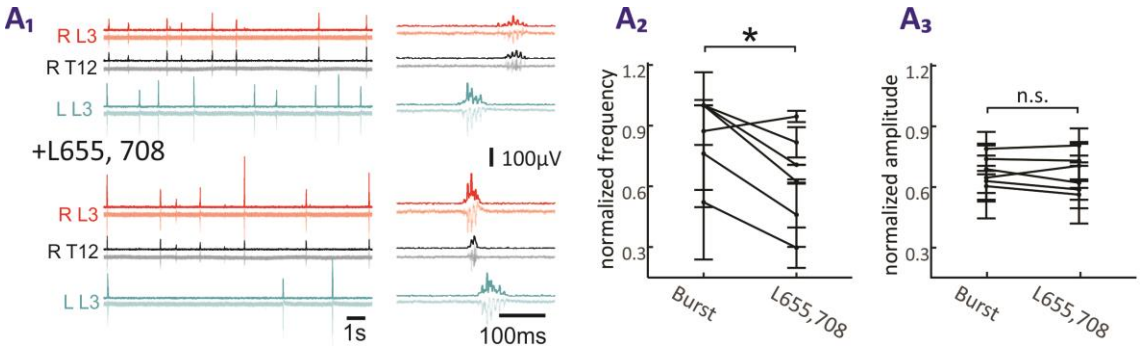

Figure 3-9: Evidence of extrasynaptic $GABA_A$ receptor modulation of bursting

***(A_1)** Representative example of three roots recorded from a single naïve + 10μM 4-AP preparation before and after administration of 10 μM L655, 708. **(A_2)** L655, 708 significantly reduced normalized burst frequency in the tested preparations (n=6) (paired t-test, t= 3.39, df = 5, p-value = 0.019; Burst = 0.88±0.19Hz, L655,708 = 0.64±0.24 Hz [mean±sd]). **(A_3)** L655,708 had no significant effect on burst amplitude, as measured by normalized average peak amplitude during burst event (n=6) (Burst = 0.59±0.08μV, L655,708 = 0.58±0.11μV [mean±sd]).*

3.4.8 Bursting and involvement of dorsal horn circuitry

To elucidate burst generation and propagation through dorsal horn circuitry, recordings were performed in Lissauer's Tract (LT), which carries long range Aδ collaterals, likely including Aδ-LTMRs (unpublished histology data from Garraway lab showing expression of Aδ-LTMR axons in LT, unpublished optogenetic electrophysiology data from Dr. Shaquia Idlett recording TrkB:ChR2 afferent volleys in LT) and shorter-range projections of C-fibers, as well as axons of superficial dorsal horn interneurons [16, 214]. Dual recordings of DREZs and LT revealed coordinated spiking activity between LT and nearby DREZs, suggesting burst propagation through LT-projecting afferent and/or interneuron axons (n = 4) **(Figure 3-10A_1)**. More interestingly, recordings also included bursting events in LT that did not coordinate with nearby DREZs, consistent with direct recording of superficial dorsal horn interneuron activity organized into a bursting pattern (n = 4) **(Figure 3-10A_2)**. This represented the first direct evidence in this work that superficial dorsal horn interneurons themselves exhibit bursting, consistent with the hypothesis that bursting of these neurons underlies the afferent bursting recorded in DREZs.

To determine whether bursting exerted reentrant actions on superficial dorsal horn interneuron circuitry, extracellular recordings on DREZs were performed simultaneously with EFP recordings of superficial dorsal horn at a depth consistent with lamina II (~90μM below LT) (n = 7; 5 experiments performed by Shaquia Idlett). EFP recordings capture synchronous electrical changes in neurons nearby the recording electrode, in this case interneuron networks in lamina II, which is comprised of a wide variety of interneurons responsible for somatosensory processing, including processing of pain information [17, 171, 300, 301]. As burst-generating circuitry would be in its refractory period immediately following a burst event, assuming recruited Aδ and C afferents feed back onto the same population of interneurons, EFP recordings at this depth would be expected to consist of only subthreshold population EPSPs (i.e. EFPs). Indeed, EFP recordings revealed subthreshold potentials following bursts in nearby DREZs (n=7) **(Figure 3-10B)**, consistent with the hypothesis that ectopic bursts propagate orthodromically into the spinal cord and exert synaptic actions on superficial dorsal horn networks responsible for burst generation. While the recordings demonstrated subthreshold EFPs, some spiking activity also followed bursts **(Figure 3-10B expanded example)**, consistent with reentrant propagation involving actions on both burst-generating circuitry (subthreshold) and interneuron populations not involved with burst generation (spiking).

Given evidence of reentrant actions of bursting, I sought to determine whether burst circuitry also activated other neurons, particularly excitatory superficial dorsal horn neurons associated with recruitment of pain circuitry, I performed Fos histology experiments as an indicator of activity on 4-AP treated and control spinal cords (n = 2 in each condition). These experiments, which labeled Fos on lamina I neurokinin 1 receptor (Nk1R) cellular internalization, supported

recruitment of pain-encoding spinal neurons during bursting after 4-AP administration compared to non-bursting controls **(Figure 3-10C$_{1,2}$)** [269, 291].

Together, these results suggest that ectopic bursts are evoked by bursting of superficial dorsal horn interneurons and that orthodromically propagating bursts recruit superficial dorsal horn circuitry through re-entrant actions. Based on histology results, these actions include activation of spinal neurons implicated in nociception, which would include lamina I ascending tract neurons encoding pain [269].

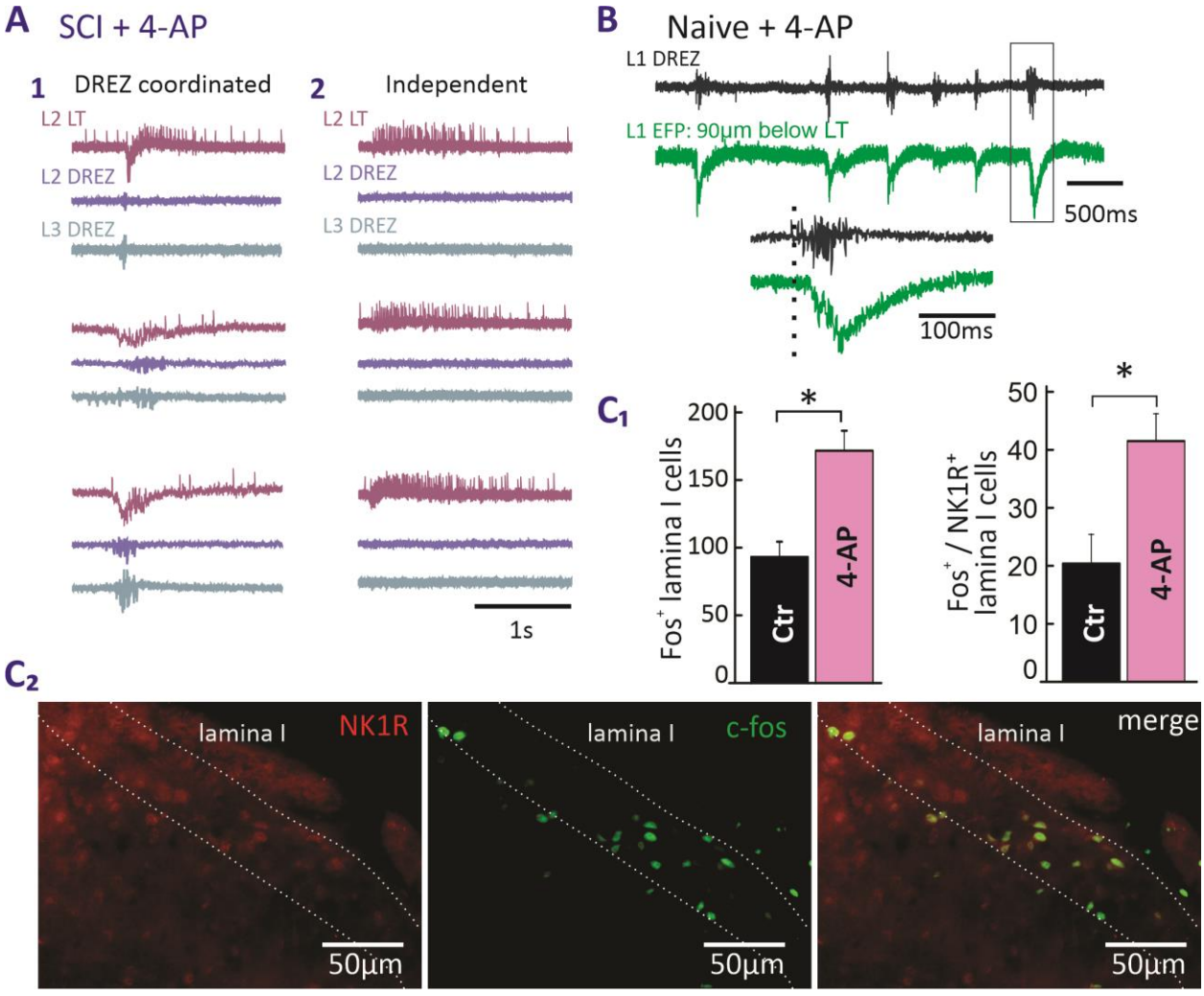

Figure 3-10: Evidence that bursts propagate orthodromically for reentrant effects

(A$_1$) *Example of spontaneous bursting extracellular recordings of L2 LT, L2 DREZ, and L3 DREZ reveal coordinated bursting between LT and nearby DREZs. Synchronous activity between LT and DREZ was recorded in four preparations. Two of those experiments included clear examples of independent LT bursting as shown here.* ***(A$_2$)*** *Recordings of the same locations in the same preparation as A$_1$ also reveal bursting events occurring exclusively in LT, not nearby DREZs, implicating bursting of superficial dorsal horn interneurons. 4 experiments were performed with similar results.* ***(B*** *Example of coordination between DR bursts and superficial dorsal horn EFPs in a 4-AP preparation. As EFP events are subthreshold, they likely represent re-entrant actions from orthodromically propagating bursts. 7 experiments were performed with similar results. Expanded example below demonstrates the temporal delay between recorded DREZ burst and EFP onset and highlights spiking overlying the low frequency EFP event.* ***(C$_1$)*** *4-AP increased the number of Fos+ neurons in lamina I ($p<0.001$) with greater than double expression in neurons with NK1 receptor internalization ($P<0.005$) (n=2 mice each). Values are averages per 20µm section.* ***(C$_2$)*** *Example images from 4-AP-treated spinal cord section demonstrate co-expression of Fos and NK1R and internalization of NK1R in Fos+ neurons. Brightness and contrast increased equivalently in all panels to improve NK1R staining visibility.*

3.4.9 Spinally driven bursts propagate to the cutaneous periphery

Previous work suggests that DRRs, and therefore presumably ectopic bursts, propagate to the periphery, where cutaneous mechanoreception could be altered by afferent-driven release of inflammatory and other factors [45, 49]. To assess whether bursts propagated to the periphery, I used 4-AP to induce bursting in a deeply anesthetized *in vivo* preparation while recording dissected dorsal cutaneous nerves in the cutaneous periphery **(Figure 3-11A$_1$**; (n=3)**)**. Emergent epileptiform bursts were observed with maintained waveform and synchrony across dermatomes

(Figure 3-11A$_{2,3}$). Dual electrode recordings from a single dorsal cutaneous nerve demonstrated that the fastest conducting afferents were Aδ fibers (3±2.5ms at 36 ˚C; n = 2 preparations). Dual in-vivo recording of a dissected dorsal cutaneous nerve and undissected hindpaw plantar surface with a sharp electrode revealed synchronous bursts in both locations (n = 2) **(Figure 3-11B)**. Similar recordings were also obtained from undissected dorsal truncal skin and tail skin (data not shown), indicating that bursting propagates to small branches of cutaneous nerves throughout the periphery, not just dorsal cutaneous nerves. This result suggested that bursting can be detected with relatively noninvasive recordings in-vivo.

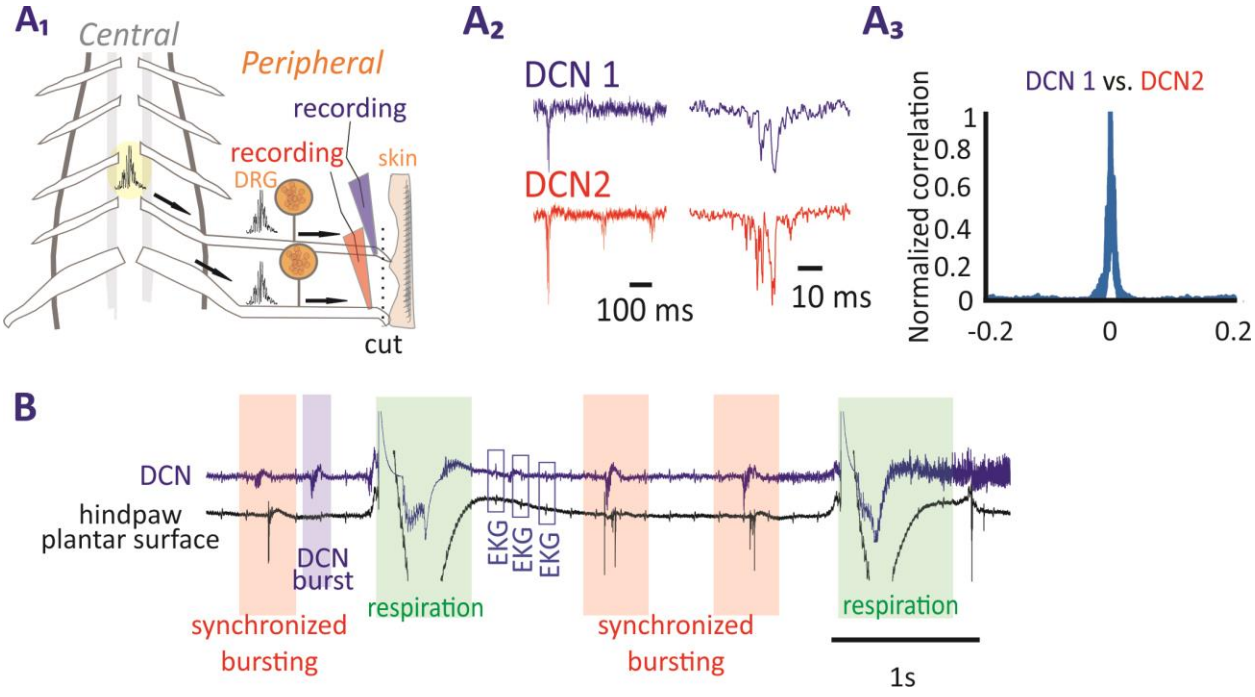

Figure 3-11 Peripheral propagation of bursts at physiological temperature

***(A$_1$)** Dorsal cutaneous nerves were dissected as peripherally as possible to allow recording from cutaneous periphery during bursting. **(A$_2$)** Administration of 4-AP in-vivo induces synchronous epileptiform bursts that can be recorded from adjacent dorsal cutaneous nerves (n = 2). **(A$_3$)** 4-AP induced synchronous bursts occur with no lag, indicating that they occur simultaneously*

across nerves. ***(B)*** *Dual in-vivo recording from dissected dorsal cutaneous nerve and undissected hindpaw plantar surface reveal synchronized bursting in the two recording locations (highlighted in orange). Other events captured were associated with respiration and heartbeat (EKG).*

To determine whether bursts could alter mechanoreceptor function in the cutaneous periphery, I sought to recapitulate spinal bursting activity in the *ex vivo* skin nerve preparation (see methods section of this chapter for detailed description). Dorsal cutaneous nerves were recorded en-passant to track afferent volleys **(Figure 3-12A)** and air-evoked recruitment of afferent spiking responses to 20 mN air stimulation, which robustly recruits a variety of LTMRs [9] **(Figure 3-12B)**. Antidromic stimulation parameters were based on recordings of spinal afferent bursting. After a series of baseline air pulse responses were recorded en-passant from dorsal cutaneous nerves (sweeps of 5 second 20mN air pulse, followed by 5 seconds of no stimulation), the cut ends of dorsal cutaneous nerves were stimulated once every second with 100ms of a 100Hz pulse train (for a total of 10 electrical stimuli) for one minute of 50μA 50μs (Aβ and Aδ fiber recruitment), 100μA 100μs (Aβ and Aδ fiber recruitment), or 200μA 200μs (Aβ, Aδ, and C fiber recruitment) positive polarity electrical stimulation. Immediately following stimulation, ongoing sweeps of air pulse stimulation were resumed.

When stimulated at 200μA 200μs intensity (sufficient to recruit C fibers **(Figure 3-12C$_1$)**, the total number of spikes recruited by innocuous air pulse stimulus was reduced **(Figure 3-12C$_2$)** without a corresponding change in afferent volleys **(Figure 3-12C$_3$)**, suggesting that changes were not due to reduced afferent conduction. This change persisted for ~5 minutes post-stimulation **(Figure 3-12D$_1$)** before recovering to baseline response. Stimulation at equivalent frequency at lower electrical stimulation intensities had no effect on spike recruitment **(Figure 3-**

12D2). Together, these results suggest that changes in response to air stimulation are due to alterations at the receptor rather than changes in axonal conduction and are consistent with the hypothesis that ongoing spinal bursting in C but not Aδ fibers could perturb peripheral mechanosensitivity through antidromic actions in the cutaneous periphery.

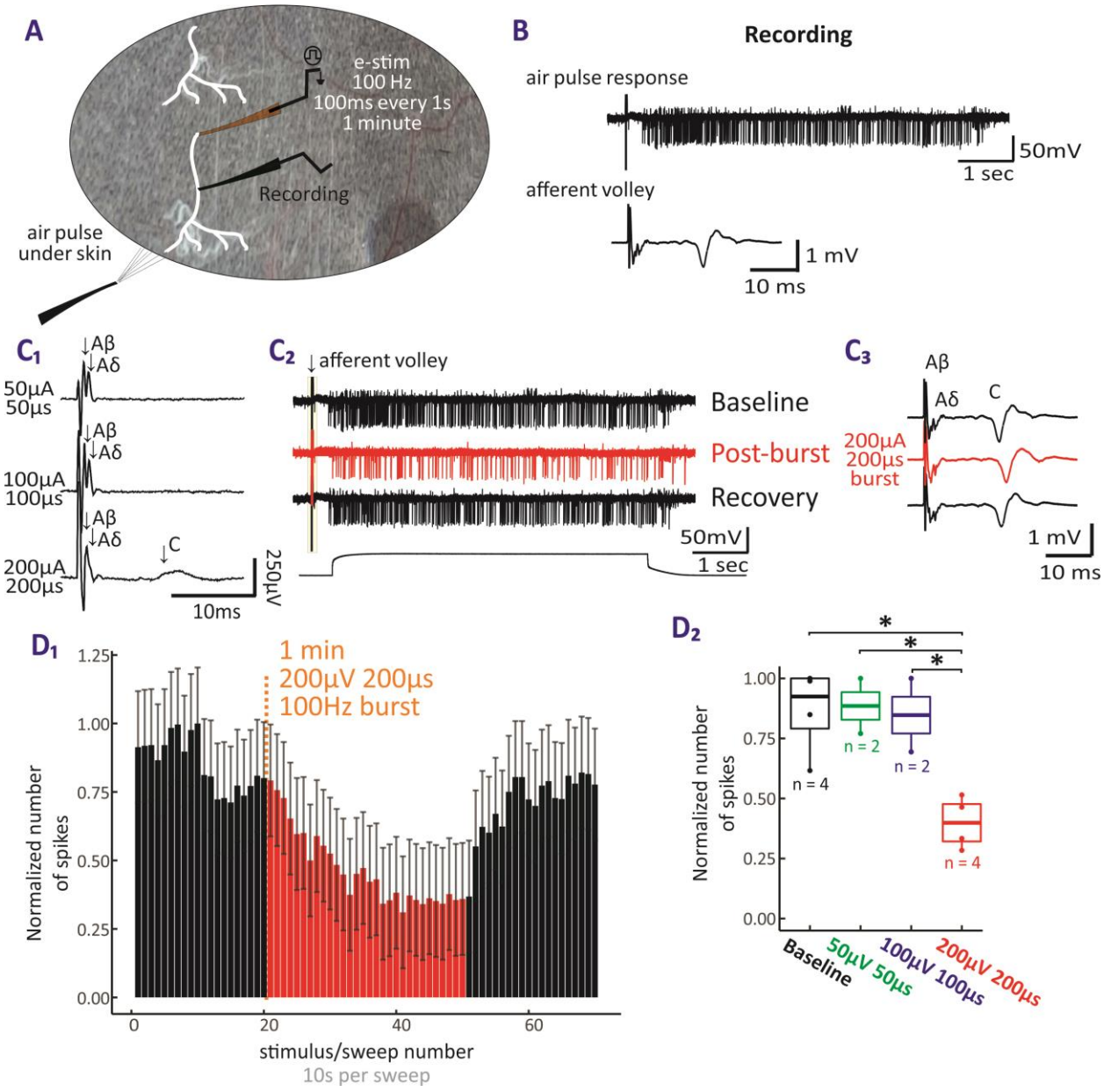

Figure 3-12 Antidromic stimulation reduces cutaneous mechanosensitivity

(A) *Diagram of recording configuration: a dorsal cutaneous nerve was electrically stimulated with pulse trains matching recorded burst fiber recruitment, burst frequency, and spike frequency (100ms, 100 Hz pulse train delivered once per second for one minute).* ***(B)*** *Representative traces of air pulse stimulation and electrical stimulation volleys recorded en-passant at baseline.* ***(C_1)*** *Representative afferent volleys demonstrate that 200µA, 200µs stimulation recruits Aβ, Aδ, and C fibers, while 50µA, 50µs and 100µA, 100µs stimulation recruit Aδ and Aβ fibers, but not C fibers.* ***(C_2)*** *Representative traces of air pulse stimulation recording at baseline, immediately following 200µA, 200µs 100Hz antidromic stimulation, and after return to baseline response.* ***(C_2)*** *Electrically evoked volleys did not alter in amplitude, waveform, or latency during successive trials, suggesting that alterations were not due to changes in conduction properties.* ***(D_1)*** *Normalized number of spikes recorded during air pulse stimulation either at baseline, after high frequency antidromic stimulation, or during post-stimulation recovery (n = 4 preparations). Each stimulus represents 10 seconds of recording.* ***(D_2)*** *Normalized number of spikes recruited by air pulse stimulation following 100Hz stimulation of listed intensity. 200µA, 200µs stimulation reduced the number of recruited units compared to all other conditions (* Welch's t-test p-value < 0.05, n's shown in plot; Baseline = 0.86±0.18, 200µV, 200µs stimulation = 0.40±0.1).*

3.5 Discussion

In Chapter 2, I demonstrated that the dorsal horn expresses an epileptiform and degenerate circuit that manifests as ectopic bursting in primary afferents. In the current chapter, I used transgenic and pharmacological approaches in the ex vivo intact spinal cord to better understand afferents' involvement in epileptiform bursting and to explore the interneuron networks and basic synaptic organization of the circuitry underlying bursting. I demonstrated that epileptiform

bursting circuitry allows multimodal interactions between afferents, specifically that Aβ fibers could recruit bursting in Aδ and C fibers and that C-LTMRs could recruit DRPs and DRRs in SCI and 4-AP conditions, which they were previously shown to be unable to do in physiological conditions [42]. $GABA_A$ receptor antagonists completely blocked C-LTMR bursting, but were not tested with Aδ-LTMR bursting. I also demonstrated that bursting occurs along a continuum associated with underlying hyperexcitability, can be generated monosynaptically via conversion of superficial dorsal horn interneurons to a bursting phenotype, and exerts reentrant effects on spinal circuitry as well as antidromic effects in the cutaneous periphery.

Bursts are evoked by multiple afferent fiber types

Although conduction velocity measurements indicated that bursts propagate through Aδ and C fibers **(Figure 3-2)** and Aδ and C fiber intensity stimulation always recruited bursts in SCI and 4-AP preparations, electrical stimulation experiments indicated that Aβ afferents were also able to recruit bursts in conditions of SCI or 4-AP evoked bursting **(Figure 3-3)**. These results suggest that bursting is a mechanism of multimodal afferent interactivity mediated through common or overlapping bursting dorsal horn circuitry. Experiments testing optogenetic stimulation of Aδ- and C-LTMRs demonstrated that they too evoke bursts after SCI or administration of 4-AP. Together, these experiments demonstrated that bursts could be evoked by a wide variety of afferents, including Aβ fibers and Aδ- and C-LTMRs. Given that Aβ and Aδ-LTMR afferents form synapses onto interneurons normally responsible for PAD [17], the fact that they are both able to evoke bursts is expected given our model of dorsal horn circuitry generating bursts through interneurons responsible for PAD and DRRs. However, the fact that C-LTMRs evoked bursts and PADs after SCI or administration of 4-AP **(Figure 3-5A$_2$)** was surprising, given that previous researchers reported that these afferents are unable to produce

DRPs [42]. Based on results presented here, C-LTMRs are able to recruit PAD and bursts state-dependently, but it remains unclear whether they do so through the same synaptic interconnectivity as Aβ and Aδ fibers. Future work should establish whether synaptic suppression experiments exhibit similar effects on bursts evoked by electrical, Aδ-LTMR optogenetic, and C-LTMR optogenetic stimulation.

Epileptiform bursting occurs along a continuum of hyperexcitability

Results presented here, including the correlation between severity of mechanical hypersensitivity and burst frequency (**Figure 2-2C**), and correlations between burst frequency and burst amplitude and duration (**Figure 3-4C**), suggest that bursting behavior manifests along a gradient associated with underlying circuit hyperexcitability. Interpreted in relation to the observed dose-dependent effect of 4-AP on burst frequency (**Figure 2-5A$_1$**), these results suggest that bursting behavior occurs on a continuum, ostensibly based on the level of underlying circuit hyperexcitability. In the cohorts discussed here, these differences in hyperexcitability are likely based on injury severity and age. With this hypothesis, progressive increases in excitability would express a gradient of circuit phenotypes, beginning with slow frequency and low amplitude bursting that can be evoked with afferent stimulation but rarely presents spontaneously. Next, more frequent, and more synchronous bursting would arise from higher frequency bursting in GABAergic interneurons, which would increase amplitude in recorded DRs, as more afferents would be recruited and DRPs would feasibly be larger with greater GABAergic drive. Increased ectopic afferent burst duration and amplitude would be expected to arise from stronger GABAergic synaptic drive via $GABA_A$ receptors, either by increasing the number of GABAergic interneurons (e.g. activation of a greater number of axoaxonic synapses) and/or their spiking frequency. Increased recruitment could also occur via greater depolarization

in afferent resting membrane potential based on increased afferent NKCC1 expression [234]. However, as demonstrated by the 4-AP dose-response curve shown in chapter 2 (**Figure 2-5**), progressive hyperexcitability induced increases in burst amplitude and duration are likely constrained by refractory periods at frequencies above those observed in SCI animals.

SCI is a systemic injury that involves local and systemic changes in ion channel expression, synaptic relationships, glial function, inflammatory signaling, and cellular signaling cascades [75, 109, 110, 117]. Based on the evidence that bursting exhibits degeneracy demonstrated in Chapter 2, it is not surprising that different spinal cords develop different levels of hyperexcitability after an insult like SCI, particularly with differences in injury severity and age. Future study should further examine the development of bursting over time, including identifying the earliest timepoint that bursting develops after injury and how it changes throughout recovery, as well as how severity of injury correlates with burst frequency and amplitude.

Bursts recruit Aδ- and C-LTMRs

A key feature of perturbation (such as bursting) to a sensory circuit like the superficial dorsal horn is the extent to which it corrupts the expected input and output of the circuit. After SCI or administration of 4-AP, optical stimulation of C-LTMRs and Aδ-LTMRs could evoke bursts with the same characteristics as those recruited by electrical stimulation evoking a broader variety of afferents. Recruitment of Aδ- and C-LTMRs during bursting **(Figure 3-7)** provides a substrate for cross-modal afferent activation, given that bursts could also be evoked by Aβ afferent stimulation **(Figure 3-2)**. Given the diversity of afferents that receive PAD axo-axonic synapses [27] and the role that LTMR-evoked PAD plays in modulating nociceptive circuits [40,

53], it is plausible that burst could directly activate nociceptive fibers as well, but this must be confirmed with future study.

Insights into the burst-generating network

As discussed in Chapter 2, afferent bursting is ostensibly driven by bursting in GABAergic interneurons leading to excessive axoaxonic drive that recruits suprathreshold spiking in afferents **(Figure 2-9)**. PAD, and assumedly associated suprathreshold spikes, can be mediated by non-GABAergic mechanisms [42] and is canonically thought to involve a trisynaptic pathway [53], but can clearly operate by more direct mechanisms [60, 302]. The evidence presented here suggests that disynaptic afferent- GABA interneuron-afferent connections are sufficient for afferent stimulation-evoked afferent bursting and that monosynaptic GABA interneuron-afferent axoaxonic connections are sufficient to generate spontaneous bursting in afferents. Demonstrated bursting in superficial dorsal horn interneurons provides further evidence that interneuron bursting underlies ectopic bursting in afferents and that bursting in dorsal horn circuitry in the absence of afferent recruitment **(Figure 3-10A)**. Based on the reduction of frequency in conditions of synaptic blockade **(Figure 3-8A)** and reduction of frequency and synchrony during glutamate receptor blockade **(Figure 2-9)**, bursting circuitry ostensibly receives functionally excitatory input from sources of polysynaptic input that facilitate spontaneous bursting. These sources of input could increase burst frequency either through direct recruitment of burst generating interneurons or depolarization of burst generating interneurons, increasing the chances of bursting interneurons stochastically reaching threshold through normally subthreshold inputs. Results from glutamate receptor blockade experiments definitively demonstrate that glutamatergic transmission plays a facilitatory role in the GABAergic burst circuit. These results are summarized graphically in **Figure 3-13.**

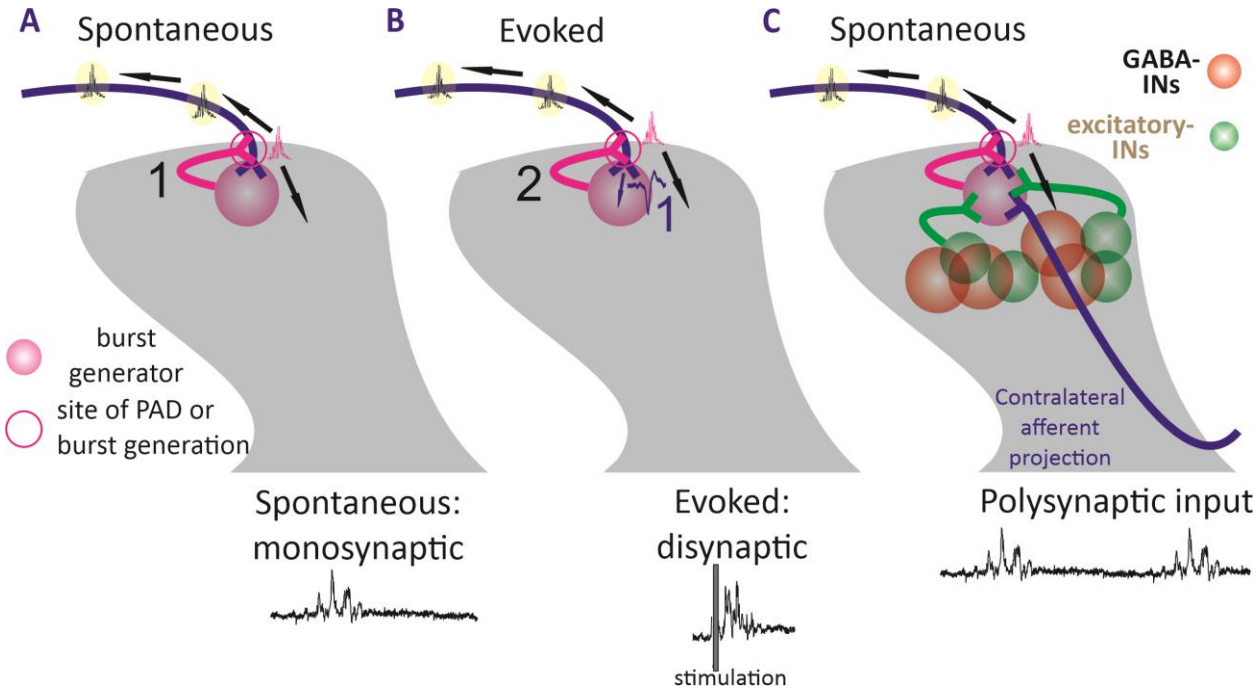

Figure 3-13: Proposed synaptic organization of bursting circuitry

In all cases, bursts propagate orthodromically for central effects and antidromically for peripheral effects. ***(A)*** *Spontaneous bursting: burst generators (presumably GABAergic interneurons normally responsible for PAD) independently generate bursts* ***(1)*** *through hyperexcitability-driven conversion to a bursting electrophysiological phenotype. Bursts travel orthodromically back into the cord and antidromically to the periphery.* ***(B)*** *Evoked bursting: In a corruption of a disynaptic PAD pathway, primary afferent stimulation* ***(1)*** *evokes activity in the burst-generating interneuron, which evokes a burst through axoaxonic synapses normally responsible for PAD* ***(2)****. These bursts travel orthodromically back into the cord and antidromically to the periphery.* ***(C)*** *Spontaneous bursting: without synaptic blockade, burst-generating interneurons may receive input from a variety of polysynaptic sources, including contralateral afferent projections [238] and a constellation of local excitatory input, allowing higher frequency generation of bursts than in conditions of polysynaptic block.*

There is anatomical evidence that Aβ fibers and Aδ-LTMRs form synapses on GABAergic parvalbumin^{+} and cadherin^{+} inhibitory interneuron subpopulations that form reciprocal axoaxonic connections back onto them [17], which would explain Aδ-LTMR access to di-synaptic burst evoking circuitry. C-LTMRs, however, exhibit only a small number of contacts with cadherin+ interneurons [17], suggesting either that their limited contacts are sufficient to evoke bursting or that they may evoke bursts through polysynaptic networks. The difference in refractory period results between electrical stimulation and Aδ- and C-LTMR optogenetic stimulation suggests that LTMR stimulation exerts a stronger effect on spontaneous bursting than spontaneous bursting exerts on LTMR-evoked bursting. Stimulation of smaller pools of afferents through optogenetic stimulation was able to recruit bursts during the refractory period suggested by electrical stimulation experiments **(Figure 3-5, 3-6)**. The most plausible interpretation of this result is that bursts are driven by pools of burst generators, each of which can be recruited by afferent input, but all of which share a refractory period. This would explain why smaller subpopulations of afferents are able to evoke bursting immediately after a spontaneous burst while electrical recruitment of many afferents in a root fails to do so. To further explore this hypothesis, future work should unravel whether all afferents exhibit monosynaptic access to burst circuitry or if there is some heterogeneity in afferent connectivity to burst generators. Identifying the neurons responsible for burst generation and determining whether there is heterogeneity in their identity would also explore this hypothesis. Given the rostrocaudal distribution of bursting and the apparent di-synaptic nature of burst generators, I hypothesize that cadherin^{+}, and likely parvalbumin^{+} inhibitory interneurons are the last-order GABAergic interneurons responsible for generating bursting in afferents and that they receive functionally excitatory drive from underlying interneuron networks, likely including widely distributed

lamina I interneurons [288, 295], and afferent collaterals. Indeed, dysfunction in parvalbumin^{+} inhibitory interneurons has been implicated as one method by which gate control can fail, resulting in allodynia [303].

In addition, lamina I GABAergic interneurons, which are known to convert to a bursting phenotype after SCI and receive synaptic input from Aδ and C fibers, but not C-LTMRs [240, 304], could contribute to bursting circuitry if they are disinhibited by SCI. In addition to their known conversion to a bursting phenotype, presumably through alterations in persistent Na^{+} and L-type Ca^{2+} channel function [240], lamina I GABAergic interneurons are known to form intersegmental and interlaminar connections consistent with the observed rostrocaudal spread of bursting noted in this work [288].

Bursting can be modulated by extrasynaptic GABAergic modulation

Bursting frequency was also reduced by the $GABA_A$ α-5 binding site inverse agonist L655, 708, consistent with the hypothesis that tonic GABA may act to modulate excitability [178]. This also provides a potential mechanism by which bursting and hyperexcitability could be modulated – alterations in tonic GABAergic tone through extrasynaptic receptors could alter the frequency of bursting and underlying hyperexcitability: in fact, L655, 708 is used clinically to promote recovery after stroke [305] (although in this case it is used to reduce excessive tonic inhibition – the inverse of its effect on the hyperexcitability examined in this work). Extrasynaptic $GABA_A$ receptors are known to be expressed on proprioceptive afferents [306] and recent genetic work has indicated that they are expressed at relatively low levels in mechanoreceptor DRG [307] (**Figure 3-14**) and responsible for modulation at branchpoints of sensory axons [178]. As lamina II dorsal horn neurons (as well as a broad population of spinal inhibitory and excitatory neurons) also express extrasynaptic $GABA_A$ receptors (see [308] and https://seqseek.ninds.nih.gov/), these

results could also be due to alteration in dorsal horn modulatory networks [299, 308, 309]. Indeed, given that L655, 708 reduced the frequency, but not amplitude or duration, of bursting, I hypothesize that the effects can be accounted for by actions on dorsal horn interneurons rather than afferents.

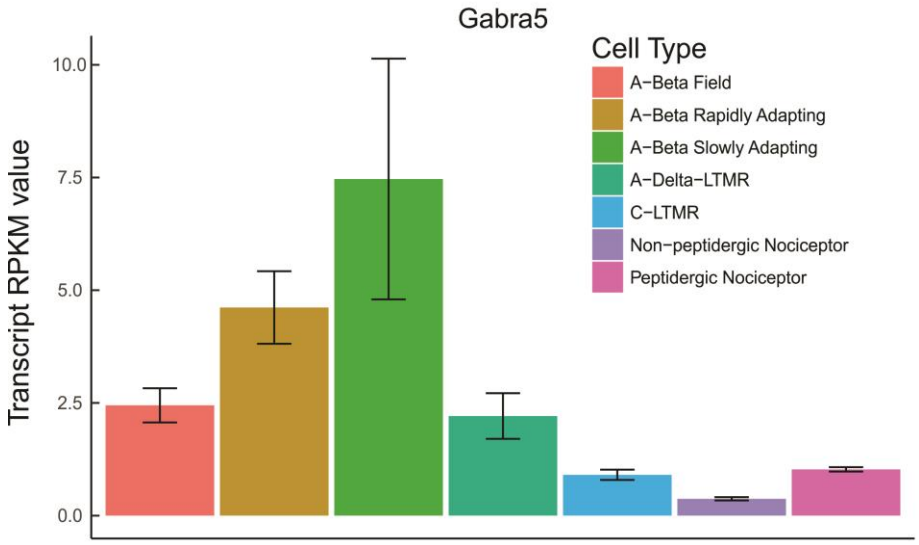

Figure 3-14: $GABA_A$ receptor α5 subunit mechanoreceptor distribution.

Distribution of reads per kilobase of transcript (RPKM) values of $GABA_A$ α5 subunit expression in mechanoreceptor DRG (gene name Gabra5). Data from [307] visualized by Matthew Bryson using R. Low levels of receptor are expressed in DRG of all listed mechanoreceptors.

Bursting and involvement of dorsal horn circuitry

Results throughout Chapters 2 and 3 suggested that GABAergic interneurons were responsible for observed afferent ectopic bursting. With recordings in Lissauer's Tract, I demonstrated that superficial dorsal horn interneurons do indeed express bursting and can even do so in the absence of afferent recruitment **(Figure 3-10A)**, consistent with the hypothesis that interneuron bursting underlies epileptiform afferent bursting. These results, in combination with previously discussed

results regarding the synaptic organization of bursting **(Figure 3-13)** further implicate dorsal horn GABAergic interneurons as the last-order drivers of ectopic bursting. GABAergic interneuron axons from laminae I, II, and III project through LT [288] and GABAergic parvalbumin^{+} interneuron axonal projections specifically have been demonstrated in LT [236].

Given the electrophysiological evidence that bursts propagate orthodromically for re-entrant actions on spinal circuitry (**Figure 3-10B**) and the histological evidence of superficial dorsal horn pain-related circuit activation by 4-AP (**Figure 3-10C**), it is at least the case that spinal pain circuitry is being aberrantly recruited in conditions in which bursting is present and likely that bursts are directly responsible for that recruitment. Spiking overlying EFP events indicated that reentrant burst propagation exerted actions not only on burst-involved interneurons in their refractory period, but also on lamina II interneurons capable of spiking **(Figure 3-10B)**. This suggested either that some burst-generating interneurons were not in a refractory period, that other interneurons were recruited by reentrant actions of burst events, or a combination of both. Given evidence suggesting that bursts are generated by interacting pools of burst-generating interneurons **(Figure 3-5, 3-6)**, this spiking could arise from burst-related interneuron pools not in a refractory period. Future study should determine which interneuron populations spike upon reentrant burst propagation. If these are the same interneurons that underly bursting, it could be concluded that separate pools of the same interneuron subtype are responsible for evoking bursting in afferents. While the consequences of epileptiform bursting in ascending tracts have yet to be established, the aberrant interactions between distinct afferent subtypes and associated refractory periods induced by bursting assuredly have deleterious effects on the ability to reliably transmit somatosensory information to the brain, particularly given the complex and sensitive somatosensory computation that takes place in the dorsal horn [172, 264, 310]. In addition to

elucidating which interneuron subtypes are the last-order drivers of bursting and which interneuron subtypes contribute to their activity, correlating bursting activity directly with pain behavior or even ascending tract activity is a critical next step in associating it directly with pain.

Spinal bursting can be detected in the cutaneous periphery

Detection of bursting in the cutaneous periphery **(Figure 3-11B)** was particularly intriguing, as it suggests that this form of spinal hyperexcitability can be observed relatively noninvasively in the cutaneous periphery. This presents an opportunity to measure epileptiform bursting *in-vivo* from cutaneous sites as an index of spinal hyperexcitability. Further, this could be incorporated as a biomarker of pain for applications such as feedback-based stimulation and suggests that ongoing bursting would corrupt incoming signals from the periphery.

Antidromic stimulation acutely alters cutaneous mechanosensitivity

Here, I show that electrical stimulation matching parameters recorded from spinal epileptiform bursts can acutely reduce the mechanosensitivity of peripheral cutaneous receptors. The relatively long time of this effect (minutes) suggests that stimulation is not simply fatiguing afferents, but rather acting through some cellular system to temporarily reduce receptor sensitivity. While bursting propagated through Aδ and C fibers, C fiber recruitment during stimulation was necessary to exert effects on cutaneous mechanoreceptors **(Figure 3-12C$_1$)**. I hypothesize that this must be due to release of a factor or combination of factors exclusively released peripherally by C-fibers, either LTMRs or nociceptors. The neuropeptides Substance P, calcitonin gene-related peptide (CGRP), galanin, vasoactive intestinal peptide, pituitary adenylate cyclase-activating peptide, neuropeptide Y, and somatostatin, along with other neuromodulators, have all been implicated in DRR's generation of neurogenic inflammation and are released by defined subsets of afferent fibers [311]. For example, the majority of CGRP+

afferents are unmyelinated, and all afferents expressing Substance P express CGRP [311], making the combination of these peptides a likely candidate for perturbation of cutaneous mechanoreception by high frequency C-fiber stimulation. Most studies focusing on DRRs demonstrate hypersensitivity and sensitization of nociceptors as a result of release of factors like CGRP [312] rather than demonstrating reduction in the sensitivity of LTMRs, adding novelty to the results presented here.

Surprisingly, the mechanisms underlying receptor sensitivity are not well understood. Recently, the first intracellular recordings were performed in individual mechanoreceptors during signal transduction [313], demonstrating mechanically activated currents from an unknown mechanosensitive ion channel (hypothesized to be Piezo2). Given the repetitive motif of bidirectional modulation in the somatosensory system, it is not surprising that mechanoreceptors are under dynamic control, but I can only hypothesize as to the mechanisms of minutes-long reduction in sensitivity in the presence of high frequency antidromic activation. One mechanism by which this reduction in mechanosensitivity could occur is by actions on T-type calcium (Cav3.2) channels, which are extensively expressed at Aδ- and C-LTMR branchpoints and implicated in modulation of conduction across branchpoints [314, 315]. As afferents, particularly LTMRs, branch extensively in the cutaneous periphery [8, 9], reduction in Cav3.2 function through secondary messengers activated by release of factors through antidromic afferent activation could reduce the overall sensitivity of LTMRs in the periphery.

The question also remains whether a state of constant antidromic stimulation, as is noted after SCI or 4-AP, would have further effects on peripheral sensitivity. In the antidromic stimulation experiments here, I gave relatively brief (1 minute of pulses every second) stimulation, but the

spontaneous activity recorded in hyperexcitable spinal conditions occurs constantly at a rate of at least 1/3 Hz.

3.6 Conclusion

In this chapter, I demonstrated that Aβ, Aδ, and C fibers, including Aδ- and C-LTMRs, can directly evoke ectopic afferent bursting. In addition, Aδ- and C-LTMRs are directly recruited during evoked burst events. Despite the lack of Aβ fiber recruitment during bursting **(Figure 3-2B)**, Aβ fiber stimulation recruited burst circuitry, indicating that bursting circuits are involved in multimodal afferent interactions. Exploration of differences between separate SCI cohorts revealed that bursting, associated with underlying dorsal horn hyperexcitability, occurred along a gradient of burst frequency and magnitude, presumably based on injury severity and age. Spontaneous bursting was shown to be driven by monosynaptic $GABA_A$ receptor-mediated interneuron-afferent axo-axonic synapses and conversion of superficial dorsal horn interneurons to a bursting phenotype. Afferent stimulation evoked bursting, then, must be minimally di-synaptic, with afferents recruiting dorsal horn interneurons, which then evoke bursts through the same GABAergic axoaxonic synapses. While bursting is dependent on $GABA_A$ synaptic transmission, it was also shown to be modulated by extrasynaptic GABA receptors. Bursting was shown to have reentrant orthodromic actions on dorsal horn circuits as well as exert antidromic modulation of cutaneous mechanosensitivity. Overall, this chapter further explored the relationships between bursting circuits and afferents and explored the basic synaptic connectivity of dorsal horn burst circuitry.

3.7 Research contribution

T12 contusion surgeries were performed by Karmarcha Martin and T10 contusion injuries by Matthew Bryson. Behavioral data were acquired by Heidi Kloefkorn-Adams and Don Noble.

Electrophysiology data were acquired by Matthew Bryson, Shawn Hochman, and Shaquia Idlett (n=4 high magnesium low calcium experiments and n=5 superficial dorsal horn recordings). Data quantification and analysis were performed by Matthew Bryson (see appendix A for details on quantification program). Matthew Bryson authored the chapter with collaboration from Dr. Shawn Hochman and Dr. Peter Wenner.

Chapter 4: Discussion and conclusions

4.1 Summary of key findings

Ectopic bursting is epileptiform

In Chapter 2, I described GABAergic interneuron-driven ectopic afferent bursting and argued that it is epileptiform in nature, exhibiting the following characteristics of epileptic activity: bursting 1) consist of episodes of stereotyped activity, 2) exhibits synchrony between normally independent circuits, 3) can be triggered by sensory input , 4) exhibits a refractory period during which another episode cannot be evoked, and 5) results from functional reorganization of circuitry. For this work, I used extracellular dorsal root entry zone recordings in an intact spinal cord preparation after lower thoracic contusion injury. I found that SCI preparations exhibited higher frequency and higher amplitude bursting, and that this bursting correlated with the extent of mechanical hypersensitivity (50% PWT) after injury. A functionally similar bursting phenotype could be recapitulated with the convulsant voltage-gated potassium channel blocker 4-AP and intensified with the KCC2 blocker VU0240551. Bursting could be reduced by the anticonvulsant retigabine and was completely abolished in all conditions by GABAergic blockade. Blockade of ionotropic glutamate receptors with CNQX+APV reduced burst frequency and synchrony, demonstrating that excitatory glutamatergic drive is not required for bursting, but rather contributes to the overall hyperexcitability of bursting circuits. This excitatory drive may arise from glutamatergic interneurons or primary afferent synapses. Overall, these results support a conceptually novel understanding of SCI -induced sensory dysfunction in which dysfunction in PAD leads to suprathreshold spiking in afferents. The observed epileptiform phenotype of segmentally propagating bursts is consistent with common

descriptions of propagating neuropathic pain and therefore provides a novel hypothetical substrate to explore underlying mechanisms of somatosensory dysfunction.

Epileptiform circuitry expresses degeneracy

Epileptiform circuitry could be unmasked through a variety of mechanisms: SCI, block of K_V channels by 4-AP and TEA, perturbation of intracellular chloride concentration by block of KCC2, and even simply letting the cord rest once removed from the animal, assumedly due to loss of descending inhibition during the dissection [115, 316]. The variety of perturbations leading to a bursting phenotype suggests that epileptiform bursting expresses degeneracy [217, 218], which draws a further connection between dorsal horn bursting and epilepsy [158]. The concept of "multiple roads leading to the same destination" is not new, but its application to conditions of neuronal hyperexcitability like neuropathic pain or epilepsy should inform our view of how these conditions develop and how they should be treated clinically. In the case of epileptiform bursting, it is possible that any of the previously discussed post-SCI cellular perturbations could be sufficient to induce a hyperexcitable bursting state in the dorsal horn. Future study should test other known SCI-related alterations (for example, increase in Na_V function or nociceptor hyperexcitability) to determine if they too are sufficient to induce the dorsal horn hyperexcitability and ectopic bursting discussed in this work. Similarly, the inverse of known SCI-induced alterations (for example, decrease in Na_V function or increase in K_V function) should be tested to determine if they are sufficient to ablate bursting and rescue a normal excitability phenotype, regardless of the perturbation that produced hyperexcitability.

Epileptiform bursting can be evoked by afferent stimulation, including Aδ- and C-LTMRs

In chapter 3, I further explored the network underlying epileptiform bursting. I established that bursting is a phenotype of hyperexcitability after SCI that can be evoked by a di-synaptic circuit

with input from Aδ-LTMR, C-LTMR, other Aδ and C afferents, and Aβ afferents. Burst-generating circuitry likely receives input from polysynaptic sources but can ostensibly be evoked by a solely di-synaptic afferent-interneuron-afferent circuit. In the absence of afferent stimulation, interneurons can ostensibly generate bursts independently, presumably through monosynaptic GABAergic axo-axonic synapses with afferents and interneuron conversion to a bursting phenotype after SCI or other hyperexcitability-inducing perturbations. Bursts propagate in both Aδ-LTMR and C-LTMR populations, and other Aδ and C fiber populations based on conduction velocity measurements, highlighting the potential of bursting circuitry to allow cross-modal activation of afferents during spontaneous and evoked events. Overall, this chapter provided insight into the afferents and networks underlying bursting and generated the hypothesis that parvalbumin^{+} and cadherin^{+} inhibitory interneurons are the last-order neurons responsible for burst propagation.

Bursting is dependent on GABAergic synaptic transmission

In Chapter 2, I demonstrated that $GABA_A$ antagonists consistently completely block spontaneous and evoked bursting. In chapter 3, I demonstrated a modulatory role for extrasynaptic $GABA_A$ receptors, presumably those expressed on dorsal horn interneurons, based on the reduction of burst frequency but not amplitude in the presence of L655,708. These results demonstrate that while synaptic $GABA_A$ receptors are necessary for bursting, extrasynaptic $GABA_A$ receptors are not necessary, but play a facilitatory role in bursting. As expected, given evidence of the necessity of $GABA_A$ receptors for burst generation, blockade of bursting in a condition of severe reduction of synaptic transmission (*High* Mg^{2+}/*Low* Ca^{2+} *solution*) demonstrated that synaptic transmission at the axo-axonic interneuron-afferent synapse is necessary for bursting to occur in afferents. This synapse is likely unnecessary for dorsal horn bursting to manifest , although

$GABA_A$ synaptic transmission still appears necessary [155]. Demonstration of bursting in superficial dorsal horn interneurons provided further evidence that afferent bursting is recruited by bursting in underlying dorsal horn interneurons, presumably the GABAergic interneurons necessary for burst recruitment. Studies in human have established that some substantia gelatinosa interneurons project through Lissauer's Tract [317] and similar studies in rat have demonstrated Lissauer's Tract projections of lamina II and III GABAergic interneurons [318].

Bursting may directly recruit pain circuitry

While a shortcoming of this work is the lack of direct connection between bursting and pain circuitry, I present several lines of evidence suggesting that bursting recruits pain circuitry. First, 4-AP evokes increased Fos expression in lamina I neurons with Nk1R internalization, consistent with activation of pain circuitry. Previous work by Shaquia Idlett similarly showed that 4-AP evokes Fos activity in superficial dorsal horn consistent with activation of pain circuitry [195]. In this work, I also demonstrated that bursting evokes subthreshold EFP activity in superficial dorsal horn consistent with re-entrant recruitment superficial dorsal horn networks. Given reentrant activation of spinal circuitry, it is possible that pain-related networks could be directly recruited by bursting. That bursts recruited activity in Lissauer's Tract, which is viewed as a pain transmitting tract [16, 214], provided further evidence of recruitment of pain circuitry.

Epileptiform bursting can acutely perturb peripheral mechanosensitivity

In chapter 3, I quantified the extent to which SCI disrupts cutaneous mechanoreception. I showed that bursts can propagate to the cutaneous periphery and that electrical stimulation matching burst intensity and frequency can acutely decrease mechanoreceptors' response to light touch stimulation. This result adds to a growing body of literature demonstrating that sensory reception at the periphery is regulated through spinal and local mechanisms.

Further, the ability to detect bursting in the cutaneous periphery provides the opportunity to use bursting as a biomarker of ongoing spontaneous pain, which is a behavioral measurement that is sorely lacking in animal models. Foreseeably, this activity could also be used as a biomarker by which to modulate feedback-based stimulation.

4.2 Contributions to the field

Overall, this dissertation offers a novel interpretation of epileptiform afferent bursting as a driver of somatosensory dysfunction after SCI. By arguing that the activity is epileptiform, this work draws critical connections between neuropathic pain and epilepsy, highlighting that both conditions fundamentally arise from hyperexcitable networks of neurons that exhibit degeneracy. These findings support further exploration of the mechanisms involved in burst generation, particularly how interneuron populations can generate a periodic bursting phenotype, as well as the orthodromic and antidromic consequences of burst propagation. In addition, demonstration of the ability to record bursting in the cutaneous periphery suggests that it could be used as a relatively noninvasive biomarker of spinal sensory hyperexcitability after SCI or in other neuropathic pain conditions.

4.3 Remaining questions and future directions

How does GABAergic circuitry synchronize to evoke bursting?

Given the evidence that inhibitory parvalbumin$^+$ and cadherin$^+$ interneurons form PAD-evoking synapses with primary afferents [42, 171, 172], I propose that these are the most likely populations to evoke bursting. To test this hypothesis and better understand bursting circuitry, I propose that calcium imaging experiments with transgenic populations of inhibitory parvalbumin$^+$ and cadherin$^+$ interneurons expressing GCaMP would allow direct observation of these interneurons' firing properties during bursting. Alternatively, parvalbumin-Cre and

cadherin-Cre lines could be crossed with a fluorescent reporter line to allow targeting with patch clamp recordings, allowing simultaneous recording of known interneuron types and DREZs during bursting. Direct observation of the temporal relationships between interneuron activity and bursting in DREZ would allow direct implication of these interneurons. If these populations are not ostensibly responsible for bursting, I hypothesize that lamina I GABAergic local circuit interneurons, which are known to convert to a bursting phenotype [240] and receive Aδ and C fiber input consistent with afferent-evoked bursts [288, 295, 319] may be another population of interest in burst generation. These neurons could similarly be investigated using a GAD67-EGFP model for localization and recording in lamina I [304]or a GAD67-GCaMP transgenic model for calcium imaging.

How does bursting interact with pain circuitry?

While I present several lines of evidence suggesting that bursting activates pain circuitry (4-AP histology, Lissauer's Tract recordings, and superficial dorsal horn recordings), a major shortcoming of this work is the lack of direct connection to pain. Future work should focus on linking ongoing bursting to activation of pain circuitry and, hopefully, to behavioral indices of pain experience. In Chapter 3, I demonstrated the ability to detect bursts in the cutaneous periphery. If streamlined and included as part of behavioral pain paradigms like conditioned place preference, respiratory rate variability tracking, or other measures of spontaneous pain (although these have been difficult to develop [119, 320]), bursting could be established as a biomarker of pain, which could be useful both in animal models and as a measurement by which to establish feedback-based stimulation paradigms for treating central neuropathic pain in human subjects.

How can SCI bursting be controlled?

Given evidence that epileptiform bursting is the result of various circuit changes that are each sufficient to induce hyperexcitability-driven bursting (i.e. bursting circuitry exhibits degeneracy), it is difficult to propose which perturbations are most likely to respond to treatment. This is especially true in light of evidence that SCI can be viewed as a systemic injury that perturbs circuit function in the spinal cord and throughout the somatosensory system through a variety of cellular mechanisms [70, 73, 117, 136, 217, 264]. In Chapter 2, I showed that the KCNQ channel opening anticonvulsant retigabine reduced the frequency of bursting. Based on these results, as well as the premise that bursting is fundamentally epileptiform, I propose that future work should test the capacity of other anticonvulsants, particularly those used as frontline neuropathic pain therapies, such as Gabapentin and Pregabalin, to reduce ongoing bursting [77, 92, 321]. I also suggest that for each mechanism used to induce bursting (e.g. K_V block with 4-AP, or more specific K_V1 block with dendrotoxin [218]), the inverse perturbation is attempted to reduce or ablate, bursting, if experimentally possible (e.g. insertion of virtual K_V conductance with dynamic clamp [218]) in order to definitively demonstrate degeneracy of mechanisms leading to bursting and explore mechanisms to restore normal circuit function. As dynamic clamp is performed at the cellular level, it would not provide therapeutic function, but it would allow investigation of the roles of specific conductances in bursting, which could better inform targeting of specific ion channels to reduce or ablate burst-related hyperexcitability.

Unaddressed in this work are non-pharmacological mechanisms of spinal circuit modulation, such as spinal cord stimulation (SCS). Dr. Shaquia Idlett previously studied the effect of SCS on 4-AP induced bursting and found that only SCS putatively recruiting postsynaptic dorsal column cells through suprathreshold dorsal column stimulation was able to modulate ongoing spiking in

Lissauer's Tract/superficial dorsal horn [195]. These results suggest that traditional SCS would be ineffective at modulating ongoing bursting, but further study is warranted.

4.4 Final words

Building on literature on SCI, somatosensory circuit organization, PAD, and principles of neural hyperexcitability, this work proposes a new lens with which to view spinal somatosensory dysfunction after SCI. Categorizing hyperexcitability-driven afferent bursting as epileptiform draws critical parallels between sensory dysfunction and epilepsy, including the concept that both exhibit degeneracy, which helps explain the difficulty in treating both conditions, but also suggests a conceptual framework to explore how to rescue normal spinal excitability after SCI.

There is still much that we don't understand about somatosensory function, even at the level of cutaneous reception in an intact and healthy model animal (here, the mouse). There is also much we don't understand about modulating neural hyperexcitability, especially in a case like SCI, where the degeneracy of hyperexcitable circuits plays out in real time: numerous cellular changes, each of which is likely sufficient to evoke hyperexcitability, occur simultaneously and interact in unpredictable ways. I propose that the best way to study these changes and interactions is at the level of spinal circuitry: how do dorsal horn processing and output change after SCI and how can these changes be modulated to minimize or ablate sensory abnormalities? Regardless of how this project moves forward, I hope that it retains a focus on circuit-level function of the spinal somatosensory system during normal function and after perturbation.

Appendices

Appendix A. Algorithmic burst detection and analysis

Section 1.01 Abstract

Bursting is a widely studied phenomenon in both individual neurons and circuits of interconnected neurons. However, recordings involving bursting activity are most commonly performed either intracellularly or with a multielectrode array. Both methods allow spatial identification of individual neurons, which is not the case with the extracellular recordings performed in this work. The lack of spatial acuity provided by our recordings left a gap in burst analysis methods. To facilitate analysis of bursts across animals and conditions, I wrote a program in Python, called BurstAnalysis, to detect, measure, and analyze spontaneous and stimulus-evoked bursts from .abf files. Spikes are measured with an adjustable threshold, after which bursts are differentiated from individual unit activity based on inter-spike interval (ISI). Once bursts are identified, measurements are taken for each bursting event (number of events per bursts, duration of burst, average amplitude of spikes within burst, frequency of bursting, etc.). Bursts are also analyzed for coordination across roots using cross-correlation. All measurements are exported to .csv files, where they can be visually inspected or compared with measurements from other preparations, drug conditions, or injury conditions. Compared to manual analysis of .abf files, BurstAnalysis is significantly faster and provides equivalent burst detection accuracy, as well as generates measurements that could not easily be performed manually. The program was designed modularly such that its functions could be used in other applications. For example, low frequency periodic activity could be detected by choosing the correct filtering settings and slightly adjusting the peak identification parameters.

Section 1.02 Introduction

Given the extent of bursting in our experiments and the large number of files recorded, it was critical to develop a reliable high throughput method to quantify bursts and compare their characteristics across injury and drug conditions both between and within animals. To this end, I developed BurstAnalysis to identify and quantify bursting waveforms from multichannel .abf files.

Bursting as a phenomenon is commonly studied in a wide variety of neuronal circuits [322, 323]. It is thought to be critical to the development of aberrant circuit states such as epilepsy and Parkinson's Disease [228, 324]. Most commonly, bursting is studied as a firing pattern of either a single neuron recorded intracellularly or a network of neurons recorded with a multielectrode array [325, 326]. These methods allow the source of spikes to be identified, often with single-neuron spatial accuracy. In this work, I used extracellular recording at the dorsal root entry zone to record bursting in an undefined population of primary afferent spinal projections. The main difference between this method and those traditionally used for burst detection is that dorsal root entry zone extracellular recordings contain spiking from a large number of axons with no way to identify the source of individual spikes. Despite the spatial limitations of this recording method, dorsal root bursting is an identifiable circuit behavior. As discussed in chapter 2, this bursting is a physiologically relevant output of spinal circuit dysfunction.

Below, I will discuss the manipulation and filtering used for preparing .abf files for burst analysis, methods for detecting and analyzing bursts, the measurements obtained from bursts, and the ways this data was intended to be compared between animals, drug, and injury conditions. I will also compare manual burst detection to programmatic burst analysis. This

chapter will serve as a description of the analysis used for much of the data presented in this dissertation.

4.4.1 Data collection

Data from all animals in the spinal injury cohorts discussed in chapter 2 were used for development of the program. A selection of 10 gap-free and stimulus-evoked .abf files recorded with Clampex were used for the initial development and testing stages. Once developed, the program was used to analyze hundreds of .abf files for inclusion in this work.

4.4.2 Code development

Ideas and algorithms from others will be cited as they are described. The program itself, including the UI, was developed de-novo with Python's tkinter library.

4.4.3 Python libraries

BurstAnalysis checks for, and if necessary, downloads and imports all necessary Python libraries. Necessary libraries are: "pyabf", "matplotlib", "numpy", "pandas", "scipy", "tkinter", and "itertools". All libraries are well-documented with robust online resources **(Table 3-1)**.

Table A-1: Python library sources and documentation

Library Name	**Source url**
Pyabf	https://pypi.org/project/pyabf/
Matplotlib	https://matplotlib.org/
Numpy	https://numpy.org/
Pandas	https://pandas.pydata.org/docs/index.html
Scipy	https://scipy.org/

Tkinter	https://docs.python.org/3/library/tkinter.html
Itertools	https://docs.python.org/3/library/itertools.html

4.4.4 Data

Data were obtained as described in previous chapters. Briefly, Clampex software was used to digitally record spontaneous and evoked bursting activity from ex-vivo spinal cord preparations as .abf files. These files can be directly opened by BurstAnalsysis (and Python in general) through use of the "pyabf" library. Note that this library is unable to open .abf files with numeric values saved as float, which is the format needed for import into Spike2. By default, Clampex saves .abf files in integer format, which is usable by pyabf.

Section 1.03 Explanation of program functionality

4.4.5 Opening and filtering raw data

First, .abf data is opened according to the specifications of the user. By default, pyabf loads files sweep by sweep. I implemented a system that concatenates sweeps and displays all data as continuous to be able to work with gap-free and stimulus-evoked files using the same UI. If chosen, the file can be simultaneously and automatically opened in Clampfit by turning on the "Open in Clampfit" option. Once the .abf file is opened in the BurstAnalysis UI, data is filtered according to the user's selections in the command window by pressing "Filter channels". In the example shown here, as well as all analysis throughout this work, data was high pass filtered at 10Hz, median filtered with a kernel size of 3, and rectified **(Figure 3-1A)**. I selected a median kernel size of 3 to minimize loss of biologically relevant peaks while reducing background noise **(Figure 3-1B)**. High pass filtering was performed to remove recording drift and any DRP

component of bursts, as spontaneous DRP presence was highly dependent on recording quality. A 10Hz cutoff frequency was determined to accomplish these goals most effectively after testing of 1, 10, 30 Hz filters between test files. SciPy's "filtfilt" function was used in order to eliminate phase shift during filtering. As shown in figure 3-1A, most bursts consisted of both positive and negative components, so all traces were rectified to ensure that peaks were not double counted based on recording configuration.

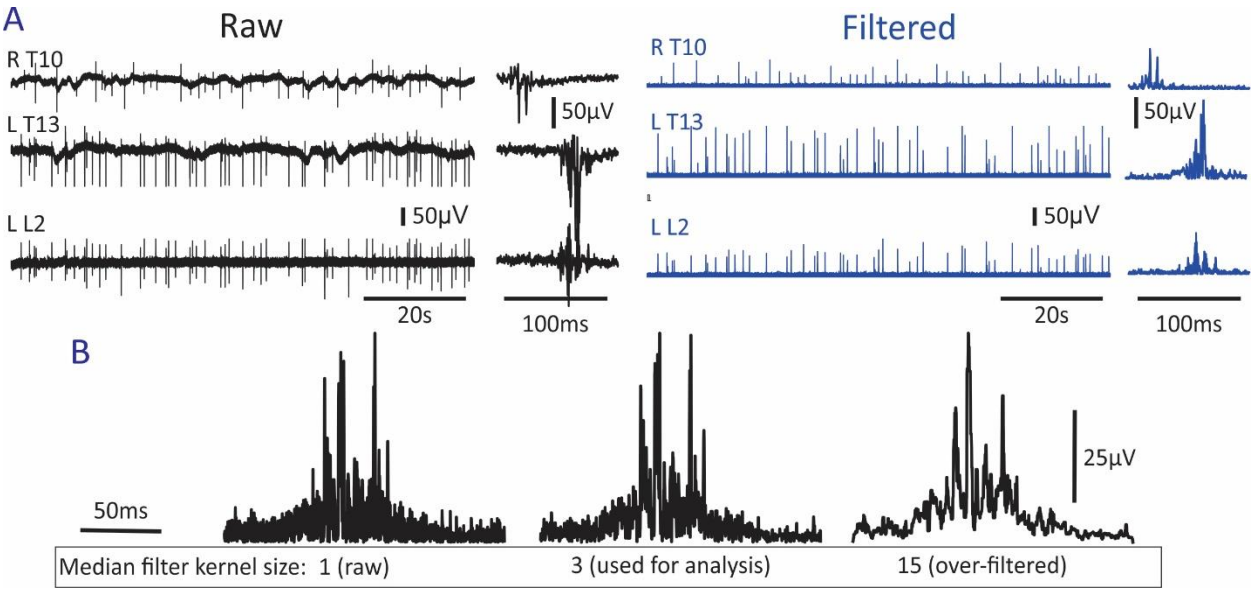

Figure A-1: Filtering parameters for burst detection

***(A)** Example raw traces and individual bursts shown in black. Same trace and same individual bursts are shown in blue after 10Hz high pass filter, median filter with a kernel size of 3, and rectification. **(B)** Example of individual burst that has been high pass filtered at 10Hz, median filtered with kernel sizes of 1, 3, and 15, respectively, and rectified.*

4.4.6 Stimulus detection and artifact removal

As discussed in chapter 2, a goal of this work was to explore afferent-evoked bursting and its interaction with spontaneous bursts. Thus, a critical aspect of analysis was identifying electrical

and optogenetic stimulation. To this end, I sought to develop a lightweight method to identify stimulation, remove stimulus artifacts, and save stimulation times for later analysis. As Clampex saves optical stimulation voltage output files, detecting optical stimulation was simple **(Figure 3-2A)**. Optical stimulation timing was saved as part of the final exported .csv file. More complex was detecting electrical stimulation and removing electrical artifacts. As electrical stimulation artifacts vary in amplitude across channels and are often in the same amplitude range as biological spiking, I chose to identify them with slope rather than amplitude **(Figure 3-2B)**. Because .abf files are digitized and the smallest unit of time is discrete and equal to 1 sample, slope can be calculated by simply subtracting each point from the preceding point. Plotting slope rather than amplitude visually clarifies the difference between electrical stimulation artifacts and other peaks, particularly in noisy channels, such as L T10 shown below **(Figure 3-2C)**. Once slope was calculated for each point in the file, time points with a slope greater than or equal to 1/15 of the maximum slope were selected as possible stimulation times. This threshold was selected to be relatively permissive so as not to miss any potential stimuli. I then took advantage of Clampex's method of recording consecutive sweeps with identical stimulation timing. For each recording channel, points from the possible stimulation time list were compared between sweeps and only points with identical timing between sweeps were stored as potential stimulation times. Identical timing between sweeps suggested that these points were in fact stimulation artifacts and not biological activity. This process was completed for each channel, with possible points continually being added to a single list **(Figure 3-2D$_1$)**. Next, points on this multi-channel possible stimulation time list were compared to all other points and saved as a confirmed stimulation time if they matched a point on the list from another channel with a buffer of 5 samples in either direction. This match indicated that a stimulus artifact was present not only

between sweeps but also between channels. Duplicates were removed and the remaining points were saved as stimulation times **(Figure 3-2D$_2$)**. To remove electrical stimulation artifact, data values 30 samples to the left and 100 samples to the right of the stimulation time were set to 0 and stimulus times marked on channel plots **(Figure 3-2E)**. Note that in the example shown, stimulus times are marked without removal of artifact in order to demonstrate accuracy. While this stimulus artifact removal method is relatively crude, more complex methods of artifact removal [327] were determined to be unnecessary for this application as stimuli were infrequent compared to bursts.

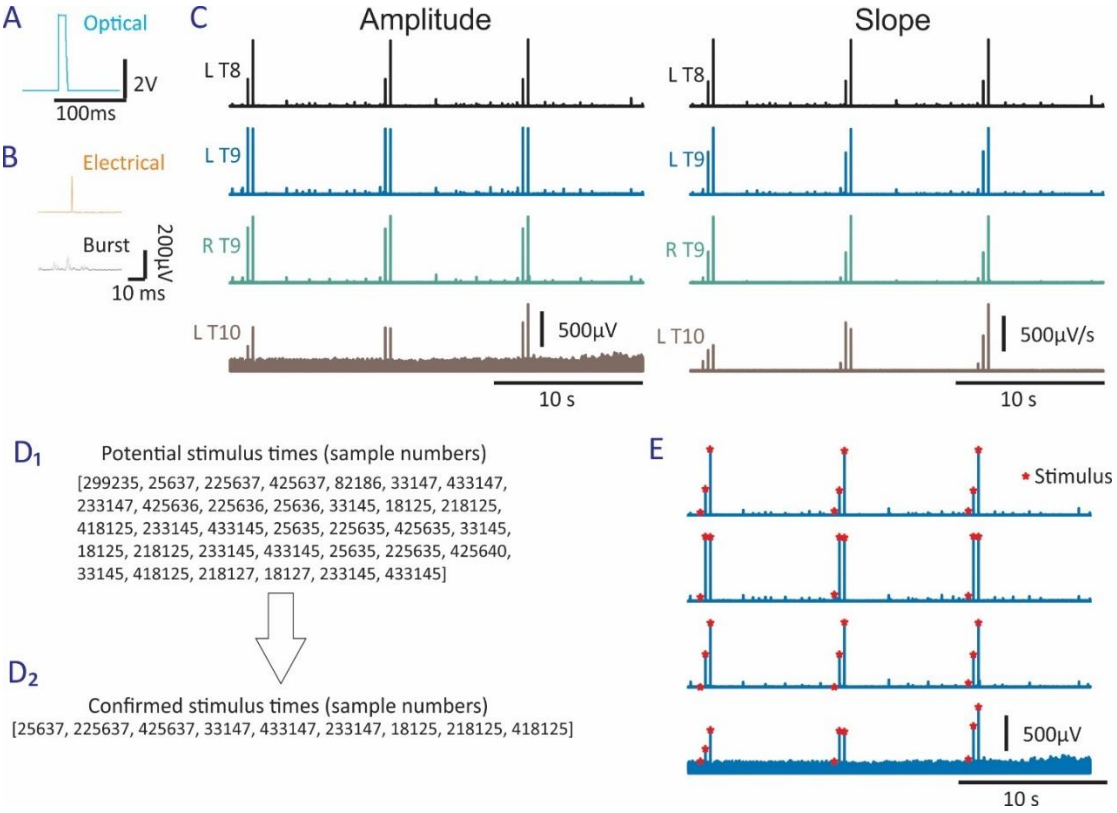

Figure A-2: Stimulus identification algorithm

***(A)** Optical stimuli are stored in a separate channel and simple to identify in Clampfit. **(B)** Electrical stimulation artifact and burst waveforms are stored in the same channel and can be similar in amplitude, making them difficult to differentiate. **(C)** Plotting amplitude often*

obfuscates low threshold electrical stimulation. In this example, 3 sweeps are shown, each with three electrical stimuli (50µVx50µs, 200µVx200µs, and 500µVx500µs). ***(D)*** *Same file as shown in C, but plotted with slope rather than amplitude. This plotting method better differentiates electrical stimuli from biological spiking and background noise.* ***(D_1)*** *All potential stimulus times stored from slope thresholds in each channel.* ***(D_2)*** *Confirmed stimulus times, based on matching times between channels.* ***(E)*** *Amplitude plot shown in C with confirmed stimulus times superimposed as red asterisks. In this example, stimulus artifacts were not removed in order to aid visualization.*

4.4.7 Burst identification

First, for the purposes of this chapter, a "spike" is any event that rises above a threshold amplitude set for spike detection. In this work, 3.5x RMS of the entire trace is used as the default threshold. Any peak with a local maximum above this value was considered a spike **(Figure 3-3A)**. One of the most common measurements used when discussing bursting activity is the inter-spike interval (ISI) [323, 328]. This value is obtained by measuring the time between individual spikes. Mathematically, bursting is defined as spiking such that the standard deviation of ISIs is greater than the mean ISI ($ISI_{SD} > ISI_{mean}$) [329], which is indicative of discreet packets of spikes occurring together at high frequency rather than tonic continuous activity **(Figure 3-3B)**. After filtering the .abf file as above, the time signatures of all spikes detected in the entire trace were added to an array. From this array, spikes were grouped as part of a burst if greater than 5 spikes occured within 20ms of one another. Burst start and end were marked by the first spike of the burst minus 10 samples and the last spike of the burst plus 50 samples, respectively **(Figure 3-3C)**. These hardcoded buffers ensured that the entire burst was captured, while being a small enough unit of time not to affect burst duration measurements. This packet was saved as an

individual burst for measurement and the process continued for the next presumptive burst for the entire loaded .abf file **(Figure 3-3D)**. If any of the above criteria were not met (not enough spikes, spikes too far apart, etc.), the spike was not counted as part of a burst and is ignored. The program takes ~10 seconds to filter and identify bursts from a 300 second long 4 channel .abf file.

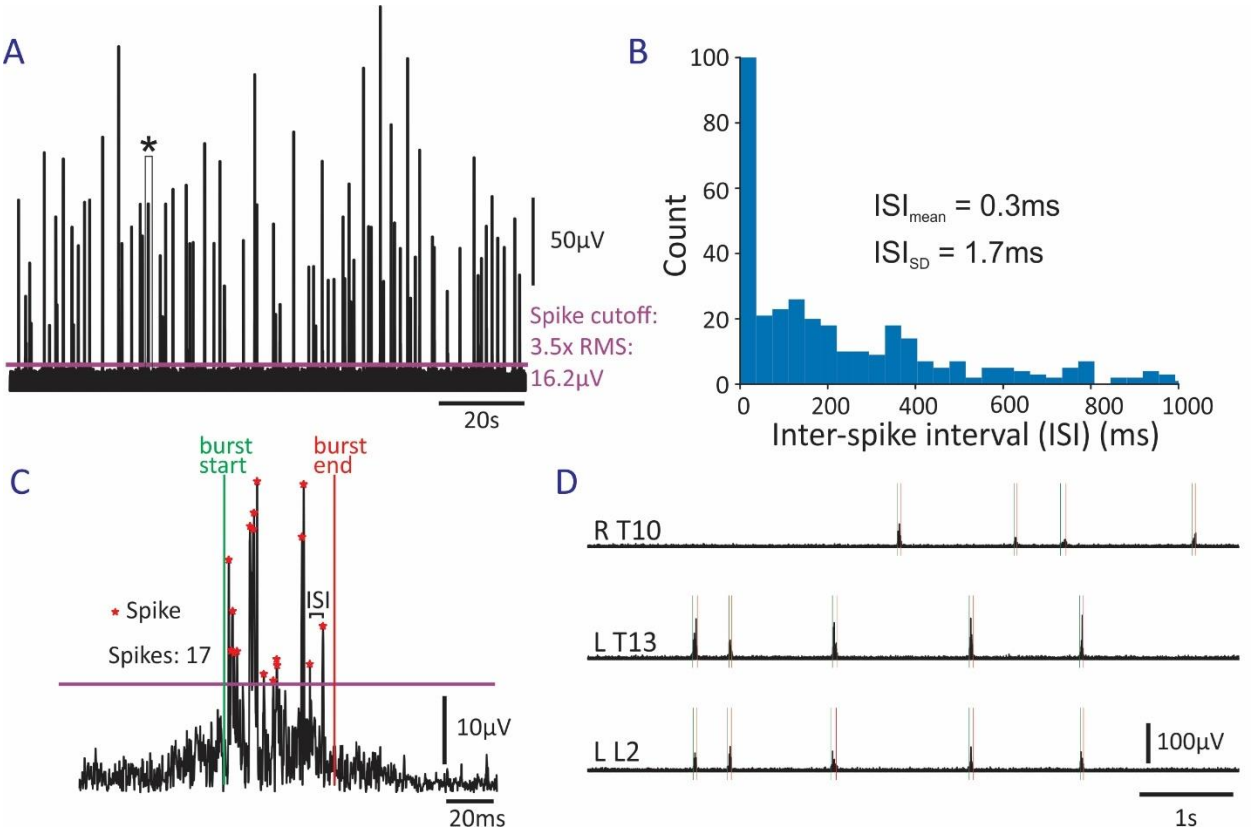

Figure A-3: Burst identification details

***(A)** Example of filtered .abf file with spike cutoff marked at 3.5x RMS, or 16.2 µV in this example. Burst with asterisk is shown zoomed in C. **(B)** Histogram of ISIs for all peaks above spike cutoff shown in A. Most spikes occur within a few milliseconds of each other, but peaks at ~180 and 400 ms indicate that activity is occurring in packets of bursts rather than tonically. Mean ISI for the entire file was 0.3ms, while the standard deviation of ISI for the whole file was*

1.7ms. ***(C)*** *Example of a single burst as labeled by the algorithm described. 17 spikes were detected according to the spike cutoff shown in A. Note that only local maxima are detected, not all values rising above the threshold amplitude. Burst start and end are based on the initial and final bursts detected within this packet with buffer time added. An example ISI is shown as the time between two identified spikes.* ***(D)*** *Example of spikes identified across multiple channels illustrates consecutive detection of bursts independently in each channel.*

4.4.8 Burst quantification

After bursts were identified and labeled, measurements were taken to compare bursts within and between preparations. These measurements included burst start time, burst end time, burst duration, average spike amplitude during burst, rectified and integrated filtered burst, rectified and integrated raw waveform, and cumulative frequency of bursts throughout the file **(Figure 3-4A)**. These measurements, along with information about the file itself and raw data values for all detected bursts **(Figure 3-4B)**, were exported for analysis and visualization in R.

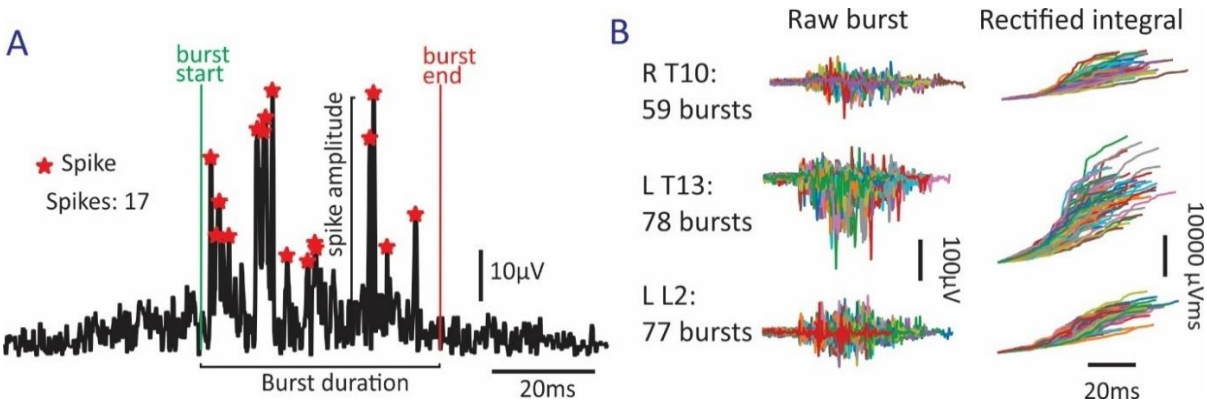

Figure A-4: Diagram of individual burst measurements

(A) *Same burst shown in 3-2C with measurements labeled.* ***(B_1)*** *Example overlay of all bursts detected in three channels of .abf file shown in figure 3-2. Data values from these traces are*

exported for later plotting or analysis. Number of bursts in each channel are shown to the left. ***(B2)*** *Example overlay of rectified integrals of bursts shown in panel to the left. The final value of each line is exported as the value of the integral.*

4.4.9 Cross-correlation

Cross-correlation is a method of analysis that provides a measurement of the similarity between two series of data as a function of the delay between them (referred to here as "lag"). It has long been used as a measurement of coordination between recorded channels in electrophysiology [330]. Cross-correlation, like convolution or wavelet analysis, is performed by sliding a kernel across a signal and measuring the similarity between the kernel and the signal. In the case of cross-correlation, the kernel is a second signal, and the measurement is the integral of the product of the signals at each delay (or lag), which here is measured in seconds. For the purposes of the analysis in this work, the integral of the product of the signals (termed cor) is normalized and is unitless, with 1 being the maximum value. If two signals are identical, or perfectly temporally correlated, they will have a cor of 1 at a lag of 0 and no other peaks on a cross-correlogram. This is also called an autocorrelation. If the signals are offset by a certain time value, they will have maximum correlation at a nonzero lag. In this way, cross-correlation allows measurement not only of whether a correlation exists but also of the temporal relationship between two signals. This was particularly useful for quantifying burst relationships across channels.

After bursts were identified, new reduced data lists were saved for each channel containing values only from bursts (all noise, non-burst spikes, etc. were removed) **(Figure 3-5A)**. Using scipy's signal.correlate function, cross-correlations were calculated for every permutation of channels loaded into the program. Correlation values were normalized for each combination and

lags were restricted from -200 to 200 ms, as any relationships outside of that range were likely spurious and not based on synaptic relationships. Channels were determined to be coordinated if the cross correlation exhibited a sharp peak at any value between -200 and 200 **(Figure 3-5B)**.

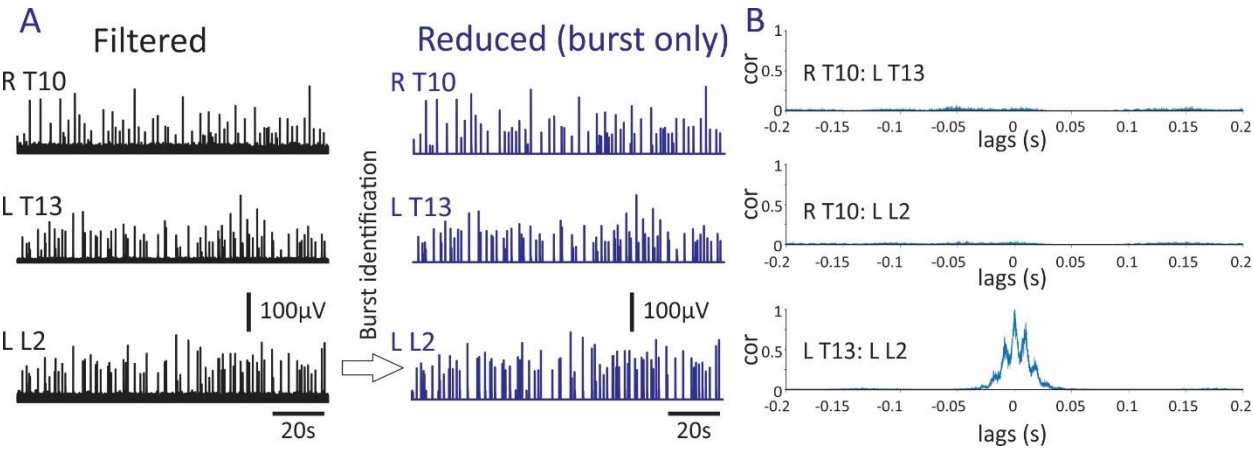

Figure A-5: Burst data reduction and cross correlation

***(A)** After identification of bursts, a new list is saved with only burst data (all noise and other activity is removed and forced to a value of 0). **(B)** Cross-correlograms for each of the channel combinations listed. Only L T13 and L L2 show coordination with the tallest peak at a lag of 0, indicating that bursts occur simultaneously across the channels. Peaks at other nonzero values indicate strong coordination with minor lag and lead without a strong preference in either direction. As discussed above, cor is a normalized value with no units. A value of 1 indicates maximum coordination.*

4.4.10 Data export and visualization

Burst measurements were exported in case formatting to an excel spreadsheet. If a cross-correlation was performed for the file, the top 5 lag and cor values were exported as a separate .csv file for each channel permutation. If selected by the user, data values for each identified burst were exported as a separate spreadsheet. All exported files followed Clampfit naming

conventions with data type added at the end of the file name (_Burst_Quant, Cross_Correlation, or Burst_Waveforms, respectively). Data from multiple files, injury, and drug conditions were collated in R for statistical analysis and visualization. At the end of analysis, the collated list of all burst measurements contained data on 192,010 bursts from 315 .abf files.

4.4.11 Verification and comparison to manual analysis

To verify burst detection accuracy and compare efficiency between manual and programmatic burst detection, I picked 5 random .abf files from all recording days, manually counted bursts from all channels for a random 60 second recording period, then saved the file and analyzed the same period with BurstAnalysis. BurstAnalysis analysis included filtering, burst identification, cross-correlation, and exporting all burst quantification, cross correlation, and burst waveform spreadsheets. Manual burst detection included counting bursts with no measurements taken. Burst counts for the two methods were 92% similar (mean manual burst count = 122.4, sd = 127.5; mean program burst count = 133.4, sd = 132.6) **(Figure 3-6A)**. However, BurstAnalysis was notably faster to identify bursts **(Figure 3-6B)**. On average, manual burst detection took 90.8 seconds (mean = 90.8, sd = 70.4) per file, while BurstAnalysis took an average of 18.4 seconds (mean = 18.4, sd = 7.7) to identify and quantify bursts and export related files.

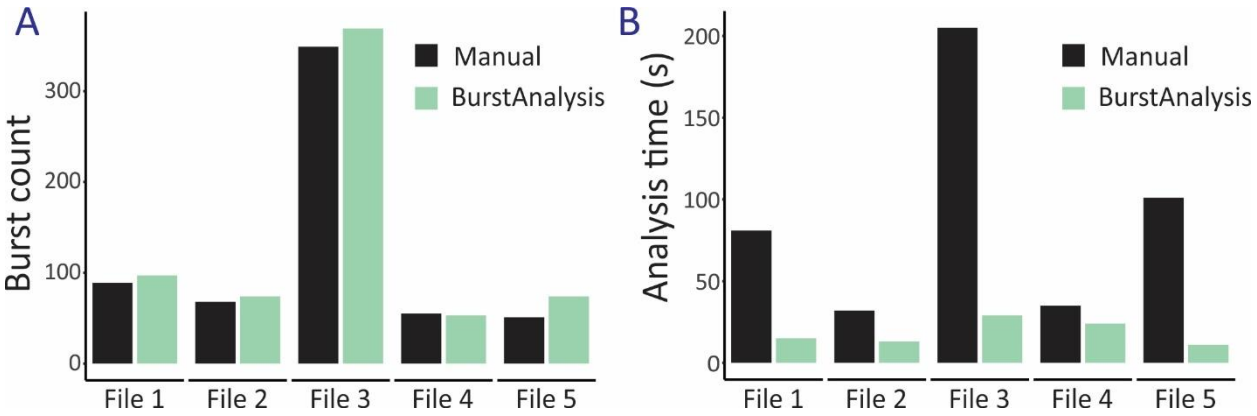

Figure A-6: Comparison between manual burst counting and BurstAnalysis

(A) *Manual counting and BurstAnalysis resulted in similar burst counts across the 5 tested files.*

(B) *BurstAnalysis was notably faster than manual burst counting on each of the 5 files tested.*

Section 1.04 Discussion

BurstAnalysis was written to enable high throughput analysis of bursting data as recorded in the intact spinal cord preparation. As shown above, the program allows consistent and efficient loading of raw .abf files, filtering and burst detection by user-set parameters, measurements of identified bursts, and export of files for further analysis. It was critical to the completion of the rest of this work.

Automated vs. manual data analysis

Semi-automated data analysis, as is performed by BurstAnalysis, presents several advantages over manual data analysis. The program is semi-automated in that analysis is completed in multiple steps with user-set thresholds, user input throughout the period of analysis, and the ability to change settings throughout the analysis of a single file. This allows the advantage of user-based quality control and the advantage of programmatic consistency. I argue that the primary advantages of automated/semi-automated analysis are 1) increased efficiency and 2) built-in reproducibility and reliability of measurements.

As shown in figure 3-6, programmatic burst detection is significantly faster than manual detection with no loss of accuracy. Analyzing a single file with BurstAnalysis took approximately 25% the time of identifying bursts manually. This is particularly relevant when files need to be analyzed multiple times, for example for multiple types of activity, or when new parameters of interest are introduced (i.e. addition of a new burst measurement). This establishes a much more efficient workflow and allows batches of files to be analyzed more quickly than

traditional methods. For example, a set of files can be analyzed on the same day of an experiment, which allows for quicker decision-making and changes to experimental design/recording configuration if needed. BurstAnalysis also allows measurements of bursts in numbers that would be near-impossible to achieve manually. For example, the program could simultaneously detect and generate measurements for every single burst in a file with 600 bursting events across channels, while manual analysis would require individual identification and measurement of each event. This eliminates the need for interpolating data (i.e. manually analyzing 10 seconds of a file and interpolating results for the entire 300 second recording), allowing more accurate and better temporal resolution.

The second advantage is a general argument for the increased reliability of semi-automated analysis over manual analysis. Manual detection and measurement are prone to user error and bias. While there is certainly room for bias in the way that burst criteria are defined for a program (i.e. higher amplitude bursts are more likely to be detected than lower amplitude bursts in a noisy file), I argue that setting numerical thresholds and maintaining them for analysis over multiple files is more internally reliable than attempting to detect similar looking spiking behavior across files by hand. By detecting and measuring bursts with user-defined criteria, BurstAnalysis allows the same file to be analyzed multiple times with identical results, as long as thresholds are maintained between replicates.

Potential for repurposing

The program is intended to be used for .abf files in which bursting is present as high frequency spiking in discreet packets of time. However, its functions were intentionally written modularly such that it could be modified to detect other kinds of activity. For example, low frequency

potentials, such as those that are present during locomotion, could be detected and quantified by simply altering filtering and detection parameters.

Potential for improvement

Bursts recorded in this work appeared to consist of high frequency spiking riding atop a low frequency DRP. To detect bursts most efficiently by thresholding, I used a 10Hz high pass filter to eliminate low threshold components. While I exported measurements from the unfiltered recording, the main purpose of the work was to compare high frequency bursting components. Future work should improve the ability of the program to recognize and quantify the low frequency DRP component of bursts, as they may be a useful secondary measurement of hyperexcitability. As a concrete example, I attempted to use this program to analyze files with Lissauer's Tract (LT) EFP recordings, which critically involve a low threshold component. Using the program as tuned to detect bursts, I failed to analyze LT EFP signals.

Section 1.05 Research contributions

Initial attempts to quantify bursts were based on the SpinalMod program, written in MATLAB by Elizabeth Gozal in 2012. Throughout development of BurstAnalysis, most resemblance to the initial program was lost, but it remains an important contribution to the final product. All Python code, outside of cited libraries, was written by Matthew Bryson. The chapter was authored by Matthew Bryson.

Appendix B: additional skin-nerve preparation results

Section 1.01 SCI does not obviously induce chronic changes in cutaneous mechanoreception

Initially, I sought to determine whether peripheral mechanoreceptors experienced chronic changes in mechanosensitivity following SCI. In the wild-type cohort of SCI and sham animals, I performed simultaneous experiments with the skin-nerve preparation and the ex-vivo spinal cord preparation (results discussed in chapter 2). All SCI (n = 7/7) and sham (n = 4/4) skin-nerve preparations exhibited random spontaneous individual spiking, thus there was no difference in prevalence in spontaneous spiking between the two injury conditions **(Figure 4-2A)**. In both conditions, spontaneous activity was highly variable in amplitude and frequency between preparations and even between individual DCNs within the same preparation. In addition to spontaneous activity, both injury groups exhibited robust response to air pulse stimulation with stronger stimulation evoking more individual spike responses **(Figure 4-2B, 4-2C)**. The general organization of receptive fields of SCI and sham preparations did not appear to differ in response to calibrated air pulse stimulation (n = 4 per injury condition) **(Figure 4-2D, 4-2E)**.

I also attempted to generate recruitment curves for individual DCNs in SCI and sham preparations to determine if SCI altered LTMR recruitment thresholds. However, differences in placement of the air stimulus and inter-day differences in the mN force of air stimulation (lowest force ranging from 2 to 6mN), made threshold recruitment comparisons between preparations difficult.

Overall, the wide variability between preparations made it difficult to draw conclusions regarding the effect of injury and I could only conclude that there were no obvious differences in baseline peripheral mechanosensitivity between the SCI and sham groups.

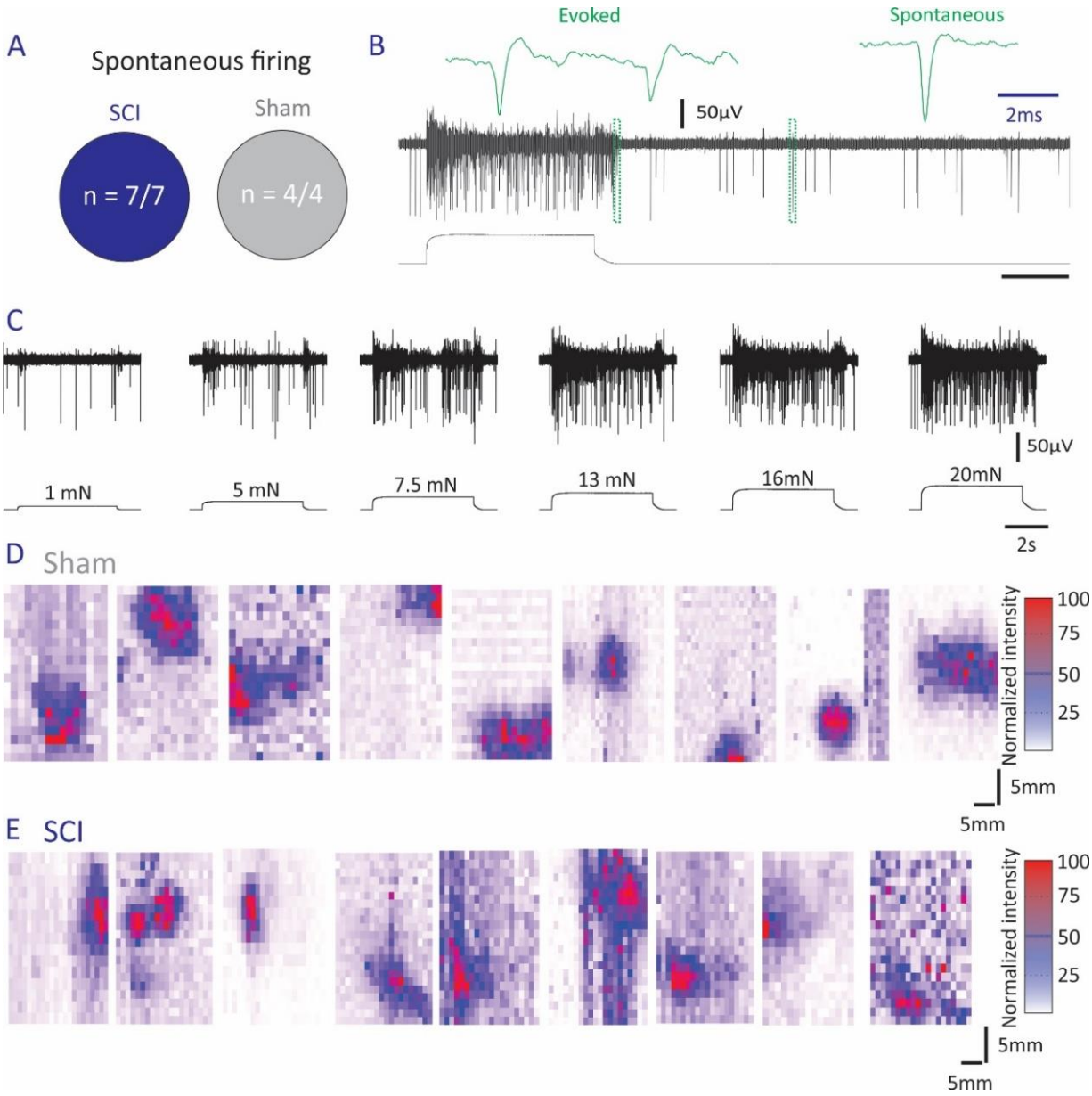

Figure B-1: SCI does not obviously alter cutaneous mechanosensitivity

***(A)** All skin-nerve preparations from SCI and sham groups exhibited spontaneous activity in the form of single-unit spiking. **(B)** Representative examples of evoked response to 20mN air*

stimulation and spontaneous spiking after stimulation. Green outlines represent areas that are zoomed above to show individual spikes. ***(C)*** *Representative example of increased evoked spiking in response to stronger air pulse stimulation.* ***(D)*** *Example single-DCN receptive fields from sham preparations. Random examples of single DCNs were taken from 4 preparation. Receptive fields exhibited wide variability in shape, size, and definition between levels and between animals.* ***(E)*** *Examples of single-DCN receptive fields from SCI preparations. Random examples were taken from 4 preparations. Receptive fields exhibited wide variability in shape, size, and definition between levels and between animals.*

Section 1.02 Trial and error with skin-nerve preparation

While potentially a strange inclusion in this section, I believe that the difficulties presented by the skin-nerve preparation merit discussion. It is theoretically a simple preparation, consisting only of axons and their cutaneous receptor terminations, lacking cell bodies or circuitry that requires oxygenation. However, the inside of the skin is surrounded by sheets of fascia, a fatty tissue that underlies the entirety of the epidermis and individually ensheathes DCNs, requiring careful dissection to enable recording en-passant. Furthermore, the fascia is hydrophobic and leaves the cutaneous surface of the preparation functionally impenetrable to drugs introduced by bath perfusion. Throughout the completion of this project, I tried multiple approaches to overcome the difficulties posed by the fascia. First, I attempted an artificially perfused mouse preparation to systemically deliver drugs through the circulation. This approach was extremely difficult and the small capillaries in the skin did not ostensibly achieve proper circulation despite larger vasculature functioning properly. Next, I tried treating the entire preparation with an oxygenated 2% collagenase solution for one hour at 37˚C. The fascia stayed completely intact, but the texture became mucosal, and it became even more likely to clog suction electrodes. Next,

I tried dissecting as much fascia away from the skin as I could. This often damaged the cutaneous DCN projections and left DCNs without peripheral innervation. Lastly, I tried locally injecting drug under the fascia into the putative receptive field of a single DCN. This seemed to allow drug to reach the cutaneous endings of DCNs, but it is an extremely delicate process. The cutaneous nerve branches are widely distributed and extremely fragile. However, this seemed to be the most effective approach for any pharmacological manipulation of the preparation. Injected solutions stayed in place remarkably well and could be easily marked with a dye such as methylene blue.

As a secondary difficulty, recordings from the preparation exhibited massive variability between preparations and even between DCNs within the same preparation. Given the variability of receptive fields, it was impossible to have a directly comparable recording between one DCN and another. For some purposes (defining receptive fields in an individual), this does not present experimental difficulty, but given that the overall goal of this project was to perform between-animals comparisons with different injury and drug conditions, the levels of variability made comparison near-impossible. Overall, this preparation presented a plethora of unexpected difficulties and provided relatively little useful data in the overall context of this work. From the skin-nerve preparation, I have included only what I believe contributes to this work as a whole.

Section 1.03 Research contributions

T10 contusion surgeries were performed by Karmarcha Martin and Matthew Bryson. Behavioral data were acquired by Heidi Kloefkorn-Adams. Electrophysiology data were acquired by Matthew Bryson, Dr. Shawn Hochman, and Dr. Heidi Kloefkorn-Adams. Data quantification and analysis were performed by Matthew Bryson (see appendix for details on quantification program). Matthew Bryson authored the chapter.

References

1. Abraira, V.E. and D.D. Ginty, *The Sensory Neurons of Touch.* Neuron, 2013. **79**(4).
2. Huang, J., et al., *Sodium channel Na_V1.9 mutations associated with insensitivity to pain dampen neuronal excitability.* The Journal of Clinical Investigation, 2017. **127**(7): p. 2805-2814.
3. Chang, W.S. and J. Bae, *Clinical Presentation of the Thoracic Spinal Compression*, in *Minimally Invasive Thoracic Spine Surgery*, S.-H. Lee, J. Bae, and S.-H. Jeon, Editors. 2021, Springer Singapore: Singapore. p. 43-45.
4. Lee, M.W.L., R.W. McPhee, and M.D. Stringer, *An evidence-based approach to human dermatomes.* Clinical Anatomy, 2008. **21**(5): p. 363-373.
5. Jr, W.D.W. and R.E. Coggeshall, *Sensory Mechanisms of the Spinal Cord: Volume 1 Primary Afferent Neurons and the Spinal Dorsal Horn*. 3 ed. 2004: Springer US.
6. !!! INVALID CITATION !!! [7].
7. !!! INVALID CITATION !!! [8, 9].
8. Zimmerman, A., L. Bai, and D.D. Ginty, *The gentle touch receptors of mammalian skin.* Science, 2014. **346**(6212): p. 950-954.
9. Abraira, Victoria E. and David D. Ginty, *The Sensory Neurons of Touch.* Neuron, 2013. **79**(4): p. 618-639.
10. Li, Y., et al., *Branching points of primary afferent fibers are vital for the modulation of fiber excitability by epidural DC polarization and by GABA in the rat spinal cord.* Journal of Neurophysiology, 2020. **124**(1): p. 49-62.
11. Li, L., et al., *The Functional Organization of Cutaneous Low-Threshold Mechanosensory Neurons.* Cell, 2011. **147**(7): p. 1615-1627.
12. Liljencrantz, J., *The role of the human C-tactile system in affective somatosensation and pain*. 2014.
13. Liljencrantz, J., et al., *Pain and Touch: Roles for C-Tactile Afferents in Pain Inhibition and Tactile Allodynia*, in *Affective Touch and the Neurophysiology of CT Afferents*, H. Olausson, et al., Editors. 2016, Springer: New York, NY. p. 409-420.
14. Kuehn, E.D., et al., *Tiling and somatotopic alignment of mammalian low-threshold mechanoreceptors.* Proceedings of the National Academy of Sciences, 2019: p. 201901378.
15. Peirs, C., et al., *Dorsal Horn Circuits for Persistent Mechanical Pain.* Neuron, 2015. **87**(4): p. 797-812.
16. Lidierth, M., *Long-range projections of Aδ primary afferents in the Lissauer tract of the rat.* Neuroscience Letters, 2007. **425**(2): p. 126-130.
17. Abraira, V.E., et al., *The Cellular and Synaptic Architecture of the Mechanosensory Dorsal Horn.* Cell, 2017. **168**(1): p. 295-310.e19.
18. Boyle, K.A., et al., *Defining a Spinal Microcircuit that Gates Myelinated Afferent Input: Implications for Tactile Allodynia.* Cell Reports, 2019. **28**(2): p. 526-540.e6.
19. Choi, S., et al., *Parallel ascending spinal pathways for affective touch and pain.* The Journal of Pain, 2021. **22**(5): p. 578.
20. Mendell, L.M., *Physiological properties of unmyelinated fiber projection to the spinal cord.* Experimental Neurology, 1966. **16**(3): p. 316-332.

21. Choi, S., et al., *Parallel ascending spinal pathways for affective touch and pain.* Nature, 2020. **587**(7833): p. 258-263.
22. Melzack, R. and P.D. Wall, *Pain Mechanisms: A New Theory.* Science, 1965. **150**(3699): p. 971-979.
23. Kasemeier-Kulesa, J.C., *Imaging neural crest cell dynamics during formation of dorsal root ganglia and sympathetic ganglia.* Development, 2005. **132**(2): p. 235-245.
24. Duan, B., et al., *Identification of Spinal Circuits Transmitting and Gating Mechanical Pain.* Cell, 2014. **159**(6): p. 1417-1432.
25. Zhang, Y., et al., *Timing Mechanisms Underlying Gate Control by Feedforward Inhibition.* Neuron, 2018. **99**(5): p. 941-955.e4.
26. Duan, B., L. Cheng, and Q. Ma, *Spinal Circuits Transmitting Mechanical Pain and Itch.* Neuroscience Bulletin, 2018. **34**(1): p. 186-193.
27. Fernandes, E.C., et al., *Primary afferent-driven presynaptic inhibition of C-fiber inputs to spinal lamina I neurons.* Prog Neurobiol, 2020. **188**: p. 101786.
28. Jiménez, I., M. Rudomin P Fau - Solodkin, and M. Solodkin, *Mechanisms involved in the depolarization of cutaneous afferents produced by segmental and descending inputs in the cat spinal cord.* 1987(0014-4819 (Print)).
29. Maxwell, D.J., et al., *FINE STRUCTURE OF PRIMARY AFFERENT AXON TERMINALS PROJECTING FROM RAPIDLY ADAPTING MECHANORECEPTORS OF THE TOE AND FOOT PADS OF THE CAT.* Quarterly Journal of Experimental Physiology, 1984. **69**(2): p. 381-392.
30. Maxwell, D.J., et al., *Synaptic connections of dorsal horn group II spinal interneurons: synapses formed with the interneurons and by their axon collaterals.* 1997(0021-9967 (Print)).
31. Vyklický, L., et al., *Primary Afferent Depolarization Evoked by a Painful Stimulus.* Science, 1969. **165**(3889): p. 184-186.
32. Levy, R., *The role of gaba in primary afferent depolarization.* Progress in Neurobiology, 1977. **9**(4): p. 211-267.
33. Martin, R.F., L.H. Haber, and W.D. Willis, *Primary afferent depolarization of identified cutaneous fibers following stimulation in medial brain stem.* Journal of Neurophysiology, 1979. **42**(3): p. 779-790.
34. Carlton, S.M., S. Zhou, and R.E. Coggeshall, *Peripheral GABAA receptors: evidence for peripheral primary afferent depolarization.* Neuroscience, 1999. **93**(2): p. 713-722.
35. Eccles, J.C., R.F. Schmidt, and W.D. Willis, *DEPOLARIZATION OF THE CENTRAL TERMINALS OF CUTANEOUS AFFERENT FIBERS.* Journal of Neurophysiology, 1963. **26**(4): p. 646-661.
36. Price, T.J. and S.A. Prescott, *Inhibitory regulation of the pain gate and how its failure causes pathological pain.* Pain, 2015. **156**(5): p. 789-792.
37. Graham, B. and S. Redman, *A simulation of action potentials in synaptic boutons during presynaptic inhibition.* Journal of Neurophysiology, 1994. **71**(2): p. 538-549.
38. Willis, W.D., *John Eccles' studies of spinal cord presynaptic inhibition.* Progress in Neurobiology, 2006. **78**(3): p. 189-214.
39. Bardoni, R., et al., *Pre- and postsynaptic inhibitory control in the spinal cord dorsal horn.* Ann N Y Acad Sci, 2013. **1279**: p. 90-6.
40. Guo, D. and J. Hu, *Spinal presynaptic inhibition in pain control.* Neuroscience, 2014. **283**: p. 95-106.

41. Hochman, S., et al., *Presynaptic inhibition of primary afferents by depolarization: observations supporting nontraditional mechanisms.* Annals of the New York Academy of Sciences, 2010. **1198**(1): p. 140-152.
42. Zimmerman, A.L., et al., *Distinct Modes of Presynaptic Inhibition of Cutaneous Afferents and Their Functions in Behavior.* Neuron, 2019. **102**(2): p. 420-434.e8.
43. Mendell, L.M., *Constructing and deconstructing the gate theory of pain.* Pain, 2014. **155**(2): p. 210-216.
44. Prescott, S.A., *Chapter Twelve - Synaptic Inhibition and Disinhibition in the Spinal Dorsal Horn,* in *Progress in Molecular Biology and Translational Science*, T.J. Price and G. Dussor, Editors. 2015, Academic Press. p. 359-383.
45. Willis Jr, W.D., *Dorsal root potentials and dorsal root reflexes: a double-edged sword.* Experimental Brain Research, 1999. **124**(4): p. 395-421.
46. Toennies, J.F., *Reflex discharge from the spinal cord over the dorsal roots.* Journal of Neurophysiology, 1938. **1**(4): p. 378-390.
47. Lucas-Romero, J., et al., *Origin and classification of spontaneous discharges in mouse superficial dorsal horn neurons.* Sci Rep, 2018. **8**(1): p. 9735.
48. Gossard, J.-P., L. Bouyer, and S. Rossignol, *The effects of antidromic discharges on orthodromic firing of primary afferents in the cat.* Brain Research, 1999. **825**(1): p. 132-145.
49. Sluka, K.A., W.D. Willis, and K.N. Westlund, *The role of dorsal root reflexes in neurogenic inflammation.* Pain Forum, 1995. **4**(3): p. 141-149.
50. Levine, J.D., et al., *Contribution of sensory afferents and sympathetic efferents to joint injury in experimental arthritis.* Journal of Neuroscience, 1986. **6**(12): p. 3423-3429.
51. Brooks, C.M. and K. Koizumi, *Origin of the dorsal root reflex.* Journal of Neurophysiology, 1956. **19**(1): p. 61-74.
52. Carlton, S.M., *Nociceptive primary afferents: they have a mind of their own.* J Physiol, 2014. **592**(16): p. 3403-11.
53. Rudomin, P. and R.F. Schmidt, *Presynaptic inhibition in the vertebrate spinal cord revisited.* Experimental Brain Research, 1999. **129**(1): p. 1-37.
54. Tinnermann, A., C. Sprenger, and C. Buchel, *Opioid analgesia alters corticospinal coupling along the descending pain system in healthy participants.* Elife, 2022. **11**.
55. Liebeskind, J.C., et al., *Analgesia from electrical stimulation of the periaqueductal gray matter in the cat: Behavioral observations and inhibitory effects on spinal cord interneurons.* Brain Research, 1973. **50**: p. 441-446.
56. Calvino, B. and R.M. Grilo, *Central pain control.* Joint Bone Spine, 2006. **73**(1): p. 10-6.
57. Basbaum, A.I. and H.L. Fields, *Endogenous pain control systems: brainstem spinal pathways and endorphin circuitry.* Annual review of neuroscience, 1984. **7**(1): p. 309-338.
58. Yoshimura, M. and H. Furue, *Mechanisms for the anti-nociceptive actions of the descending noradrenergic and serotonergic systems in the spinal cord.* J Pharmacol Sci, 2006. **101**(2): p. 107-17.
59. Liu, Y., et al., *Touch and tactile neuropathic pain sensitivity are set by corticospinal projections.* Nature, 2018. **561**(7724): p. 547-550.
60. Shreckengost, J., et al., *Bicuculline-sensitive primary afferent depolarization remains after greatly restricting synaptic transmission in the mammalian spinal cord.* J Neurosci, 2010. **30**(15): p. 5283-8.

61. Rudomin, P., *In search of lost presynaptic inhibition.* Exp Brain Res, 2009. **196**(1): p. 139-51.
62. Eccles Jc Fau - Schmidt, R., W.D. Schmidt R Fau - Willis, and W.D. Willis, *PHARMACOLOGICAL STUDIES ON PRESYNAPTIC INHIBITION.* 1963(0022-3751 (Print)).
63. Raja, S.N., et al., *The revised International Association for the Study of Pain definition of pain: concepts, challenges, and compromises.* 2020(1872-6623 (Electronic)).
64. Siddall, P.J., et al., *Pain report and the relationship of pain to physical factors in the first 6 months following spinal cord injury.* Pain, 1999. **81**(1): p. 187-197.
65. Siddall, P.J. and J.D. Loeser, *Pain following spinal cord injury.* Spinal Cord, 2001. **39**(2): p. 63-73.
66. Siddall, P.J., et al., *A longitudinal study of the prevalence and characteristics of pain in the first 5 years following spinal cord injury.* Pain, 2003. **103**(3): p. 249-257.
67. Sun, X., et al., *Multiple organ dysfunction and systemic inflammation after spinal cord injury: a complex relationship.* Journal of Neuroinflammation, 2016. **13**(1): p. 260.
68. Walters, E.T., *Neuroinflammatory contributions to pain after SCI: Roles for central glial mechanisms and nociceptor-mediated host defense.* Experimental Neurology, 2014. **258**: p. 48-61.
69. Walters, E.T., *Adaptive mechanisms driving maladaptive pain: how chronic ongoing activity in primary nociceptors can enhance evolutionary fitness after severe injury.* Philosophical Transactions of the Royal Society B: Biological Sciences, 2019. **374**(1785): p. 20190277.
70. Walters, E.T., *Chapter 17 - Peripheral mechanisms contributing to central neuropathic pain following SCI*, in *Spinal Cord Injury Pain*, C.N. Sang and C.E. Hulsebosch, Editors. 2022, Academic Press. p. 353-371.
71. Yang, Q., et al., *Persistent Pain after Spinal Cord Injury Is Maintained by Primary Afferent Activity.* Journal of Neuroscience, 2014. **34**(32): p. 10765-10769.
72. Jensen, T.S. and N.B. Finnerup, *Allodynia and hyperalgesia in neuropathic pain: clinical manifestations and mechanisms.* The Lancet Neurology, 2014. **13**(9): p. 924-935.
73. Widerström-Noga, E., *Neuropathic Pain and Spinal Cord Injury: Phenotypes and Pharmacological Management.* Drugs, 2017. **77**(9): p. 967-984.
74. Glare, P., K.R. Aubrey, and P.S. Myles, *Transition from acute to chronic pain after surgery.* The Lancet, 2019. **393**(10180): p. 1537-1546.
75. Hulsebosch, C.E., *Chapter 3 - Central neuropathic pain after spinal cord injury: Therapeutic opportunities. A brief history and temporal progression of the pathophysiology from acute trauma to chronic conditions*, in *Spinal Cord Injury Pain*, C.N. Sang and C.E. Hulsebosch, Editors. 2022, Academic Press. p. 45-86.
76. Gwak, Y.S. and J.W. Leem, *Chapter 14 - Glial activation and neuropathic pain*, in *Spinal Cord Injury Pain*, C.N. Sang and C.E. Hulsebosch, Editors. 2022, Academic Press. p. 297-314.
77. Gilron, I., R. Baron, and T. Jensen, *Neuropathic pain: principles of diagnosis and treatment.* Mayo Clin Proc, 2015. **90**(4): p. 532-45.
78. Vallbo, A.B., et al., *Somatosensory, proprioceptive, and sympathetic activity in human peripheral nerves.* Physiological Reviews, 1979. **59**(4): p. 919-957.
79. Chen, Y., et al., *Causes of Spinal Cord Injury.* Topics in Spinal Cord Injury Rehabilitation, 2013. **19**(1): p. 1-8.

80. Mahnig, S., et al., *Pain assessment according to the International Spinal Cord Injury Pain classification in patients with spinal cord injury referred to a multidisciplinary pain center.* Spinal Cord, 2016. **54**(10): p. 809-815.
81. Levi, R., et al., *The Stockholm spinal cord injury study: 1. Medical problems in a regional SCI population.* Spinal Cord, 1995. **33**(6): p. 308-315.
82. Turner, J. and D. Cardenas. *Chronic pain problems in individuals with spinal cord injuries*. in *Seminars in clinical neuropsychiatry*. 1999.
83. Turner, J.A., et al., *Chronic pain associated with spinal cord injuries: A community survey.* Archives of Physical Medicine and Rehabilitation, 2001. **82**(4): p. 501-508.
84. Störmer, S., et al., *Chronic pain/dysaesthesiae in spinal cord injury patients: results of a multicentre study.* Spinal cord, 1997. **35**(7): p. 446-455.
85. Siddall, P.J., et al., *Pain report and the relationship of pain to physical factors in the first 6 months following spinal cord injury.* Pain, 1999. **81**(1-2): p. 187-197.
86. Defrin, R., et al., *Characterization of chronic pain and somatosensory function in spinal cord injury subjects.* Pain, 2001. **89**(2): p. 253-263.
87. Sang, C.N. and C.E. Hulsebosch, *Front Matter*, in *Spinal Cord Injury Pain*, C.N. Sang and C.E. Hulsebosch, Editors. 2022, Academic Press. p. i-ii.
88. Cragg, J.J., et al., *Neuropathic Pain, Depression, and Cardiovascular Disease: A National Multicenter Study.* Neuroepidemiology, 2015. **44**(3): p. 130-137.
89. Burke, D., et al., *Neuropathic pain prevalence following spinal cord injury: A systematic review and meta-analysis.* European Journal of Pain, 2017. **21**(1): p. 29-44.
90. Shinu, P.M.M.A.A.U.N.A.B.A.U.M.A.K.A.V.K.N.A.U.G.M.B.M.J. *Novel Therapies for the Treatment of Neuropathic Pain Potential*

Pitfalls,. Journal of Clinical Medicine, 2022. **11**, DOI: 10.3390/jcm11113002.
91. Rogawski, M.A. and W. Loscher, *The neurobiology of antiepileptic drugs for the treatment of nonepileptic conditions.* Nat Med, 2004. **10**(7): p. 685-92.
92. Bialer, M., *Why are antiepileptic drugs used for nonepileptic conditions?* Epilepsia, 2012. **53 Suppl 7**: p. 26-33.
93. Hatch, M.N., et al., *Neuropathic pain and SCI: Identification and treatment strategies in the 21st century.* Journal of the Neurological Sciences, 2018. **384**: p. 75-83.
94. Mei, L., et al., *Efficacy and safety of different drug treatments in patients with spinal-cord injury-related neuropathic pain: a network meta-analysis.* Spinal Cord, 2022. **60**(11): p. 943-953.
95. D'Souza, R.S., et al., *Dorsal Root Ganglion Stimulation for Lower Extremity Neuropathic Pain Syndromes: An Evidence-Based Literature Review.* Advances in Therapy, 2022. **39**(10): p. 4440-4473.
96. Zhang, T.C., J.J. Janik, and W.M. Grill, *Modeling effects of spinal cord stimulation on wide-dynamic range dorsal horn neurons: influence of stimulation frequency and GABAergic inhibition.* J Neurophysiol, 2014. **112**(3): p. 552-67.
97. Holsheimer, J. and J.R. Buitenweg, *Review: Bioelectrical Mechanisms in Spinal Cord Stimulation.* Neuromodulation: Technology at the Neural Interface, 2015. **18**(3): p. 161-170.
98. Jankowska, E., et al., *Evidence that some long-lasting effects of direct current in the rat spinal cord are activity-independent.* European Journal of Neuroscience, 2016. **43**(10): p. 1400-1411.

99. Dones, I. and V. Levi, *Spinal Cord Stimulation for Neuropathic Pain: Current Trends and Future Applications.* Brain Sciences, 2018. **8**(8): p. 138.
100. Jaggi, A.S., V. Jain, and N. Singh, *Animal models of neuropathic pain.* Fundam Clin Pharmacol, 2011. **25**(1): p. 1-28.
101. Verma, R., et al., *Animals models of spinal cord contusion injury.* The Korean Journal of Pain, 2019. **32**(1): p. 12-21.
102. Hulsebosch, C.E. and R.E. Coggeshall, *Quantitation of sprouting of dorsal root axons.* Science, 1981. **213**(4511): p. 1020-1021.
103. Hulsebosch, C.E. and C.N. Sang, *Chapter 6 - Counterpoint: Animal models are indispensable for translational pain research in spinal cord injury*, in *Spinal Cord Injury Pain*, C.N. Sang and C.E. Hulsebosch, Editors. 2022, Academic Press. p. 125-133.
104. Bedi, S.S., et al., *Chronic Spontaneous Activity Generated in the Somata of Primary Nociceptors Is Associated with Pain-Related Behavior after Spinal Cord Injury.* Journal of Neuroscience, 2010. **30**(44): p. 14870-14882.
105. Bavencoffe, A., et al., *Persistent Electrical Activity in Primary Nociceptors after Spinal Cord Injury Is Maintained by Scaffolded Adenylyl Cyclase and Protein Kinase A and Is Associated with Altered Adenylyl Cyclase Regulation.* Journal of Neuroscience, 2016. **36**(5): p. 1660-1668.
106. Baliki, M.N., A.T. Baria, and A.V. Apkarian, *The Cortical Rhythms of Chronic Back Pain.* The journal of neuroscience : the official journal of the Society for Neuroscience. **31**(39): p. 13981-13990.
107. Vierck, C., *Mechanisms of below-level pain following spinal cord injury (SCI).* The Journal of Pain, 2019.
108. Stachowski, N.J. and K.J. Dougherty, *Spinal Inhibitory Interneurons: Gatekeepers of Sensorimotor Pathways.* International Journal of Molecular Sciences, 2021. **22**(5): p. 2667.
109. Stucky, C.L. and A.R. Mikesell, *Chapter 16 - When soft touch hurts: How hugs become painful after spinal cord injury*, in *Spinal Cord Injury Pain*, C.N. Sang and C.E. Hulsebosch, Editors. 2022, Academic Press. p. 341-351.
110. Vierck, C., *Chapter 4 - Mechanisms of pain below the level of spinal cord injury (SCI)*, in *Spinal Cord Injury Pain*, C.N. Sang and C.E. Hulsebosch, Editors. 2022, Academic Press. p. 87-111.
111. Gangadharan, V., X. Wang, and C. Luo, *Cyclic GMP-dependent protein kinase-I localized in nociceptors modulates nociceptive cortical neuronal activity and pain hypersensitivity.* Molecular Pain, 2017. **13**: p. 1744806917701743.
112. Saab, C.Y. and B.C. Hains, *Remote neuroimmune signaling: a long-range mechanism of nociceptive network plasticity.* Trends Neurosci, 2009. **32**(2): p. 110-7.
113. Corder, G., et al., *An amygdalar neural ensemble that encodes the unpleasantness of pain.* Science, 2019. **363**(6424): p. 276-281.
114. Da Silva, J.T. and D.A. Seminowicz, *Neuroimaging of pain in animal models: a review of recent literature.* Pain Reports, 2019. **4**(4).
115. Fauss, G.N.K., K.E. Hudson, and J.W. Grau, *Role of Descending Serotonergic Fibers in the Development of Pathophysiology after Spinal Cord Injury (SCI): Contribution to Chronic Pain, Spasticity, and Autonomic Dysreflexia.* Biology (Basel), 2022. **11**(2).

116. Gwak, Y.S. and Z.D. Luo, *Chapter 13 - Spinal GABA mechanism in neuropathic pain after spinal cord injury**, in *Spinal Cord Injury Pain*, C.N. Sang and C.E. Hulsebosch, Editors. 2022, Academic Press. p. 275-296.
117. Knerlich-Lukoschus, F., *Chapter 15 - Mechanisms of CNP following SCI: Chemokines in neuronal-glial cell interaction*, in *Spinal Cord Injury Pain*, C.N. Sang and C.E. Hulsebosch, Editors. 2022, Academic Press. p. 315-338.
118. Sharif-Alhoseini, M., et al., *Animal models of spinal cord injury: a systematic review.* Spinal Cord, 2017. **55**(8): p. 714-721.
119. Tappe-Theodor, A. and R. Kuner, *Studying ongoing and spontaneous pain in rodents--challenges and opportunities.* Eur J Neurosci, 2014. **39**(11): p. 1881-90.
120. Finnerup, N.B., et al., *Phenotypes and Predictors of Pain Following Traumatic Spinal Cord Injury: A Prospective Study.* The Journal of Pain, 2014. **15**(1): p. 40-48.
121. Hulsebosch, C.E., et al., *Mechanisms of Chronic Central Neuropathic Pain after Spinal Cord Injury.* Brain research reviews, 2009. **60**(1): p. 202-213.
122. Gwak, Y.S., C.E. Hulsebosch, and J.W. Leem, *Neuronal-Glial Interactions Maintain Chronic Neuropathic Pain after Spinal Cord Injury.* Neural Plasticity, 2017.
123. Walters, E.T., *Nociceptors as chronic drivers of pain and hyperreflexia after spinal cord injury: an adaptive-maladaptive hyperfunctional state hypothesis.* Frontiers in Physiology, 2012. **3**.
124. Klein, A.H., et al., *Sodium Channel Nav1.8 Underlies TTX-Resistant Axonal Action Potential Conduction in Somatosensory C-Fibers of Distal Cutaneous Nerves.* Journal of Neuroscience, 2017. **37**(20): p. 5204-5214.
125. Zemel, B.M., et al., *A-Type KV Channels in Dorsal Root Ganglion Neurons: Diversity, Function, and Dysfunction.* Frontiers in Molecular Neuroscience, 2018. **11**.
126. Ritter, D.M., et al., *Dysregulation of Kv3.4 Channels in Dorsal Root Ganglia Following Spinal Cord Injury.* Journal of Neuroscience, 2015. **35**(3): p. 1260-1273.
127. Walters, E.T., *How is chronic pain related to sympathetic dysfunction and autonomic dysreflexia following spinal cord injury?* Autonomic Neuroscience, 2018. **209**: p. 79-89.
128. Wang, J., M. Kawamata, and A. Namiki, *Changes in Properties of Spinal Dorsal Horn Neurons and Their Sensitivity to Morphine after Spinal Cord Injury in the Rat.* Anesthesiology, 2005. **102**(1): p. 152-164.
129. Hains, B.C., et al., *Upregulation of sodium channel Nav1.3 and functional involvement in neuronal hyperexcitability associated with central neuropathic pain after spinal cord injury.* (1529-2401 (Electronic)).
130. Hains, B.C., et al., *Upregulation of Sodium Channel Na_v1.3 and Functional Involvement in Neuronal Hyperexcitability Associated with Central Neuropathic Pain after Spinal Cord Injury.* The Journal of Neuroscience, 2003. **23**(26): p. 8881-8892.
131. Bilchak, J.N., et al., *Enhancing KCC2 activity decreases hyperreflexia and spasticity after chronic spinal cord injury.* Experimental Neurology, 2021. **338**: p. 113605.
132. Doyon, N., et al., *Treating pathological pain: is KCC2 the key to the gate?* Expert Review of Neurotherapeutics, 2013. **13**(5): p. 469-471.
133. Lu, Y., et al., *Spinal cord injury-induced attenuation of GABAergic inhibition in spinal dorsal horn circuits is associated with down-regulation of the chloride transporter KCC2 in rat.* The Journal of Physiology, 2008. **586**(23): p. 5701-5715.

134. Lee, K.Y., S. Ratté, and S.A. Prescott, *Excitatory neurons are more disinhibited than inhibitory neurons by chloride dysregulation in the spinal dorsal horn.* eLife, 2019. **8**: p. e49753.
135. Gwak, Y.S. and C.E. Hulsebosch, *GABA and central neuropathic pain following spinal cord injury.* Neuropharmacology, 2011. **60**(5): p. 799-808.
136. Huang, Y.-J., et al., *Acute spinal cord injury (SCI) transforms how GABA affects nociceptive sensitization.* Experimental Neurology, 2016. **285**: p. 82-95.
137. Walters, E.T., *How is chronic pain related to sympathetic dysfunction and autonomic dysreflexia following spinal cord injury?* Autonomic neuroscience : basic & clinical, 2018. **209**: p. 79-89.
138. Lee, H.J., et al., *Central Plasticity of Cutaneous Afferents Is Associated with Nociceptive Hyperreflexia after Spinal Cord Injury in Rats.* Neural Plasticity, 2019.
139. Woolf, C.J. *The Pathophysiology of Peripheral Neuropathic Pain—Abnormal Peripheral Input and Abnormal Central Processing*. 1993. Springer.
140. Kinnman, E. and J.D. Levine, *Sensory and sympathetic contributions to nerve injury-induced sensory abnormalities in the rat.* Neuroscience, 1995. **64**(3): p. 751-767.
141. Michaelis, M., M. Devor, and W. Janig, *Sympathetic modulation of activity in rat dorsal root ganglion neurons changes over time following peripheral nerve injury.* Journal of Neurophysiology, 1996. **76**(2): p. 753-763.
142. Deng, Y.-S., J.-H. Zhong, and X.-F. Zhou, *BDNF is involved in sympathetic sprouting in the dorsal root ganglia following peripheral nerve injury in rats.* Neurotoxicity Research, 1999. **1**(4): p. 311-322.
143. Menorca, R.M.G., T.S. Fussell, and J.C. Elfar, *Peripheral Nerve Trauma: Mechanisms of Injury and Recovery.* Hand clinics, 2013. **29**(3): p. 317-330.
144. Nascimento, F.P., et al., *Sympathetic fibre sprouting in the skin contributes to pain-related behaviour in spared nerve injury and cuff models of neuropathic pain.* Molecular Pain, 2015. **11**(1): p. 59.
145. Smith, P.A., *K(+) Channels in Primary Afferents and Their Role in Nerve Injury-Induced Pain.* Front Cell Neurosci, 2020. **14**: p. 566418.
146. Bagust, J., I.D. Forsythe, and G.A. Kerkut, *An investigation of the dorsal root reflex using an in vitro preparation of the hamster spinal cord.* Brain Research, 1985. **331**(2): p. 315-325.
147. Lidierth, M. and P.D. Wall, *Synchronous inherent oscillations of potentials within the rat lumbar spinal cord.* Neurosci Lett, 1996. **220**(1): p. 25-8.
148. Manjarrez, E., et al., *Modulation of synaptic transmission from segmental afferents by spontaneous activity of dorsal horn spinal neurones in the cat.* J Physiol, 2000. **529 Pt 2**: p. 445-60.
149. Fisher, R.S., et al., *Epileptic seizures and epilepsy: definitions proposed by the International League Against Epilepsy (ILAE) and the International Bureau for Epilepsy (IBE).* Epilepsia, 2005. **46**(4): p. 470-2.
150. Thijs, R.D., et al., *Epilepsy in adults.* Lancet, 2019. **393**(10172): p. 689-701.
151. Allen, N.M., et al., *Genetic potassium channel-associated epilepsies: Clinical review of the K(v) family.* Eur J Paediatr Neurol, 2020. **24**: p. 105-116.
152. Kohling, R., *Voltage-gated sodium channels in epilepsy.* Epilepsia, 2002. **43**(11): p. 1278-95.

153. Moore, Y.E., et al., *Seizing Control of KCC2: A New Therapeutic Target for Epilepsy.* Trends Neurosci, 2017. **40**(9): p. 555-571.
154. Treiman, D.M., *GABAergic mechanisms in epilepsy.* Epilepsia, 2001. **42 Suppl 3**: p. 8-12.
155. Ruscheweyh, R. and J. Sandkühler, *Epileptiform activity in rat spinal dorsal horn in vitro has common features with neuropathic pain.* Pain, 2003. **105**(1): p. 327-338.
156. Valentín, A., et al., *Responses to single pulse electrical stimulation identify epileptogenesis in the human brain in vivo.* Brain, 2002. **125**(8): p. 1709-1718.
157. Shorvon, S.D., *The etiologic classification of epilepsy.* Epilepsia, 2011. **52**(6): p. 1052-7.
158. Stober, T.M., et al., *Degeneracy in epilepsy: multiple routes to hyperexcitable brain circuits and their repair.* Commun Biol, 2023. **6**(1): p. 479.
159. Kandel, E.R., et al., *Touch*, in *Principles of Neural Science, 6e*. 2021, McGraw Hill: New York, NY.
160. Kuner, R. and T. Kuner, *Cellular Circuits in the Brain and Their Modulation in Acute and Chronic Pain.* Physiological Reviews, 2020. **101**(1): p. 213-258.
161. Vierck Jr, C.J. and A.R. Light, *Allodynia and hyperalgesia within dermatomes caudal to a spinal cord injury in primates and rodents.* 2000.
162. Hansen, A.P., et al., *Pain following stroke: A prospective study.* European Journal of Pain, 2012. **16**(8): p. 1128-1136.
163. Finnerup, N.B., *A review of central neuropathic pain states.* Current Opinion in Anesthesiology, 2008. **21**(5).
164. O'Donnell, M.J., et al., *Chronic Pain Syndromes After Ischemic Stroke.* Stroke, 2013. **44**(5): p. 1238-1243.
165. Delpont, B., et al., *Pain after stroke: A review.* Revue Neurologique, 2018. **174**(10): p. 671-674.
166. Price, T.J., F. Cervero, and Y.d. Koninck, *Role of Cation-Chloride-Cotransporters (CCC) in Pain and Hyperalgesia.* Current Topics in Medicinal Chemistry, 2005. **5**(6): p. 547-555.
167. Gagnon, M., et al., *Chloride extrusion enhancers as novel therapeutics for neurological diseases.* Nature Medicine, 2013. **19**(11): p. 1524-1528.
168. Fransen, E. and J. Tigerholm, *Role of A-type potassium currents in excitability, network synchronicity, and epilepsy.* Hippocampus, 2010. **20**(7): p. 877-87.
169. Todd, A.J., *GABA and Glycine in Synaptic Glomeruli of the Rat Spinal Dorsal Horn.* European Journal of Neuroscience, 1996. **8**(12): p. 2492-2498.
170. Todd, A.J., *Neuronal circuitry for pain processing in the dorsal horn.* Nature Reviews Neuroscience, 2010. **11**(12): p. 823-836.
171. Todd, A.J., *Identifying functional populations among the interneurons in laminae I-III of the spinal dorsal horn.* Molecular Pain, 2017. **13**: p. 174480691769300.
172. Peirs, C., R. Dallel, and A.J. Todd, *Recent advances in our understanding of the organization of dorsal horn neuron populations and their contribution to cutaneous mechanical allodynia.* Journal of Neural Transmission, 2020. **127**(4): p. 505-525.
173. Hughes, D.I. and A.J. Todd, *Central Nervous System Targets: Inhibitory Interneurons in the Spinal Cord.* Neurotherapeutics, 2020. **17**(3): p. 874-885.
174. Bolzoni, F. and E. Jankowska, *Presynaptic and postsynaptic effects of local cathodal DC polarization within the spinal cord in anaesthetized animal preparations.* The Journal of Physiology, 2015. **593**(4): p. 947-966.

175. Bardoni, R., et al., *Pre- and postsynaptic inhibitory control in the spinal cord dorsal horn.* Annals of the New York Academy of Sciences, 2013. **1279**(1): p. 90-96.
176. Todd, A.J., *Identifying functional populations among the interneurons in laminae I-III of the spinal dorsal horn.* Molecular Pain, 2017. **13**: p. 1744806917693003.
177. Paixão, S., et al., *Identification of Spinal Neurons Contributing to the Dorsal Column Projection Mediating Fine Touch and Corrective Motor Movements.* Neuron, 2019. **104**(4): p. 749-764.e6.
178. Hari, K., et al., *GABA facilitates spike propagation through branch points of sensory axons in the spinal cord.* Nat Neurosci, 2022. **25**(10): p. 1288-1299.
179. Ki-Wug, S., et al., *Abnormal GABA_A Receptor-Mediated Currents in Dorsal Root Ganglion Neurons Isolated from Na–K–2Cl Cotransporter Null Mice.* The Journal of Neuroscience, 2000. **20**(20): p. 7531.
180. Vicente-Baz, J., J.A. Lopez-Garcia, and I. Rivera-Arconada, *Central sensitization of dorsal root potentials and dorsal root reflexes: An in vitro study in the mouse spinal cord.* Eur J Pain, 2022. **26**(2): p. 356-369.
181. Lin, Q., J. Wu, and W.D. Willis, *Dorsal Root Reflexes and Cutaneous Neurogenic Inflammation After Intradermal Injection of Capsaicin in Rats.* Journal of Neurophysiology, 1999. **82**(5): p. 2602-2611.
182. Bagust, J., I.D. Forsythe, and G.A. Kerkut, *An investigation of the dorsal root reflex using an in vitro preparation of the hamster spinal cord.* Brain Res, 1985. **331**(2): p. 315-25.
183. Garcia, C.A., et al., *Effects of spinal and peripheral nerve lesions on the intersegmental synchronization of the spontaneous activity of dorsal horn neurons in the cat lumbosacral spinal cord.* Neurosci Lett, 2004. **361**(1-3): p. 102-5.
184. Rudomin, P., *Primary afferent depolarization produced in Aδ and C fibres by glutamate spillover? New ways to look at old things.* The Journal of Physiology, 2000. **528**(Pt 1): p. 1.
185. Bos, R., F. Brocard, and L. Vinay, *Primary afferent terminals acting as excitatory interneurons contribute to spontaneous motor activities in the immature spinal cord.* J Neurosci, 2011. **31**(28): p. 10184-8.
186. Scheff, S. and K.N. Roberts, *Infinite Horizon Spinal Cord Contusion Model*, in *Animal Models of Acute Neurological Injuries*, J. Chen, et al., Editors. 2009, Humana Press: Totowa, NJ. p. 423-432.
187. Kramer, J.L.K., et al., *Neuropathic pain following traumatic spinal cord injury: Models, measurement, and mechanisms.* Journal of Neuroscience Research, 2017. **95**(6): p. 1295-1306.
188. Drew, G.M., P.J. Siddall, and A.W. Duggan, *Mechanical allodynia following contusion injury of the rat spinal cord is associated with loss of GABAergic inhibition in the dorsal horn.* Pain, 2004. **109**(3): p. 379-388.
189. Lampert, A., B.C. Hains, and S.G. Waxman, *Upregulation of persistent and ramp sodium current in dorsal horn neurons after spinal cord injury.* Exp Brain Res, 2006. **174**(4): p. 660-6.
190. Carlton, S.M., et al., *Peripheral and central sensitization in remote spinal cord regions contribute to central neuropathic pain after spinal cord injury.* PAIN®, 2009. **147**(1): p. 265-276.

191. Noble, D.J., et al., *Use of electric field sensors for recording respiration, heart rate, and stereotyped motor behaviors in the rodent home cage.* Journal of Neuroscience Methods, 2017. **277**: p. 88-100.
192. Chaplan, S.R., et al., *Quantitative assessment of tactile allodynia in the rat paw.* Journal of Neuroscience Methods, 1994. **53**(1): p. 55-63.
193. Keizer, D., et al., *Quantitative Sensory Testing With Von Frey Monofilaments in Patients With Allodynia: What Are We Quantifying?* The Clinical Journal of Pain, 2008. **24**(5).
194. Trierweiler, J., D.N. Göttert, and G. Gehlen, *Evaluation of Mechanical Allodynia in an Animal Immobilization Model Using the Von Frey Method.* Journal of Manipulative and Physiological Therapeutics, 2012. **35**(1): p. 18-25.
195. Idlett, S., *INVESTIGATIONS OF SPONTANEOUS PAIN AND MODULATION WITH SPINAL CORD STIMULATION*. 2020, Georgia Institute of Technology.
196. Ting, J.T., et al., *Acute Brain Slice Methods for Adult and Aging Animals: Application of Targeted Patch Clamp Analysis and Optogenetics*, in *Patch-Clamp Methods and Protocols*, M. Martina and S. Taverna, Editors. 2014, Springer New York: New York, NY. p. 221-242.
197. Eide, E., *Stimulation and recording with closely spaced microelectrodes.* 1971(0001-6772 (Print)).
198. Kocsis, J.D., et al., *Functional differences between 4-aminopyridine and tetraethylammonium-sensitive potassium channels in myelinated axons.* Neuroscience Letters, 1987. **75**(2): p. 193-198.
199. Targ, E.F. and J.D. Kocsis, *4-aminopyridine leads to restoration of conduction in demyelinated rat sciatic nerve.* Brain Research, 1985. **328**(2): p. 358-361.
200. Bostock, H., T.A. Sears, and R.M. Sherratt, *The effects of 4-aminopyridine and tetraethylammonium ions on normal and demyelinated mammalian nerve fibres.* The Journal of Physiology, 1981. **313**(1): p. 301-315.
201. Smith, K.J., P.A. Felts, and G.R. John, *Effects of 4-aminopyridine on demyelinated axons, synapses and muscle tension.* Brain, 2000. **123**(1): p. 171-184.
202. Targ, E.F. and J.D. Kocsis, *Action potential characteristics of demyelinated rat sciatic nerve following application of 4-aminopyridine.* Brain Research, 1986. **363**(1): p. 1-9.
203. Albrecht, P., et al., *Prolonged-release fampridine in multiple sclerosis: clinical data and real-world experience. Report of an expert meeting.* 2018(1756-2856 (Print)).
204. Segal, J.L., et al., *Safety and Efficacy of 4-Aminopyridine in Humans with Spinal Cord Injury: A Long-Term, Controlled Trial.* Pharmacotherapy: The Journal of Human Pharmacology and Drug Therapy, 1999. **19**(6): p. 713-723.
205. Hayes, K.C., *Fampridine-SR for multiple sclerosis and spinal cord injury.* Expert Review of Neurotherapeutics, 2007. **7**(5): p. 453-461.
206. Sandkühler, J., *Models and Mechanisms of Hyperalgesia and Allodynia.* Physiological Reviews, 2009. **89**(2): p. 707-758.
207. Gonzalez-Sulser, A., et al., *The 4-aminopyridine in vitro epilepsy model analyzed with a perforated multi-electrode array.* Neuropharmacology, 2011. **60**(7-8): p. 1142-53.
208. Scalmani, P., et al., *Involvement of GABAergic Interneuron Subtypes in 4-Aminopyridine-Induced Seizure-Like Events in Mouse Entorhinal Cortex in Vitro.* J Neurosci, 2023. **43**(11): p. 1987-2001.
209. Fueta, Y. and M. Avoli, *Tetraethylammonium-induced epileptiform activity in young and adult rat hippocampus.* Developmental Brain Research, 1993. **72**(1): p. 51-58.

210. Mapplebeck, J.C.S., et al., *Chloride Dysregulation through Downregulation of KCC2 Mediates Neuropathic Pain in Both Sexes.* Cell Reports, 2019. **28**(3): p. 590-596.e4.
211. Cramer, S.W., et al., *The Role of Cation-Dependent Chloride Transporters in Neuropathic Pain Following Spinal Cord Injury.* Molecular Pain, 2008. **4**: p. 1744-8069-4-36.
212. Hasbargen, T., et al., *Role of NKCC1 and KCC2 in the development of chronic neuropathic pain following spinal cord injury.* Annals of the New York Academy of Sciences, 2010. **1198**(1): p. 168-172.
213. Tang, B.L., *The Expanding Therapeutic Potential of Neuronal KCC2.* Cells, 2020. **9**(1): p. 240.
214. Idlett, S.L., et al., *Assessment of axonal recruitment using model-guided preclinical spinal cord stimulation in the ex vivo adult mouse spinal cord.* Journal of Neurophysiology, 2019.
215. Avoli, M., et al., *Extracellular free potassium and calcium during synchronous activity induced by 4-aminopyridine in the juvenile rat hippocampus.* J Physiol, 1996. **493 (Pt 3)**(Pt 3): p. 707-17.
216. Dubuc, R.j. and S. Rossignol, *Unitary discharges in dorsal and ventral roots after the administration of 4-aminopyridine in the cat.* Brain Research, 1989. **491**(2): p. 349-355.
217. Ratte, S. and S.A. Prescott, *Afferent hyperexcitability in neuropathic pain and the inconvenient truth about its degeneracy.* Curr Opin Neurobiol, 2016. **36**: p. 31-7.
218. Ratté, S., et al., *Criticality and degeneracy in injury-induced changes in primary afferent excitability and the implications for neuropathic pain.* eLife, 2014. **3**: p. e02370.
219. J, B., K. Ga, and R. Ni, *The dorsal root reflex in isolated mammalian spinal cord.* Comparative Biochemistry and physiology. A, Comparative Physiology, 1989. **93**(1): p. 151-160.
220. Łuszczki, J.J., *Third-generation antiepileptic drugs: mechanisms of action, pharmacokinetics and interactions.* Pharmacological Reports, 2009. **61**(2): p. 197-216.
221. Dost, R., A. Rostock, and C. Rundfeldt, *The anti-hyperalgesic activity of retigabine is mediated by KCNQ potassium channel activation.* Naunyn Schmiedebergs Arch Pharmacol, 2004. **369**(4): p. 382-90.
222. Wu, Z., et al., *Activation of KCNQ Channels Suppresses Spontaneous Activity in Dorsal Root Ganglion Neurons and Reduces Chronic Pain after Spinal Cord Injury.* Journal of Neurotrauma, 2017. **34**(6): p. 1260-1270.
223. Bardoni, R., et al., *Delta Opioid Receptors Presynaptically Regulate Cutaneous Mechanosensory Neuron Input to the Spinal Cord Dorsal Horn.* Neuron, 2014. **81**(6): p. 1312-1327.
224. Khasabov, S.G., et al., *Modulation of afferent-evoked neurotransmission by 5-HT3 receptors in young rat dorsal horn neurones in vitro: a putative mechanism of 5-HT3 induced anti-nociception.* British Journal of Pharmacology, 1999. **127**(4): p. 843-852.
225. Ahuja, C.S., et al., *Spinal Cord Injury—What Are the Controversies?* Journal of Orthopaedic Trauma, 2017. **31**.
226. Ralf, W., et al., *Outcome heterogeneity and bias in acute experimental spinal cord injury.* Neurology, 2019. **93**(1): p. e40.
227. Hagains, C.E., et al., *Contributions of dorsal root reflex and axonal reflex to formalin-induced inflammation.* Brain Research, 2010. **1359**: p. 90-97.

228. Bertram, E.H., *Neuronal circuits in epilepsy: do they matter?* Exp Neurol, 2013. **244**: p. 67-74.
229. Jiruska, P., et al., *Synchronization and desynchronization in epilepsy: controversies and hypotheses.* J Physiol, 2013. **591**(4): p. 787-97.
230. Magloire, V., et al., *GABAergic Interneurons in Seizures: Investigating Causality With Optogenetics.* Neuroscientist, 2019. **25**(4): p. 344-358.
231. Calin, A., A.S. Ilie, and C.J. Akerman, *Disrupting Epileptiform Activity by Preventing Parvalbumin Interneuron Depolarization Block.* J Neurosci, 2021. **41**(45): p. 9452-9465.
232. Bagust, J., G.A. Kerkut, and N.I.A. Rakkah, *The dorsal root reflex in isolated mammalian spinal cord.* Comparative Biochemistry and Physiology Part A: Physiology, 1989. **93**(1): p. 151-160.
233. Lucas-Romero, J., I. Rivera-Arconada, and J.A. Lopez-Garcia, *Synchronous firing of dorsal horn neurons at the origin of dorsal root reflexes in naïve and paw-inflamed mice.* Frontiers in Cellular Neuroscience, 2022.
234. Rocha-González, H.I., F.J. Mao S Fau - Alvarez-Leefmans, and F.J. Alvarez-Leefmans, *Na+,K+,2Cl- cotransport and intracellular chloride regulation in rat primary sensory neurons: thermodynamic and kinetic aspects.* 2008(0022-3077 (Print)).
235. Häring, M., et al., *Neuronal atlas of the dorsal horn defines its architecture and links sensory input to transcriptional cell types.* Nature Neuroscience, 2018. **21**(6): p. 869-880.
236. Hughes, D.I., et al., *Morphological, neurochemical and electrophysiological features of parvalbumin-expressing cells: a likely source of axo-axonic inputs in the mouse spinal dorsal horn.* J Physiol, 2012. **590**(16): p. 3927-51.
237. Grudt, T.J. and E.R. Perl, *Correlations between neuronal morphology and electrophysiological features in the rodent superficial dorsal horn.* J Physiol, 2002. **540**(Pt 1): p. 189-207.
238. Luz, L.L., et al., *Contralateral Afferent Input to Lumbar Lamina I Neurons as a Neural Substrate for Mirror-Image Pain.* J Neurosci, 2023. **43**(18): p. 3245-3258.
239. Bannatyne, B.A., et al., *Differential Projections of Excitatory and Inhibitory Dorsal Horn Interneurons Relaying Information from Group II Muscle Afferents in the Cat Spinal Cord.* The Journal of Neuroscience, 2006. **26**(11): p. 2871.
240. Dougherty, K.J. and S. Hochman, *Spinal cord injury causes plasticity in a subpopulation of lamina I GABAergic interneurons.* J Neurophysiol, 2008. **100**(1): p. 212-23.
241. Thaweerattanasinp, T., et al., *Bursting interneurons in the deep dorsal horn develop increased excitability and sensitivity to serotonin after chronic spinal injury.* J Neurophysiol, 2020. **123**(5): p. 1657-1670.
242. Coull, J.A.M., et al., *Trans-synaptic shift in anion gradient in spinal lamina I neurons as a mechanism of neuropathic pain.* Nature, 2003. **424**(6951): p. 938-942.
243. Doyon, N., et al., *Chloride regulation: a dynamic equilibrium crucial for synaptic inhibition.* Neuron, 2016. **89**(6): p. 1157-1172.
244. Maxwell, D.J., et al., *Morphology of inhibitory and excitatory interneurons in superficial laminae of the rat dorsal horn.* J Physiol, 2007. **584**(Pt 2): p. 521-33.
245. Jolivalt, C.G., et al., *Allodynia and hyperalgesia in diabetic rats are mediated by GABA and depletion of spinal potassium-chloride co-transporters.* PAIN, 2008. **140**(1): p. 48-57.
246. Bao, F. and D. Liu, *Peroxynitrite generated in the rat spinal cord induces apoptotic cell death and activates caspase-3.* Neuroscience, 2003. **116**(1): p. 59-70.

247. Rafati, D.S., et al., *Nuclear factor-κB decoy amelioration of spinal cord injury-induced inflammation and behavior outcomes.* Journal of neuroscience research, 2008. **86**(3): p. 566-580.
248. Sah, R., et al., *Modulation of the GABAA-gated chloride channel by reactive oxygen species.* Journal of neurochemistry, 2002. **80**(3): p. 383-391.
249. West, S.J., et al., *Circuitry and plasticity of the dorsal horn--toward a better understanding of neuropathic pain.* Neuroscience, 2015. **300**: p. 254-75.
250. Di Cristo, G., et al., *KCC2, epileptiform synchronization, and epileptic disorders.* Progress in Neurobiology, 2018. **162**: p. 1-16.
251. Rash, J.E., et al., *Mixed synapses discovered and mapped throughout mammalian spinal cord.* Proceedings of the National Academy of Sciences, 1996. **93**(9): p. 4235-4239.
252. Chiang, C.Y., et al., *Central sensitization in medullary dorsal horn involves gap junctions and hemichannels.* Neuroreport, 2010. **21**(3): p. 233-7.
253. Tonkin, R.S., et al., *Gap junction proteins and their role in spinal cord injury.* Front Mol Neurosci, 2014. **7**: p. 102.
254. Wu, A., et al., *Role of gap junctions in chronic pain.* Journal of Neuroscience Research, 2012. **90**(2): p. 337-345.
255. Wang, H., et al., *The gap junction blocker carbenoxolone attenuates nociceptive behavior and medullary dorsal horn central sensitization induced by partial infraorbital nerve transection in rats.* PAIN®, 2014. **155**(2): p. 429-435.
256. Ouachikh, O., et al., *Electrical Synapses are Involved in Orofacial Neuropathic Pain.* Neuroscience, 2018. **382**: p. 69-79.
257. Paredes-Cruz, M., et al., *Functional improvement in individuals with chronic spinal cord injury treated with 4-aminopyridine: A systematic review.* Front Neurol, 2022. **13**: p. 1034730.
258. Cardenas, D.D., et al., *Phase 2 trial of sustained-release fampridine in chronic spinal cord injury.* Spinal Cord, 2007. **45**(2): p. 158-168.
259. Passmore, G.M., et al., *KCNQ/M Currents in Sensory Neurons: Significance for Pain Therapy.* Journal of Neuroscience, 2003. **23**(18): p. 7227-7236.
260. Marder, E. and A.A. Prinz, *Modeling stability in neuron and network function: the role of activity in homeostasis.* BioEssays, 2002. **24**(12): p. 1145-1154.
261. Prinz, A.A., D. Bucher, and E. Marder, *Similar network activity from disparate circuit parameters.* Nature Neuroscience, 2004. **7**(12): p. 1345-1352.
262. Bagust, J., Y. Chen, and G.A. Kerkut, *Spread of the dorsal root reflex in an isolated preparation of hamster spinal cord.* Experimental Physiology, 1993. **78**(6): p. 799-809.
263. Vicente-Baz, J., J.A. Lopez-Garcia, and I. Rivera-Arconada, *Central sensitization of dorsal root potentials and dorsal root reflexes: An in vitro study in the mouse spinal cord.* European Journal of Pain, 2022. **26**(2): p. 356-369.
264. Medlock, L., et al., *Multiscale Computer Model of the Spinal Dorsal Horn Reveals Changes in Network Processing Associated with Chronic Pain.* J Neurosci, 2022. **42**(15): p. 3133-3149.
265. Rémi, B., B. Frédéric, and V. Laurent, *Primary Afferent Terminals Acting as Excitatory Interneurons Contribute to Spontaneous Motor Activities in the Immature Spinal Cord.* The Journal of Neuroscience, 2011. **31**(28): p. 10184.
266. Cervero, F. and J.M.A. Laird, *Mechanisms of touch-evoked pain (allodynia): a new model.* Pain, 1996. **68**(1): p. 13-23.

267. Takkala, P., Y. Zhu, and S.A. Prescott, *Combined Changes in Chloride Regulation and Neuronal Excitability Enable Primary Afferent Depolarization to Elicit Spiking without Compromising its Inhibitory Effects.* PLOS Computational Biology, 2016. **12**(11): p. e1005215.
268. Vítor, P., et al., *Multisegmental Aδ- and C-Fiber Input to Neurons in Lamina I and the Lateral Spinal Nucleus.* The Journal of Neuroscience, 2010. **30**(6): p. 2384.
269. Andrew, J.T., et al., *Projection Neurons in Lamina I of Rat Spinal Cord with the Neurokinin 1 Receptor Are Selectively Innervated by Substance P-Containing Afferents and Respond to Noxious Stimulation.* The Journal of Neuroscience, 2002. **22**(10): p. 4103.
270. Delfini, M.-C., et al., *TAFA4, a Chemokine-like Protein, Modulates Injury-Induced Mechanical and Chemical Pain Hypersensitivity in Mice.* Cell Reports, 2013. **5**(2): p. 378-388.
271. Charline, K., et al. *Activation of spinal dorsal horn inhibitory networks by the CLTMR derived chemokine TAFA4*. in *10th FENS Forum of Neuroscience*. 2016.
272. Kambrun, C., et al., *TAFA4 Reverses Mechanical Allodynia through Activation of GABAergic Transmission and Microglial Process Retraction.* Cell Reports, 2018. **22**(11): p. 2886-2897.
273. Liljencrantz, J., et al., *Altered C-tactile processing in human dynamic tactile allodynia.* PAIN, 2013. **154**(2): p. 227-234.
274. Liljencrantz, J. and H. Olausson, *Tactile C fibers and their contributions to pleasant sensations and to tactile allodynia.* Frontiers in Behavioral Neuroscience, 2014. **8**.
275. Nagi, S.S., et al., *Allodynia mediated by C-tactile afferents in human hairy skin.* J Physiol, 2011. **589**(Pt 16): p. 4065-75.
276. Noble, D.J., et al. *C-low threshold mechanoreceptor activation becomes sufficient to trigger affective pain in spinal cord-injured mice in association with increased respiratory rates*. Frontiers in integrative neuroscience, 2022. **16**, 1081172 DOI: 10.3389/fnint.2022.1081172.
277. Rutlin, M., et al., *The Cellular and Molecular Basis of Direction Selectivity of Aδ-LTMRs.* Cell, 2014. **159**(7): p. 1640-1651.
278. Garraway, S.M. and J.R. Huie, *Spinal Plasticity and Behavior: BDNF-Induced Neuromodulation in Uninjured and Injured Spinal Cord.* Neural Plasticity, 2016.
279. Pitcher, M., C.E. Le Pichon, and A. Chesler, *Functional Properties of C-Low Threshold Mechanoreceptors (C-LTMRs) in Nonhuman Mammals*, in *Affective Touch and the Neurophysiology of CT Afferents*, H. Olausson, et al., Editors. 2016, Springer: New York, NY. p. 31-48.
280. Pitcher, M.H., C.E.L. Pichon, and A.T. Chesler. *Chapter 2 Functional Properties of CLow Threshold Mechanoreceptors (C-LTMRs) in Nonhuman Mammals*. 2018.
281. Emanuel, A.J., et al., *Cortical responses to touch reflect subcortical integration of LTMR signals.* Nature, 2021. **600**(7890): p. 680-685.
282. Handler, A. and D.D. Ginty, *The mechanosensory neurons of touch and their mechanisms of activation.* Nat Rev Neurosci, 2021. **22**(9): p. 521-537.
283. Moehring, F., et al., *Uncovering the Cells and Circuits of Touch in Normal and Pathological Settings.* Neuron, 2018. **100**(2): p. 349-360.
284. Peirs, C., et al., *Mechanical Allodynia Circuitry in the Dorsal Horn Is Defined by the Nature of the Injury.* Neuron, 2021. **109**(1): p. 73-90 e7.

285. Qi, L., S.H. Lin, and Q. Ma, *Spinal VGLUT3 lineage neurons drive visceral mechanical allodynia but not sensitized visceromotor reflexes.* Neuron, 2022.
286. Ting, J.T., et al., *Acute brain slice methods for adult and aging animals: application of targeted patch clamp analysis and optogenetics.* (1940-6029 (Electronic)).
287. Provost, M., *The effects of adrenergic, serotonergic, and cholinergic modulation on hairy skin low threshold mechanoreceptors*. 2019.
288. Szucs, P., et al., *Axon diversity of lamina I local-circuit neurons in the lumbar spinal cord.* Journal of Comparative Neurology, 2013. **521**(12): p. 2719-2741.
289. Szentágothai, J., *Neuronal and synaptic arrangement in the substantia gelatinosa rolandi.* Journal of Comparative Neurology, 1964. **122**(2): p. 219-239.
290. Dragunow, M. and R. Faull, *The use of c-fos as a metabolic marker in neuronal pathway tracing.* Journal of Neuroscience Methods, 1989. **29**(3): p. 261-265.
291. Torsney, C. and A.B. MacDermott, *Disinhibition Opens the Gate to Pathological Pain Signaling in Superficial Neurokinin 1 Receptor-Expressing Neurons in Rat Spinal Cord.* Journal of Neuroscience, 2006. **26**(6): p. 1833-1843.
292. Rahman, W., et al., *Superficial NK1 expressing spinal dorsal horn neurones modulate inhibitory neurotransmission mediated by spinal GABA(A) receptors.* Neurosci Lett, 2007. **419**(3): p. 278-83.
293. Zhang, L., et al., *c-fos expression in isolated rat spinal cord.* Journal of Neuroscience Methods, 1998. **79**(1): p. 105-113.
294. Alexander, S.P., et al., *The Concise Guide to PHARMACOLOGY 2015/16: Overview.* British Journal of Pharmacology, 2015. **172**(24): p. 5729-5743.
295. Fernandes, E.C., et al., *Diverse firing properties and Abeta-, Adelta-, and C-afferent inputs of small local circuit neurons in spinal lamina I.* Pain, 2016. **157**(2): p. 475-487.
296. Pinto, V., V.A. Derkach, and B.V. Safronov, *Role of TTX-Sensitive and TTX-Resistant Sodium Channels in Aδ- and C-Fiber Conduction and Synaptic Transmission.* Journal of Neurophysiology, 2008. **99**(2): p. 617-628.
297. Jessell, T.M., K. Yoshioka, and C.E. Jahr, *Amino Acid Receptor-Mediated Transmission at Primary Afferent Synapses in Rat Spinal Cord.* Journal of Experimental Biology, 1986. **124**(1): p. 239-258.
298. Salio, C., A. Merighi, and R. Bardoni, *GABA(B) receptors-mediated tonic inhibition of glutamate release from Abeta fibers in rat laminae III/IV of the spinal cord dorsal horn.* Mol Pain, 2017. **13**: p. 1744806917710041.
299. Ataka, T. and J.G. Gu, *Relationship between tonic inhibitory currents and phasic inhibitory activity in the spinal cord lamina II region of adult mice.* Mol Pain, 2006. **2**: p. 36.
300. Heise, C. and G. Kayalioglu, *Chapter 6 - Cytoarchitecture of the Spinal Cord*, in *The Spinal Cord*, C. Watson, G. Paxinos, and G. Kayalioglu, Editors. 2009, Academic Press: San Diego. p. 64-93.
301. Koch, S.C., D. Acton, and M. Goulding, *Spinal Circuits for Touch, Pain, and Itch.* Annual Review of Physiology, 2018. **80**(1): p. 189-217.
302. Russo, R.E., R. Delgado-Lezama, and J. Hounsgaard, *Dorsal root potential produced by a TTX-insensitive micro-circuitry in the turtle spinal cord.* The Journal of Physiology, 2000. **528**(Pt 1): p. 115.
303. Petitjean, H., et al., *Dorsal Horn Parvalbumin Neurons Are Gate-Keepers of Touch-Evoked Pain after Nerve Injury.* Cell Reports, 2015. **13**(6): p. 1246-1257.

304. Dougherty, K.J., M.A. Sawchuk, and S. Hochman, *Properties of Mouse Spinal Lamina I GABAergic Interneurons.* Journal of Neurophysiology, 2005. **94**(5): p. 3221-3227.
305. Clarkson, A.N., et al., *Reducing excessive GABA-mediated tonic inhibition promotes functional recovery after stroke.* Nature, 2010. **468**(7321): p. 305-309.
306. Lucas-Osma, A.M., et al., *Extrasynaptic alpha(5)GABA(A) receptors on proprioceptive afferents produce a tonic depolarization that modulates sodium channel function in the rat spinal cord.* J Neurophysiol, 2018. **120**(6): p. 2953-2974.
307. Zheng, Y., et al., *Deep Sequencing of Somatosensory Neurons Reveals Molecular Determinants of Intrinsic Physiological Properties.* Neuron, 2019. **103**(4): p. 598-616.e7.
308. Russ, D.E., et al., *A harmonized atlas of mouse spinal cord cell types and their spatial organization.* Nature Communications, 2021. **12**(1): p. 5722.
309. Takahashi, A., T. Mashimo, and I. Uchida, *GABAergic tonic inhibition of substantia gelatinosa neurons in mouse spinal cord.* NeuroReport, 2006. **17**(12).
310. Brown, E.V., et al., *Differential Activation of Pain Circuitry Neuron Populations in a Mouse Model of Spinal Cord Injury-Induced Neuropathic Pain.* J Neurosci, 2022. **42**(15): p. 3271-3289.
311. Sorkin, L.S., et al., *Origins of antidromic activity in sensory afferent fibers and neurogenic inflammation.* Seminars in Immunopathology, 2018. **40**(3): p. 237-247.
312. Li, D., et al., *Sensitization of Primary Afferent Nociceptors Induced by Intradermal Capsaicin Involves the Peripheral Release of Calcitonin Gene-Related Peptide Driven by Dorsal Root Reflexes.* The Journal of Pain, 2008. **9**(12): p. 1155-1168.
313. Ziolkowski, L.H., E.O. Gracheva, and S.N. Bagriantsev, *Mechanotransduction events at the physiological site of touch detection.* Elife, 2023. **12**.
314. Dubreuil, A.-S., et al., *Role of T-Type Calcium Current in Identified D-Hair Mechanoreceptor Neurons Studied In Vitro.* Journal of Neuroscience, 2004. **24**(39): p. 8480-8484.
315. François, A., et al., *The Low-Threshold Calcium Channel Cav3.2 Determines Low-Threshold Mechanoreceptor Function.* Cell Reports, 2015. **10**(3): p. 370-382.
316. Mills, E.P., et al., *Brainstem Pain-Control Circuitry Connectivity in Chronic Neuropathic Pain.* Journal of Neuroscience, 2018. **38**(2): p. 465-473.
317. Schoenen, J., *The dendritic organization of the human spinal cord: The dorsal horn.* Neuroscience, 1982. **7**(9): p. 2057-2087.
318. Barber, R.P., J.E. Vaughn, and E. Roberts, *The cytoarchitecture of gabaergic neurons in rat spinal cord.* Brain Research, 1982. **238**(2): p. 305-328.
319. Luz, L.L., P. Szucs, and B.V. Safronov, *Peripherally driven low-threshold inhibitory inputs to lamina I local-circuit and projection neurones: a new circuit for gating pain responses.* J Physiol, 2014. **592**(7): p. 1519-34.
320. Heinsinger, N.M., et al., *Facial grimace testing as an assay of neuropathic pain-related behavior in a mouse model of cervical spinal cord injury.* Experimental Neurology, 2020. **334**: p. 113468.
321. Hagen, E.M. and T. Rekand, *Management of Neuropathic Pain Associated with Spinal Cord Injury.* Pain and Therapy, 2015. **4**(1): p. 51-65.
322. Dekhuijzen, A.J. and J. Bagust, *Analysis of neural bursting: nonrhythmic and rhythmic activity in isolated spinal cord.* Journal of Neuroscience Methods, 1996. **67**(2): p. 141-147.

323. Chen, L., et al., *Detection of bursts in neuronal spike trains by the mean inter-spike interval method.* Progress in Natural Science, 2009. **19**(2): p. 229-235.
324. Lobb, C., *Abnormal Bursting as a Pathophysiological Mechanism in Parkinson's Disease.* Basal Ganglia, 2014. **3**(4): p. 187-195.
325. Van Pelt, J., et al., *Longterm stability and developmental changes in spontaneous network burst firing patterns in dissociated rat cerebral cortex cell cultures on multielectrode arrays.* Neurosci Lett, 2004. **361**(1-3): p. 86-9.
326. Cotterill, E. and S.J. Eglen, *Burst Detection Methods*, in *In Vitro Neuronal Networks: From Culturing Methods to Neuro-Technological Applications*, M. Chiappalone, V. Pasquale, and M. Frega, Editors. 2019, Springer International Publishing: Cham. p. 185-206.
327. Heffer, L.F. and J.B. Fallon, *A novel stimulus artifact removal technique for high-rate electrical stimulation.* J Neurosci Methods, 2008. **170**(2): p. 277-84.
328. Bakkum, D.J., et al., *Parameters for burst detection.* Front Comput Neurosci, 2013. **7**: p. 193.
329. Robin, K., et al., *Assessment of bursting activity and interspike intervals variability: A case study for methodological comparison.* Journal of Neuroscience Methods, 2009. **179**(1): p. 142-149.
330. Bagust, J., *Analysis of extracellular potentials using an IBM PC.* Comparative Biochemistry and Physiology Part A: Physiology, 1989. **93**(1): p. 161-170.